THE UNIVERSITY OF MICHIGAN
INDUSTRY PROGRAM OF THE COLLEGE OF ENGINEERING

HEAT TRANSFER IN A PIPE WITH TURBULENT FLOW AND ARBITRARY WALL-TEMPERATURE DISTRIBUTION

Charles A. Sleicher, Jr.

August 1955

IP-127

ACKNOWLEDGMENT

The Industry Program of the College of Engineering wishes to express its appreciation to the author for making it possible to distribute this dissertation under the Industry Program cover.

This dissertation was submitted in partial fulfillment of the requirements for the degree of Doctor of Philosophy in the University of Michigan.

PREFACE

The purpose of this investigation is to determine the effect of wall-temperature distribution on heat transfer and radial temperature distribution for the turbulent flow of fluids in pipes. The program of work was divided into two distinct phases: the first phase involved the construction of equipment and the taking of experimental data on heat transfer and radial temperature distribution for the flow of air. In the second phase the air data and the investigations of others were used to determine functions by means of which the temperature distribution could be extended to other fluids and flow rates by use of an electronic analog computer.

The author is indebted to Professor Donald L. Katz, Chairman of the Doctoral Committee, who, despite the pressure of other duties, was always available for advice and guidance. Professor Myron Tribus, now of the University of California at Los Angeles, deserves special mention for his help in initiating the investigation and his continued interest while in California. The author wishes also to thank Professors Stuart W. Churchill, Richard G. Folsom, and John R. Sellars for serving as members of the Committee and for their willingness to be of help at any time.

Special credit for the investigation is due to the staff and facilities of the Chemical and Metallurgical Engineering Department for help during all phases of the work; the Aeronautical Engineering Department for the use of equipment for the construction of hot-wire anenometers; the Instrumentation Section of the Aeronautical Engineering Department for the use of its electronic analog computer equipment and for the helpful advice of its staff; the DuPont Company for a fellowship during part

of the work; and the Engineering Research Institute for reproduction of the manuscript.

The author wishes to pay particular tribute to Professor Harold Mickley of M.I.T. for providing earlier stimulation to a basic and analytical approach to chemical engineering, and to Professor Josiah Carberry of Brown University for inspiration and guidance during the author's undergraduate years.

TABLE OF CONTENTS

LIST OF TABLES

LIST OF FIGURES

LIST OF FIGURES (concluded)

ABSTRACT

The purpose of this investigation is to determine the effect of wall-temperature distribution on the rate of heat transfer to fluids flowing in turbulent flow in pipes. The subject is of interest primarily because in any pipe heat exchanger the wall temperature undergoes a sudden change where heating begins. This change in wall temperature causes the heat-transfer coefficients to be abnormally high for a distance down the pipe termed the thermal entrance region.

The problem is approached through the partial differential equation governing the temperature distribution within the fluid. The equation is solved for fully developed velocity distribution and the uniform wall-temperature boundary condition, i.e., a step-change in wall temperature. It is shown that this solution may be used to solve the case of an arbitrary wall-temperature distribution by the method of superposition of solutions. The solution is presented as the first three terms of an infinite series in which the eigenfunctions and constants are functions of the Prandtl and Reynolds numbers.

The first step in solving the equation was to determine the eddy conductivity in pipe flow. This was done in an apparatus of the following description: Recirculated, dry air at a controlled temperature entered an entrance section of straightening vanes, screens, 46 diameters of 1-1/2-in. copper pipe, and 4 diameters of plastic pipe before entering the heated test section. The test section was of 1-1/2-in. copper pipe electrically heated in such a way that the wall temperature was uniform. In the test section 31 diameters from its beginning the following were measured: heat flux at the wall by a calorimeter, velocity distribution with a hot-wire

anemometer, and temperature distribution with the anemometer serving as a resistance thermometer.

The second step was to use an electronic analog computer to solve the differential equation. The eddy conductivities calculated from the above measurements were input functions to the computer. For fluids other than air, the air eddy conductivity was modified by means of Jenkins' analysis (19), which resulted in lower values in the liquid-metal region.

The results of computer show that the thermal entry lengths in diameters are about 10 for water and oils, 10-15 depending on Reynolds number for air, and 5-60 for liquid metals. The results for the asymptotic Nusselt number for liquid metals may be correlated within 10% by the following two simplified equations:

For uniform heat flux at the wall

$$Nu_a = 6.3 + 0.0060\ Pe^{.9}$$

For uniform wall temperature

$$Nu_a = 4.8 + 0.0056\ Pe^{.9}$$

It is concluded that the effects of nonuniform wall temperature on the rate of heat transfer in pipes is most marked in the liquid-metal region, and that failure to consider these effects can account for much of the scatter in the reported experimental data on liquid-metal heat transfer.

I. INTRODUCTION

Heat transfer to fluids flowing in forced convection is one of the most widely used processes in industry. It is employed in equipment ranging from drinking fountains to nuclear reactors. The most widely used geometry for this type of heat transfer is a simple pipe within which a fluid flows and which may be heated or cooled externally by another fluid or some other means. It is little wonder, then, that heat transfer in pipes has been the object of hundreds of investigations, both experimental and analytical, over the past eighty years or so. These are admirably reviewed in "Heat Transmission" by McAdams (34).

One aspect of the rate of heat transfer in pipes, however, that has received relatively little attention is the effect of wall-temperature distribution. There is, however, good reason for this state of affairs. In the first place, the effects are usually quite complicated and their mathematical treatment is difficult. In the second place, the effects are unimportant in many cases, and so correlations are possible without accounting for the nonuniform temperatures. Tribus and Klein (57) have recently summarized the available analytical methods for nonisothermal flow and have shown how these solutions can be extended to an arbitrary surface-temperature distribution. Of the twelve solutions they summarize, however, only three are for pipe flow. One of these is the classical Graetz solution (18,51) for laminar flow and the others are the solutions of Poppendiek (38,39,40) for the flow of liquid metals at low flow rates. Other more recent investigations have appeared and are reviewed in the following section. The object of this investigation is to provide an analysis which will yield both rate of heat transfer and temperature

distribution within a fluid flowing turbulently in a pipe in which the wall temperature varies in an arbitrary fashion. In particular, this statement implies a direct attack on heat transfer in the thermal entrance region. Before discussing this region further, it is best to give some definitions.

For heat transfer in pipes, results are usually correlated by an equation involving the Nusselt number, hD/k, in which h is defined by

$$q(x) = h(t_w - t_{mm})$$

With this definition it is possible for h and Nu to be negative or even negatively or positively infinite. The reason for this is simply that the rate of heat transfer is in reality proportional to the temperature gradient at the wall.

$$q(x) = -k\left(\frac{\partial t}{\partial y}\right)_{y=o}$$

This temperature gradient bears no necessary relation to the mixed-mean temperature; for a given fluid it is dependent principally upon the flow field and upon the wall-temperature pattern upstream of the point concerned.

The thermal entrance region mentioned above is the region immediately downstream from the point at which the fluid is first heated. For a short distance downstream from this point the heat-transfer coefficient, h, is abnormally high. The distance that is required for the coefficient to approach within 2% of its asymptotic or final value is called the thermal entrance length or thermal entry length.

The reason for the initial coefficients being high is best understood by a consideration of the "thermal boundary layer." Suppose that a fluid

enters a steam-jacketed pipe as shown in the following sketch.

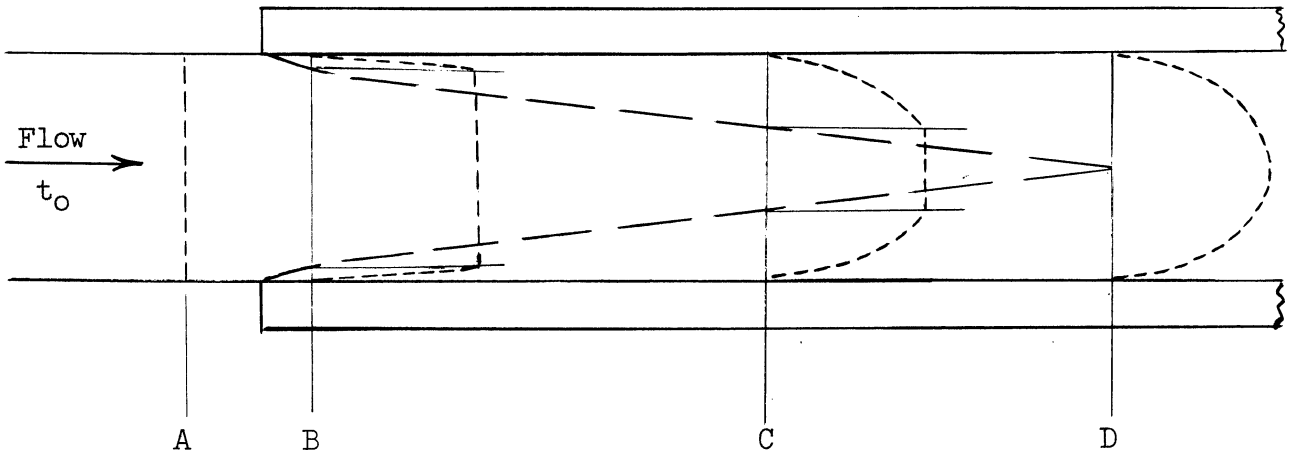

Successive temperature profiles are shown at A, B, C, and D as dotted lines. At A the temperature profile is flat since no heat transfer has yet occurred. At the jacketed section, however, the wall has a sudden change in temperature. This heats the fluid, but at first it heats only a thin layer of fluid next to the wall since the heat has not had time to penetrate the fluid very far. Because the temperature difference $t_w - t_o$ occurs across a thin layer, the temperature gradient and consequently the rate of heat transfer are high. The region in which the temperature gradient is different from zero is outlined by the dashed lines and is called the thermal boundary layer. Eventually at D the boundary layer fills the pipe and entrance effects have thus decayed to zero.

Of course, the above picture is an oversimplified one. For example, a minute amount of heat might penetrate to the center even at B. This difficulty can be circumvented by simply defining the boundary layer in a different way, such as that layer bounded by the pipe wall and a region

in which the temperature increase over t_o is less than 2% of $t_w - t_o$. With this definition the qualitative observations made before are still valid.

One more example will suffice to illustrate the effect of wall-temperature distribution on heat-transfer rate. Suppose that the wall temperature of a pipe looks as follows:

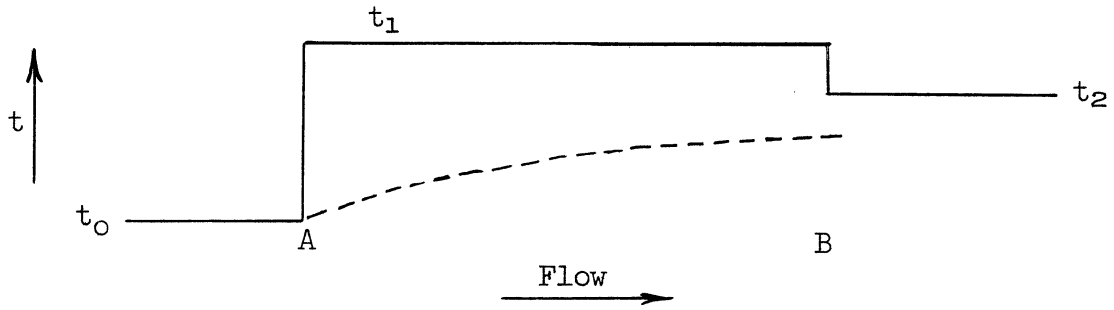

The dotted line represents the mixed-mean temperature of the fluid, which travels from left to right. Before the fluid reaches point A, it is at the wall temperature throughout its radius, but at A the wall temperature takes a sudden jump. Thus, infinitesimally beyond A the wall and the fluid next to it are at different temperatures. This in turn implies an infinite temperature gradient (a finite difference across zero depth) and therefore an infinite heat-transfer coefficient. Of course, discontinuous wall temperatures cannot be obtained in practice, but sharp changes can and, in fact, usually are obtained at some point in heat exchangers. This causes the coefficients to be high for a certain distance downstream, as explained in the previous example.

At B the wall temperature suddenly decreases but not as low as the mixed-mean temperature. Before B the fluid next to the wall is at the temperature t_1 and is above t_2 for some distance into the fluid. Therefore, as this fluid passes B, it will transfer its heat to the colder wall at t_2; i.e., the direction of heat flow is reversed whereas the difference $t_w - t_{mm}$ is still positive as before. Thus, the heat-transfer coefficient

is negative. In fact, it is negatively infinite for an infinitesimal distance beyond B. These examples have served to illustrate that the heat-transfer coefficient is dependent upon the nature of the wall-temperature distribution.

In order to calculate quantitatively the heat-transfer coefficient under conditions similar or less severe to the above, several approaches are possible, but the most general would be the solution of the partial differential equations that governs the heat transfer in a pipe. It is this approach that is used here. The equation that is solved is

$$u\sigma C_p \frac{\partial t}{\partial x} = \frac{1}{r} \frac{\partial}{\partial r} \left[r(k + \sigma C_p \epsilon_c) \right] \frac{\partial t}{\partial r} \qquad (1)$$

The assumptions and restrictions on this equation are discussed in the following section. The solution is found for fully developed velocity profile and a particular wall-temperature distribution, the constant wall-temperature case; i.e., the case in which the wall temperature takes a discontinuous jump and then remains constant. This solution can then be used to solve the equation for any wall-temperature distribution by the methods explained by Tribus and Klein (59).

The velocity, u, and the eddy conductivity ϵ_c, that appear in equation (1) are functions of radius, and the form of the functions must be determined before the equation can be solved. Velocity distribution has been experimentally determined by many authors and is sufficiently well-known for purposes of solving (1). The eddy conductivity has been reported for the flow of mercury in a pipe by Isakoff and Drew (17) and for the flow of air between parallel plates by Corcoran, et al. (7). There is a wide difference between their results that can be attributed to marked differences in the physical properties of air and mercury and

to the difference in the flow geometry. In order to determine with more assurance the value of ϵ_c for pipe flow, an apparatus was constructed in which temperature measurements within an air stream could be measured downstream from a sharp jump in wall temperature. Values of ϵ_c were computed from these measurements, and these values were used in conjunction with the analysis of Jenkins (19) for the solution of equation (1).

The equation was solved with the aid of an electronic analog computer, and the results are presented as the first three terms of an infinite series. The results cover Reynolds numbers from about 7,000 to 700,000 and Prandtl numbers from 0 to 7.5. It is shown that the results are of particular interest in the low Prandtl number or liquid metal region because wall-temperature distribution has the most marked effect on heat transfer and temperature distribution in that region.

II. MATHEMATICAL METHODS AND PREVIOUS WORK

As stated in the Introduction, the determination of heat flux and temperature distribution can be accomplished by solving the partial differential equation or equations that govern the transfer of energy in the system concerned. The system of concern here is that of a fluid of constant physical properties in turbulent flow in a smooth pipe, for which the energy equation (1) may also be written:

$$u \frac{\partial t}{\partial x} = \frac{1}{r} \frac{\partial}{\partial r} \left[r \left(\frac{\nu}{Pr} + \epsilon_c \right) \frac{\partial t}{\partial r} \right] \tag{2}$$

The system satisfying this equation is subject to the following restriction:

1. Fluid properties are constant.
2. Mean velocity in axial direction is independent of angular position.
3. Mean radial velocity is zero.
4. Mean temperature at any radius does not vary with time or axial position.
5. Frictional dissipation of energy is negligible.
6. The molecular thermal diffusivity, ν/Pr, may be directly added to the eddy diffusivity or eddy conductivity, ϵ_c.
7. Axial diffusion is negligible with respect to bulk transport of energy in the x direction.

The last assumption would lead to greatest error at low Prandtl and low Reynolds numbers. Deissler (10) checked the assumption at a Prandtl number of 0.01. The ratio of axial conduction to bulk transport was

found to be 0.009 at x/D = 1.1 at a Reynolds number of 13,000. At a Reynolds number of 21,000 the ratio was 0.008 at x/D = 0.8 and 0.002 at x/D = 3.1. The assumption, therefore, appears to be a good one.

To solve equation (2) further assumptions are necessary as well as a statement of the boundary conditions. Two hydrodynamic conditions are of primary interest. They are the case of fully developed velocity distribution and that of uniform initial velocity distribution, i.e., the hydronamic and thermal boundary layers begin at the same point. In this paper only the condition of fully developed velocity distribution is considered.

There are also two boundary conditions of particular interest, constant or uniform wall temperature and uniform wall-heat flux. The case of uniform wall temperature is considered here because, since equation (2) is linear, the solution to that problem can be easily used to solve not only the case of an arbitrary wall-temperature distribution, but also the case of arbitrary wall-heat flux (57). As shown later, however, calculations for the later are of limited accuracy. Equation (2) has been solved for special cases, and these are discussed later in this section.

The uniform wall-temperature boundary condition may be stated as follows: If $t = t(x,r)$,

$$t(x,r) = t_o \qquad x < 0$$

$$t(x,a) = t_w \qquad x > 0$$

$$t(0,r) = t_o \qquad r \neq a$$

To solve the equation it is convenient first to render it dimensionless by use of the following definitions:

$$r_* = \frac{r}{a} = \frac{2r}{D}$$

$$f(r_*) = \frac{u}{u_{av}}$$

$$x_* = \frac{2x}{RePrD} = \beta x$$

$$\theta(x_*, r_*) = \frac{t - t_w}{t_o - t_w}$$

$$g(r_*) = \frac{\nu/Pr + \epsilon_c}{\nu/Pr}$$

Substitution of the above values into (1) yields

$$f \frac{\partial \theta}{\partial r_*} = \frac{2}{r_*} \frac{\partial}{\partial r_*} \left[r_* g \frac{\partial \theta}{\partial r_*} \right] \tag{3}$$

with boundary conditions

$$\theta(x_*, r_*) = 1 \qquad x_* < 0$$

$$\theta(x_*, 1) = 0 \qquad x_* > 0$$

$$\theta(0, r_*) = 1 \qquad r_* \neq 1$$

The variables can be separated by assuming a solution of the form

$$\theta = X(x_*)R(r_*)$$

and the solution is then

$$\theta = \sum_{n=0}^{\infty} C_n R_n e^{-\lambda_n^2 x_*} \tag{4}$$

in which $R_n(r_*)$ satisfies

$$\frac{d}{dr_*} \left[r_* g R_n' \right] + \lambda_n^2 \frac{f}{2} r_* R_n = 0 \tag{5}$$

with the boundary conditions

$$R_n(1) = 0$$

$$R_n(0) = 1$$

$$q(x) = k\left(\frac{\partial t}{\partial r}\right)_{r=a} = \frac{-4k(t_o-t_w)}{D} \sum A_n e^{-\lambda_n^2 x_*} \qquad (6)$$

in which

$$A_n = -\frac{C_n R_n(1)}{2}$$

The equations are presented in the above form in order to agree with the laminar flow case in Jakob (18) and Sellars, Tribus and Klein (51).

Equation (5) with its boundary conditions falls into a well-known class of differential equations called Sturm-Liouville systems. See, for example, Churchill (6). From the theory of these systems it is known that the solution to (5) exists and that it is in the form of an infinite series of eigenfunctions, R_n, each corresponding to a discrete value of the λ_n, the eigenvalues. It is also known that the functions R_n form a complete, orthogonal set in the region $0 < r_* < 1$. From the orthogonality property of the functions the coefficients C_n are easily shown to be given by

$$C_n = \frac{\int_o^1 f r_* R_n dr_*}{\int_o^1 f r_* R_n^2 dr_*} \qquad (7)$$

The forms of the functions $f(r_*)$ and $g(r_*)$ are too complicated to enable λ_n and R_n to be found by other than some numerical method. They are found here with the aid of an electronic analog computer in which $f(r_*)$ and $g(r_*)$ are formed by a function generator.

These two functions are related as first postulated by Reynolds (43) and as explained, for example, by von Karman (59). Briefly, the argument is as follows: By definition

$$\frac{\tau_w}{\rho} = \nu\left(\frac{\partial u}{\partial y}\right)_{y=o} \tag{8}$$

and in laminar flow

$$\frac{\tau}{\rho} = \nu \frac{\partial u}{\partial y} \tag{9}$$

In turbulent flow an equation of the same form is often used, and it may be thought of as the defining equation of ϵ_ν, the eddy diffusivity for momentum or eddy viscosity.

$$\frac{\tau}{\rho} = (\nu + \epsilon_\nu) \frac{\partial u}{\partial y} \tag{10}$$

It is also easily shown that

$$\frac{\tau}{\tau_w} = \frac{r}{a} \tag{11}$$

Equations (10) and (11) may be combined to yield

$$\epsilon_\nu = \frac{\left(\frac{\tau_w}{\rho}\right)\frac{r}{a}}{\frac{\partial u}{\partial y}} - \nu \tag{12}$$

One may also define

$$\epsilon_c = \alpha\epsilon_\nu \tag{13}$$

Thus

$$g(r_*) = 1 + Pr\,\frac{\epsilon_c}{\nu} = 1 + \alpha Pr\,\frac{\epsilon_\nu}{\nu} \tag{14}$$

which when combined with (8) and (12) yields

$$g(r_*) = 1 + \alpha Pr\left[\frac{\left(\frac{\partial u}{\partial y}\right)_{y=0} r_*}{\frac{\partial u}{\partial y}} - 1\right] \qquad (15)$$

From equation (15) it can be understood why small errors in the velocity distribution can cause large errors in $g(r_*)$. Small errors in point velocity will cause much larger errors in the derivative of the velocity. Close to the wall, where the velocity distribution is difficult to determine with accuracy, the resulting error in $g(r_*)$ is greatly masked by the added 1 (corresponding to kinematic viscosity). At high Prandtl numbers, however, the errors in $g(r_*)$ are greatly magnified. This point has been emphasized by other authors (9,19).

Another difficulty in evaluating $g(r_*)$ is a knowledge of the proper value of α, the ratio of eddy diffusivities. Reynolds (43) suggested that $\alpha = 1$, a statement of the idea that heat and momentum are transferred by exactly the same mechanism. Others, notably Prandtl (41), have given firmer mathematical foundation for these mechanistic ideas of turbulence. The model he used was that of a turbulent eddy which traveled from one layer of fluid to another of different velocity or temperature. The eddy was postulated to retain the mean velocity and temperature of the original layer during its flight and to dissipate them into the second layer when it arrived there. Jenkins (19) proposed a modification of this mixing-length theory in which he supposed that an eddy can lose some of its momentum or heat during the time of its travel over the mixing length. This analysis leads to a dependency of α upon physical properties and violence of turbulence, which is not the case with Prandtl's original theory. Jenkins' theory predicts that α will approach unity as turbulence increases, a trend which is clearly indicated

by the experimental work of Isakoff and Drew (17), Corcoran, et al. (7), and the present investigation. The theory also predicts that α should decrease with decreasing Prandtl number, and this trend is indicated by a comparison of the results of Isakoff and Drew for mercury with the present results for air, both in pipe flow. The low value of α for low Prandtl numbers is also a quite reasonable explanation of the fact that most experimental values of the Nusselt number for liquid metals are below the predictions of Martinelli (33) and Lyon (31) based on the value of 1 for α.

Although Jenkins' analysis seems to predict the right trends for α, the absolute values are lower than the experimental results of Isakoff and Drew (17), Corcoran, et al. (7), the suggestions of Reichardt (42) based on the experimental work of others, and the present investigation. In view of the above, the value of ϵ_c used to determine $g(r_*)$ for the analog computer was calculated in the following way. The experimental values of this investigation were used for air, and these values were multiplied by Jenkins' prediction for fluids of different Prandtl number. The values found in this way are in fair agreement with the results of Isakoff and Drew for mercury except at Reynolds numbers above about 150,000, in which range Isakoff and Drew's results are higher. For consistency, however, the modified Jenkins' values were used throughout.

The eddy conductivity, ϵ_c, was calculated from the experimental data as follows. Temperature measurements were made far enough downstream such that the temperature distribution was fully developed. In this case $n = 0$ the first term of equation (4) is significant, or

$$\theta = C_o R_o e^{-\lambda_o \bar{x}_*} \tag{16}$$

and $$\frac{d\theta}{dr_*} = C_o R_o' e^{-\lambda_o^2 x_*} \tag{17}$$

Equation (5) can be integrated to give

$$g(r_*) = \frac{\lambda_o^2}{2r_* R_o'} \int_o^{r_*} f r_* R_o dr_* \tag{18}$$

Substitution of (16) and (17) into (18) gives

$$g(r_*) = \frac{\lambda_o^2}{2r_* \frac{dt}{dr_*}} \int_o^{r_*} f r_* (t - t_w) dr_* \tag{19}$$

The value of λ_o^2 is evaluated from the condition at the wall

$$g(1) = 1 = \frac{\lambda_o^2}{2\left(\frac{dt}{dr_*}\right)_{r_*=1}} \int_o^1 f r_* (t - t_w)\, dr_* \tag{20}$$

Equations (19) and (20) permit the calculation of $g(r_*)$ from experimental data on a uniform wall-temperature system.

Extension of the Solution to Arbitrary Wall-Temperature Distribution

Tribus and Klein (57) have shown how the solution for uniform wall temperature can be used to solve the problem of arbitrary wall-temperature distribution. The method employed is simply that of superposition of solutions, which is valid because of the linearity of equation (2). Thus, if the wall temperature, $t_w(x)$, can be approximated by a series of steps, the temperature distribution within the fluid at any point is found for each step as though it were the only one present. The solutions for all the steps are added to form the solution to the problem. In the limit as the steps become smaller, the summation is an integral. Thus, for arbitrary wall-temperature distribution the solution can be represented as a Stieltjes integral,

$$t - t_o = \int_{\xi=o}^{x_*} [1 - \theta(x_*-\xi,r_*)]\ dt_w \qquad (21)$$

This integral is evaluated by substituting $\left(\frac{dt_w}{d\xi}\right)d\xi$ for dt_w whenever t_w is continuous and adding to the resulting Riemann integral the value

$$[1 - \theta(x_*-\xi_i,r_*)][t(\xi_i^+) - t(\xi_i^-)]$$

wherever $t_w(x_*)$ has a discontinuity at ξ_i. The heat flux is given by

$$q(x) = \frac{k}{a}\left(\frac{\partial t}{\partial r_*}\right)_{r_*=1} = -\frac{k}{a}\int_o^{x_*} \frac{d\theta}{dr_*}(x_*-\xi,1)dt_w(\xi) \qquad (22)$$

Examples are given of the use of these formulas in Appendix D.

Velocity Distribution in Turbulent Pipe Flow

Many experimental determinations of velocity distribution in pipes have been made. Three of the most thorough are those of Nikuradse (37), Laufer (26), and Deissler (8). In addition, Reichardt (42), Laufer (25), and Corcoran, et al. (7) among others have made measurements between parallel flat plates, and their results are applicable to pipe flow in the important region close to the wall. The results of these investigations are not in complete agreement, but the discrepancies are not sufficient to cause enough error in $f(r_*)$ to affect the solution of (5) to a significant degree. The differences would be important, however, in the calculation of $g(r_*)$ by analogy. The values actually used for the computation of $f(r_*)$ were those found in the experimental phase of this investigation. They are compared with the results of others in Section IV, Results and Discussion.

Deissler (8,9) and Schlinger, et al. (47) report empirical equations for velocity distribution near the wall that are improvements over the

earlier Prandtl-von Karman lines. Another empirical equation, of which Schlinger's is the limiting case of $B = \infty$, is

$$\frac{\epsilon}{\nu} = Ay^{+2}\left[1-e^{-By^{+2}}\right]$$

or since near the wall

$$\frac{du^+}{dy^+} = \frac{1}{1 + \epsilon/\nu}$$

$$u^+ = \int_o^{y^+} \frac{dy^+}{1 + Ay^{+2}\left[1- \exp\left(-By^{+2}\right)\right]} \qquad (23)$$

By proper evaluation of the constants in the equation both the velocity and the slope of the velocity can be made to agree with the logarithmic law at about $y^+ = 35$, and the resulting velocity is an excellent representation of the data all the way to the wall. As this report was being written, however, Van Driest (58) published an excellent theoretical analysis of turbulent flow near a wall. His equation has a physical basis that the others lack, and it represents the data very well from the wall to nearly the pipe center. It is

$$u^+ = \int_o^{y^+} \frac{2dy^+}{1 + \sqrt{1 + 4K^2y^{+2}[1-\exp(-y^+/A)]^2}} \qquad (24)$$

A comparison of the above results with the present is made in Section IV.

Previous Solutions of the Energy Equation

Previous solutions have been given for equation (2) for special cases, and the papers of particular interest are those of Latzko (24), Martinelli (33), Lyon (31), Seban and Shimazaki (50), Deissler (9), Poppendiek (38,

39,40), Berry (3) and Levy (27). The first four of these authors based their analyses upon the analogy between heat and momentum transfer. That is, they assumed that $\epsilon_c = \alpha\epsilon_\nu$, and their numerical results were calculated with α equal to unity. Generalized velocity distributions were then used to calculate u and ϵ as functions of r_* for the solution of equation (2). These papers deal only with the case of established temperature distribution, and thus shed no light either upon thermal entrance effects or upon how far down the pipe the temperature distribution becomes sufficiently established to produce no appreciable error in the analyses. Deissler, however, in the same paper solved the boundary layer equations in integral form in order to estimate thermal entrance effects.

Martinelli, Lyon, and Deissler all consider the case of uniform heat flux at the wall, for which $\partial t(r)/\partial r$ is a constant. Martinelli further assumed that u is a constant and equal to the mean velocity, whereas Lyon and Deissler retained u as a function of r and integrated the equation numerically. Martinelli and Lyon used the generalized von Karman-Nikuradse velocity distribution (2). Deissler, however, developed an empirical formula for ϵ_ν in which a constant was evaluated from velocity distribution data. The velocity distribution calculated from his equation for ϵ_ν runs about midway between his own data and Laufer's (26) near the wall. The wall-heat fluxes for high Prandtl number fluids calculated by Deissler apparently represent the data better than the other papers.

Seban and Shimazaki (50) studied the case of uniform wall temperature, for which they assumed that after velocity and temperature profiles are fully developed,

$$\frac{\partial}{\partial x}\left(\frac{t_w - t}{t_w - t_{mm}}\right) = 0 \qquad (25)$$

Apparently this assumption was more or less intuitive. At any rate, the authors did not present a defense of the assumption. It can easily be shown, however, that this assumption is a very good one. In fact, it is as good as the assumptions inherent in the basic equation (2). Briefly, the proof is as follows: After entrance effects die out far downstream from a step increase in wall temperature, the temperature distribution is $1 - \theta$ or

$$\frac{t - t_o}{t_w - t_o} = 1 - C_o R_o e^{-\lambda_o^2 \beta x} \tag{26}$$

The mixed mean temperature is given by

$$t_{mm} = \frac{\int_o^a urt\, dr}{\int_o^a urdr} = 2\int_o^1 fr_* t dr_*$$

$$= t_w - 2(t_w - t_o)C_o e^{-\lambda_o^2 \beta x} \int_o^1 fr_* R_o dr_* \tag{27}$$

From (26) and (27)

$$\frac{\partial t}{\partial x} = (t_w - t_o)C_o R_o \beta \lambda_o^2 e^{-\lambda_o^2 \beta x} \tag{28}$$

and

$$\frac{\partial t_{mm}}{\partial x} = 2(t_w - t_o)C_o \beta \lambda_o^2 e^{-\lambda_o^2 \beta x} \int_o^1 fr_* R_o dr_* \tag{29}$$

Also

$$\frac{\partial}{\partial x}\left(\frac{t_w - t}{t_w - t_{mm}}\right) = -\frac{1}{t_w - t_{mm}} \frac{\partial t}{\partial x} + \frac{t_w - t}{(t_w - t_{mm})^2} \frac{\partial t_{mm}}{dx} \tag{30}$$

Substitution of (26), (27), (28), and (29) into (30) confirms (25). The authors solved their equations by an iterative method which, of course, involved considerable numerical calculation. As a result, they present only a limited number of cases, which were sufficient, however, to predict that the ratio of the Nusselt number for uniform wall-heat flux to that of uniform wall temperature could be significantly different from one for fluids of low Prandtl number.

Poppendiek and Harrison (40) review four pipe solutions that are not limited to an established temperature distribution. The first is the slug-flow (uniform-velocity) solution with eddy transfer negligible compared to conduction and uniform wall temperature. This solution is derived in Carslaw and Jaeger (5) and discussed also in McAdams (34). The second solution differs from the above in that the velocity distribution is given by

$$u = B\left(\frac{y}{a}\right)^{1/7}$$

This solution had been previously reported by Poppendiek (38,39). After separating variables, he found a solution in the form of an infinite series of Bessel functions.

The third solution is for uniform velocity, uniform wall temperature, and eddy diffusivity approximated by a straight line from wall to center. This assumption is, of course, increasingly better at decreasing Prandtl number and Reynolds number. This solution is also a series solution of Bessel functions. The solution is not given in the paper because it had not yet been evaluated. The final solution discussed by Poppendiek and Harrison differs from the third in that the boundary condition is that of uniform wall-heat flux instead of temperature. It also had not been evaluated.

Berry (3) discusses equation (2) and its solution by separation of variables similar to the method employed here. He did not solve the equation for any special case, but by making certain assumptions he was able to predict the thermal entry length as a function of Reynolds number and Prandtl number. It was pointed out by Schenk (46), however, that a discrepancy exists between Berry's results and the previously known results in the laminar region. Schenk states that Berry's results are valid only for very low Prandtl number.

Latzko (24) presented a remarkably thorough theoretical investigation for heat transfer in pipes for fluids with a Prandtl number of one. He presents solutions to equation (2) for uniform wall temperature and three entrance conditions: (a) both velocity and temperature distribution are uniform over the cross section; (b) fully developed velocity distribution with uniform temperature distribution; and (c) a case intermediate between the two foregoing ones. Using Prandtl's and von Karman's equations for shearing stress and velocity distribution, he wrote equation (2) as follows:

$$\frac{\partial}{\partial r}\left[r\left(\frac{a^2-r^2}{2a}\right)^{6/7}\frac{\partial\theta}{\partial r}\right] = Kr\left(1-\frac{r}{a}\right)^{1/7}\frac{\partial\theta}{\partial x}$$

in which K is a constant for a given pipe, fluid, and Reynolds number. An approximate solution was obtained by the Ritz method and the calculus of variations. The solution is in the form of the first three terms of an infinite, exponential series.

Levy (27) presents a method by means of which transient heat conduction solutions can be used to determine temperature distribution of fluids flowing in pipes, annuli, and between flat plates. The pipe radius is divided into equal parts, and then the solutions for heat conduction in

composite slabs is modified to permit calculation of the temperature in flowing fluids. The method involves considerable numerical calculations, and these were carried out for a Reynolds number of 10,000 and Prandtl numbers of 0.01, 0.1, 1, and 10. A simplified analysis for high Prandtl number is presented and the use of the slug-flow solution is recommended for fluids of very low Prandtl number.

Deissler has presented another paper (10) which deals with the entrance region only. The boundary layer equations in their integral form are evaluated for a variety of cases. Numerical calculations for the thermal entry length of low Prandtl fluids have also been made by Seban and Shimazaki (49).

Experimental Investigations of Thermal Entry Length

The most extensive experiments directed specifically at the determination of heat transfer in the thermal entrance region are those of Boelter, Young, and Iversen (4) and Hartnett (14). Boelter, et al., measured point heat transfer rates for the flow of air in a pipe at constant wall temperature with a variety of hydrodynamic entrance conditions. They used steam for heating, and so temperature differences were probably large enough to cause fluid property variations to be a complicating factor.

Hartnett studied the flow of water and several oils in an electrically heated tube (uniform heat flux). From heat flux and wall-temperature measurements, he calculated the Nusselt number at various positions downstream from the start of heating. His results with water (Prandtl number 7 to 9) covered Reynolds numbers from 16,900 to 89,200. The oil runs covered Prandtl numbers from 61 to 480 and Reynolds numbers from 1580 to 46,600.

Other authors reporting entry length values are Aladyev (1) for water at uniform wall temperature; Johnson, Hartnett, and Clabaugh (20) for lead-bismuth eutectic at uniform heat flux; and Hoffman (37) for molten sodium hydroxide at uniform heat flux.

Physical Properties of Air

For calculations from the experimental data, it was necessary to know the values of the density, viscosity, heat capacity at constant pressure, and thermal conductivity of dry air at atmospheric pressure and temperatures from 80°F to 100°F. The density was calculated from the perfect gas law and the other values were taken from the literature. There are no significant discrepancies in the literature about the values of the viscosity or heat capacity, and they were taken from the compilation of Tribus and Boelter (56). There are considerable differences in the reported thermal conductivity, however, and so a search was made for articles containing original experimental data. The articles used in the determination of k are those of Eucken (11), Stops (53), Taylor and Johnson (54), Keys and Sandell (21), and Rothman (45). The value of k chosen on the basis of these is 0.0152 Btu/hr ft °F at 90°F, and 0.0154 at 100°F. These values are almost precisely those of Rothman and Eucken. They are about 1.3% below the values employed by Córcoran, et al. (7).

III. APPARATUS AND EXPERIMENTAL PROCEDURE

In this section is a description of the heat transfer apparatus and a brief description of the analog computer equipment. Further details of the apparatus are contained in Appendix A and of the experimental and calculation procedures in Appendix B.

Heat-Transfer Apparatus

A photograph of the experimental apparatus is shown in Figure 1 and a flow diagram in Figure 2. Air from a centrifugal blower was passed through a heat exchanger (cooler) and into the entrance section. This section consisted of a small electric heater, baffles, straightening vanes, two screens, a 15° reduction from 4 to 1-1/2 inches, 46 diameters of copper pipe, and 4 diameters of Lucite pipe. The entire entrance section was insulated with 1 in. of 85% magnesia and 3 in. of glass wool. From the entrance section the air passed into the test section and then through a silica gel drier and a heat exchanger before returning to the centrifugal blower. The closed system was used to assure dry air.

The test section consisted of five pieces of 1-1/2 in. copper pipe with 0.20 in. wall thickness followed by a 6-inch length of Lucite pipe. The lengths of the pieces were 0.60, 8, 1.00, 36, and 1.00 in., respectively. They were separated from each other by gaskets of polyethylene 0.01 in. thick. Three small pins of Chromel were placed in carefully drilled holes in the edges of each piece so that the pieces would stay in position when pushed together and held by bolts through the flanges on the larger pieces. Details of this construction are described in Appendix A.

In order to remove the small steps at the junctions of sections

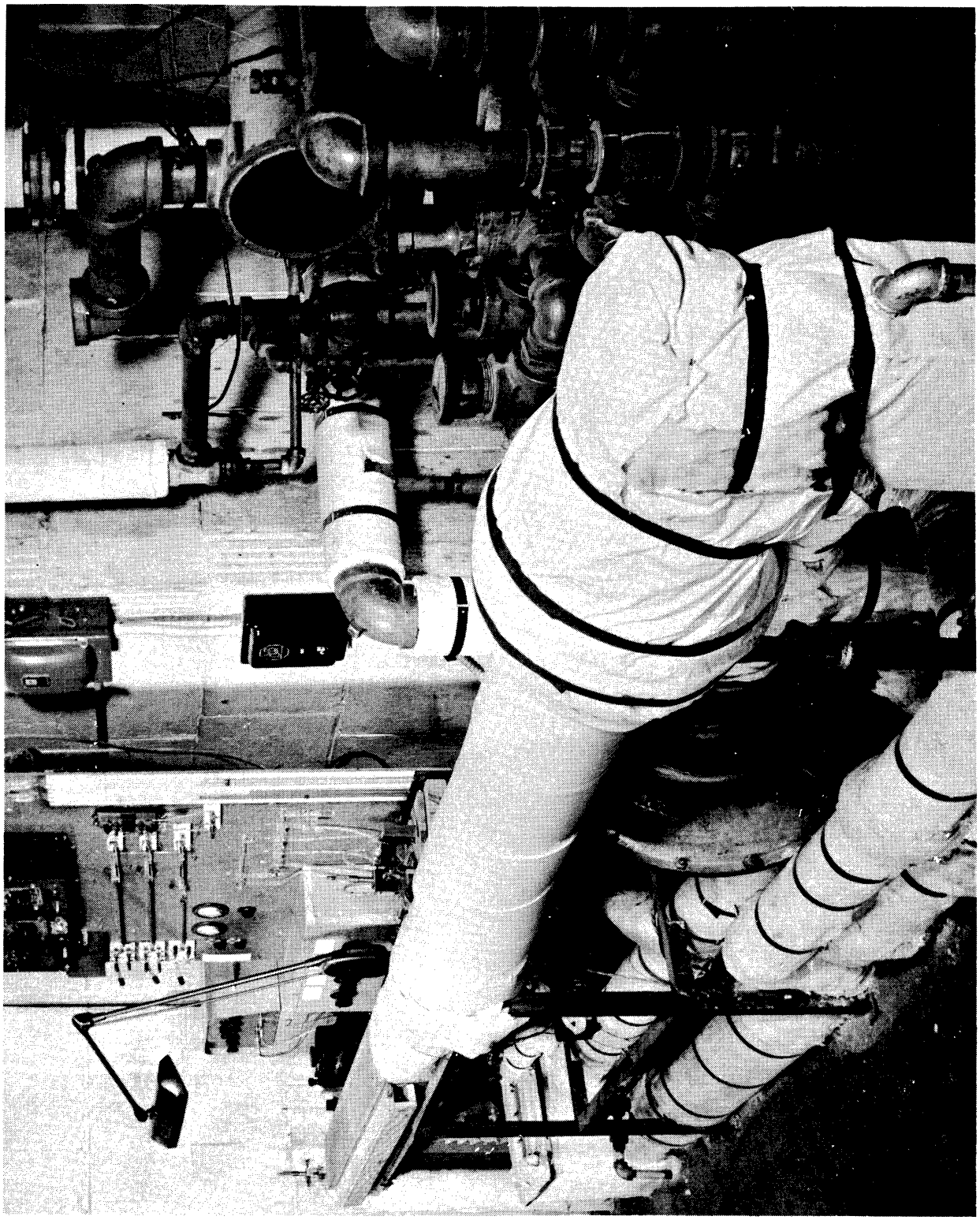

Figure 1. Experimental Apparatus.

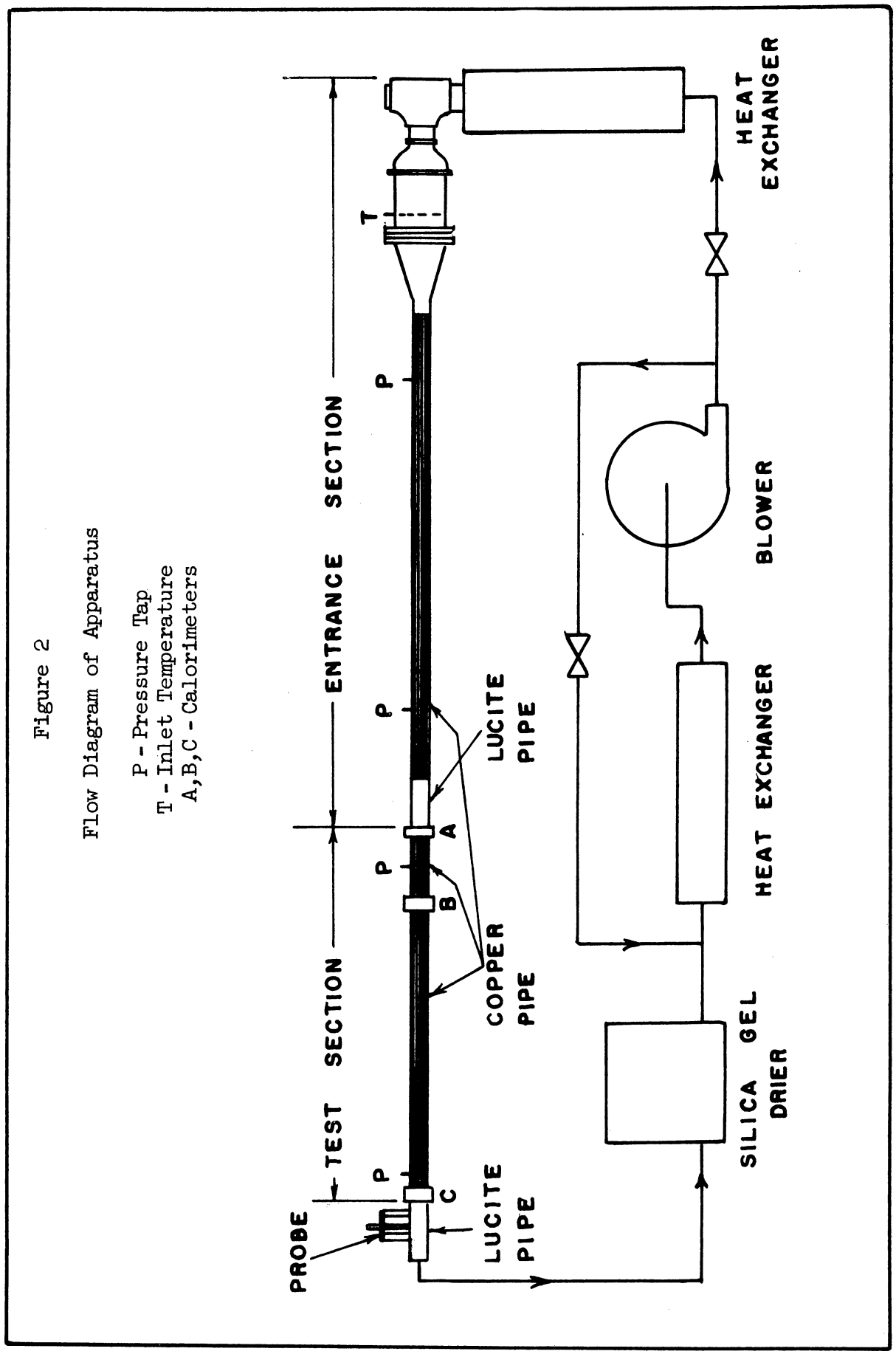

Figure 2

Flow Diagram of Apparatus

P - Pressure Tap
T - Inlet Temperature
A,B,C - Calorimeters

(eccentricity was estimated to be no greater than 0.002 in.), the entire test section and part of the entrance section were bolted together and honed from 1.496 in. to 1.504 in. in diameter. After honing, the wall roughness was about 30 microinches (36).

All of the pipe sections were wound with Chromel ribbon either 1/8, 3/16, or 1/4 in. wide and were heated electrically. At no place was the spacing between windings greater than 1/8 in. except at the flanges which separated them by about 1/4 in. The flanges were of Monel metal 1/8 to 3/16 in. thick, and were heated slightly at their edges. Taps were provided at every second winding so that some or all of the heating current could be by-passed in order to control the wall temperature distribution. For the above geometry and heat transfer to air at Reynolds numbers in the range employed (less than 80,000), calculations show that temperature ripples on the inside surface of the copper pipe were negligible, i.e., less than 0.2% of the difference between the mixed-mean temperature of the air and the wall temperature.

The three small segments of pipe served as calorimeters for measuring local heat flux. Each was surrounded by a guard heater whose construction is described in detail in Appendix A.

Forty-three thermocouples were located at various points in the equipment including one or two at either edge of each segment and one every two inches along the one generator line of the pipe. They were made of 36-gage Chromel-Constantan wire and were placed in holes 0.020 in. in diameter and drilled to within 0.040 in. of the inside surface. Since the temperature drop across the copper wall was relatively small (about 0.18°F for the highest heat fluxes), thermocouple location was not critical. A Leeds and Northrup K-2 potentiometer was used to measure the E.M.F.'s with

a precision of about 0.03°F. The potentiometer error signal was sent to a Liston-Becker Model 14 D.C. amplifier, whose output was fed to a Brown Electronik potentiometer. This system provided extreme sensitivity and rapid response. All thermocouples were calibrated in place under isothermal conditions against a Bureau of Standards thermometer.

Pressure measurements were made at two positions in the test section and two in the entrance section. The tap holes were 0.030 in. in diameter and were made free from burrs by the honing. Pressure differences over 0.80 in. of water were made on a straight manometer containing Meriam Red Oil (sp. gr. = 0.82 g/cc, calibrated), whereas for smaller differences a micromanometer was used. The micromanometer reads directly in thousandths of an inch of Meriam Red Oil and is described by Knudsen (22).

Direct current supplied by two storage batteries and a battery charger was passed through the windings of each calorimeter and adjustable, external, control resistances. Voltage drop across the windings was taken with a voltmeter, and current was determined by measuring the voltage drop across a shunt with a small potentiometer. Both meters and the shunt were calibrated. Alternating current controlled by Variacs was used for heating the 8-in. and 36-in. sections.

The entire test section was surrounded by a wooden box which was then filled with vermiculite insulation.

Velocity profiles were made with platinum hot-wire anemometers, which also served as resistance thermometers for measuring temperature profiles. The traversing mechanism was located in the Lucite section just beyond the last calorimeter. The thermometer itself was supported on needles which projected upstream so that temperature profiles could be made within

the calorimeter. The distance from the wire to the wall was determined by electrical contact, the distance from the wire center to the point of contact having been measured by microscopic observation. The distance traveled was read on a micrometer barrel whose smallest division was 0.001 in. The reproducibility of contact was ± 0.0002 in. and the overall accuracy of location from the wall was about ± 0.0005 in.

The length of the platinum anemometers and thermometers averaged about 0.038 in., so the difference in distance to the wall between the ends and the center of the wire was negligible. The diameter of the platinum wire was about 0.00016 in. and that of the supporting silver wires was about 0.003 in. These silver wires protruded in a small arc upstream from the needles in order to minimize flow disturbance. All temperature runs were made with such wire, but some of the velocity profiles were made with 0.0002-in. platinum and tungsten wire. Tungsten wire was found to be unsatisfactory for temperature measurement. The construction of the probe and needle tips is described in more detail in Appendix A.

For measuring velocity, a constant current of 40 to 60 milliamps supplied from a 24-volt storage battery was passed through the wire. The voltage drop across the probe was measured by the K-2 potentiometer, and a small correction was applied for voltage drop in the lead wires. Thermal E.M.F.'s in the circuit were less than one microvolt, which was about the limit of reproducibility of the readings. Current was determined by measuring the voltage drop across a standard 10-ohm, temperature-compensated resistance with the K-2 potentiometer. The probe was calibrated at the center of the tube with a carefully made pitot tube. The response of such wires is proportional to the square root of the velocity, so a

correction had to be applied wherever there were large fluctuations in velocity. The correction was never more than 5%. See Appendix B for details of this calculation. Average velocity in the pipe was determined by integration of velocity profiles. The accuracy of velocity measurements was about 0.5% at moderate velocities to 5% at 7 ft/sec.

Temperature measurements were made by passing 1.5 milliamps through the wire. Corrections were applied for electric and aerodynamic heating of the wire and are discussed in Appendix B. The maximum correction was about 0.5°F. The absolute accuracy of measurements is estimated to be about ± 0.2°F, but temperature differences were made with a precision of about ± 0.05°F. The probe was calibrated before and after each run against a thermocouple in the center of the tube under adiabatic conditions.

All temperature and most velocity traverses were made in the last calorimeter at the end of the test section 31 diameters downstream from the thermal entrance and 81 diameters from the hydrodynamic entrance. After all temperature runs had been completed, the test section was dismantled and several velocity traverses were made within the first calorimeter 50 diameters from the entrance.

The procedure for a heat-transfer run was as follows. The blower and heat exchangers were given about an hour to approach thermal equilibrium before the current in the test section was turned on. The current for each of the five pipe segments and resistances across the winding taps were adjusted until the entire test section was uniform within ± 0.1°F and 15 to 20°F above the entering air temperature. The procedure was very painstaking and sometimes took over 15 hours. As soon as this condition was reached, a temperature profile was taken. The measurements consumed about twenty minutes, after which all thermocouples were read

again. The inlet air temperature was kept constant by slight manual adjustment of the wire heater in the entrance section and was always within 3°F of room temperature.

Analog Computer Equipment

The analog circuit for the solution of equation (2) is shown in the following sketch.

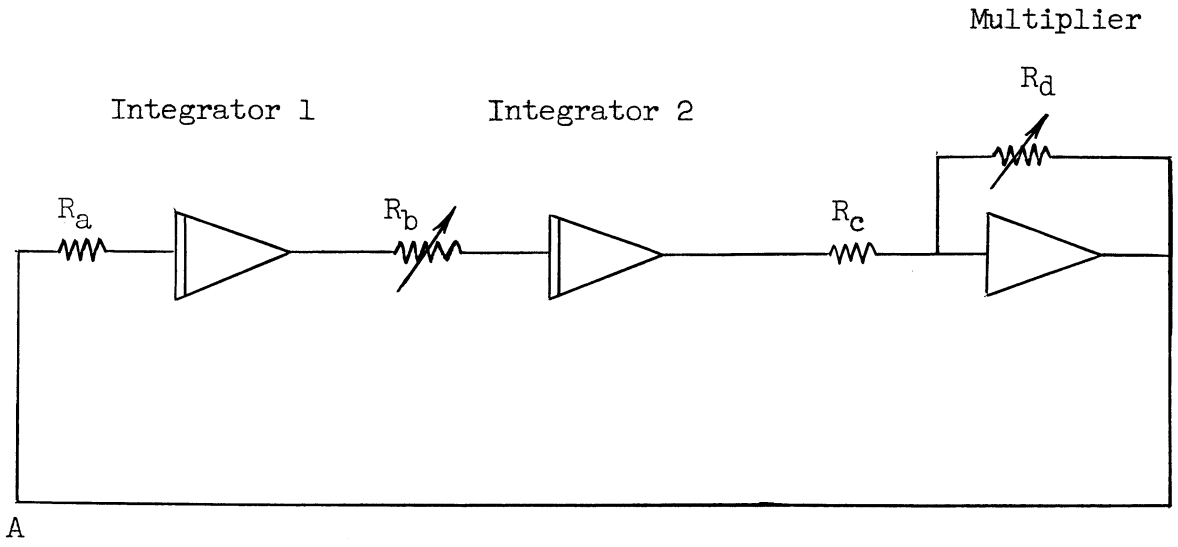

$$R_a = 2/\lambda_n^2$$

$$R_b = r_* g(r_*)$$

$$R_c = 1$$

$$R_d = r_* f(r_*)$$

In this computer time represents the independent variable, r_*, and so it is necessary that R_b and R_d change with time. This was done by means of a device which approximates the functions by twenty-four steps, each with a one-second duration. It is described in detail, as are the other parts of the computer by Hagelbarger, Howe and Howe (13).

That the above circuit will solve equation (5) is easily seen. At the point marked A, the voltage (dependent variable) is considered to be

$$\frac{2}{\lambda_n^2} \frac{d}{dr_*} \left[r_* g R_n' \right]$$

This quantity is then divided by $R_a = 2/\lambda_n^2$ and integrated. The result at the output of Integrator 1 is $-r_* g R_n'$. (Integrators and multipliers always change sign.) This voltage is then divided by $R_b = r_* g$ and integrated to form R_n at the output of Integrator 2. After multiplying by $R_d = r_* f$ and changing sign, the result is $-r_* f R_n$. But according to equation (2)

$$-r_* f R_n = \frac{2}{\lambda_n^2} \frac{d}{dr_*} \left[r_* g R_n' \right]$$

and so the circuit satisfies the equation.

Several measurements in this circuit are needed to complete the solution of the problem. First, the eigenfunctions R_n and the eigenvalues λ_n are found by varying R_a until R_n passes through zero at $r_* = 1$. $R_n'(1)$, used to evaluate A_n, can then be measured directly from the output of Integrator 1 at the end of the solution.

The coefficients C_n were evaluated by use of equation (7). For this purpose the output of the multiplier was integrated once by a third integrator to form

$$\int_0^1 f r_* R_n dr_*$$

The integral

$$\int_0^1 f r_* R_n^2 dr_*$$

was formed by multiplying R_n by $f r_* R_n$ with a servomultiplier and integrating the result.

At moderate and higher values of the product RePr, which is known as the Peclet number, the gradient of $g(r_*)$ is very steep near the wall. In

this case $g(r_*)$ cannot be closely approximated by only twenty-four steps. This difficulty was solved by changing the time constant of both integrators simultaneously during a run. In this way, for example, fourteen steps could be used for 90% of the radius and the remaining ten steps for the last 10% of the radius. The decrease in mumber of steps for the inner 90% of the radius would have little effect because of relative flatness of the temperature profile there.

In some of the runs the time constant was changed twice. The extreme example was the run for Pr = 7.5, Re = 500,000. In this case ten steps were employed for $0 < r_* < 0.997$, eight steps for $0.997 < r_* < 0.9992$, and six steps for $0.9998 < r_* < 1$.

To test the analog equipment and procedure, two known solutions were run. Five eigenfunctions and constants were calculated for the laminar case (Graetz solution) and three were found for the slug-flow case. Turbulent flow solutions were run for the combination of parameters shown in the following table.

TABLE I

NUMBER OF EIGENFUNCTIONS

CALCULATED FOR PARAMETERS SHOWN

Reynolds Number	Prandtl Number 0	.01	.024	.10	.718	7.5
8,000	3	3	3	3	3	2
14,500		3	3	3	3	2
24,000	3	3	3	3	3	
38,500		3	3	3	3	2
80,300	3	3	3	3	3	2
150,000		3	3	3	3	2
500,000	3	3	3	3	3	2

IV. RESULTS AND DISCUSSION OF RESULTS

The important experimental and analog computer results are given in this section and discussed in turn. The experimental heat transfer results are essentially a means to an end, but some of the findings are worthwhile discussing in themselves.

Velocity Distribution

In an excellent review of Nikuradse's data by Ross (44), the author shows that Nikuradse's data (37) begin to deviate from the logarithmic law at $y_* = 0.15$. In other words, for the region $0 < r_* < .85$, u^+ is not a single-valued function of y^+ but depends also upon Reynolds number. For the inner 85% of the pipe radius, they suggest the data be correlated by plotting $(u_{max} - u)/U_\tau$ vs. y_*. This suggestion has been followed here. Figure 3 shows the velocity data for $y_* < 0.15$ plotted as u^+ vs. log y^+. One set of points for the entire radius has been plotted to illustrate the deviation mentioned above. It is probably this deviation that causes variance in the constants of the equations for velocity distribution in the turbulent cone. For example, Ross states that if Nikuradse's points are plotted for $y^+ > 30$, $y_* < 0.15$, the best empirical fit is given by

$$u^+ = 5.6 + \frac{1}{K} \ln y^+$$

with $K = 0.41$. Deissler (8), on the other hand fitted one line for the entire region $y^+ > 30$ and for a relatively limited range of Reynolds numbers. Thus the high points near the center resulted in a slightly steeper line represented by $K = 0.36$. Van Driest used the value 0.40, and it is this value that was used here for the calculation of eddy viscosity discussed later.

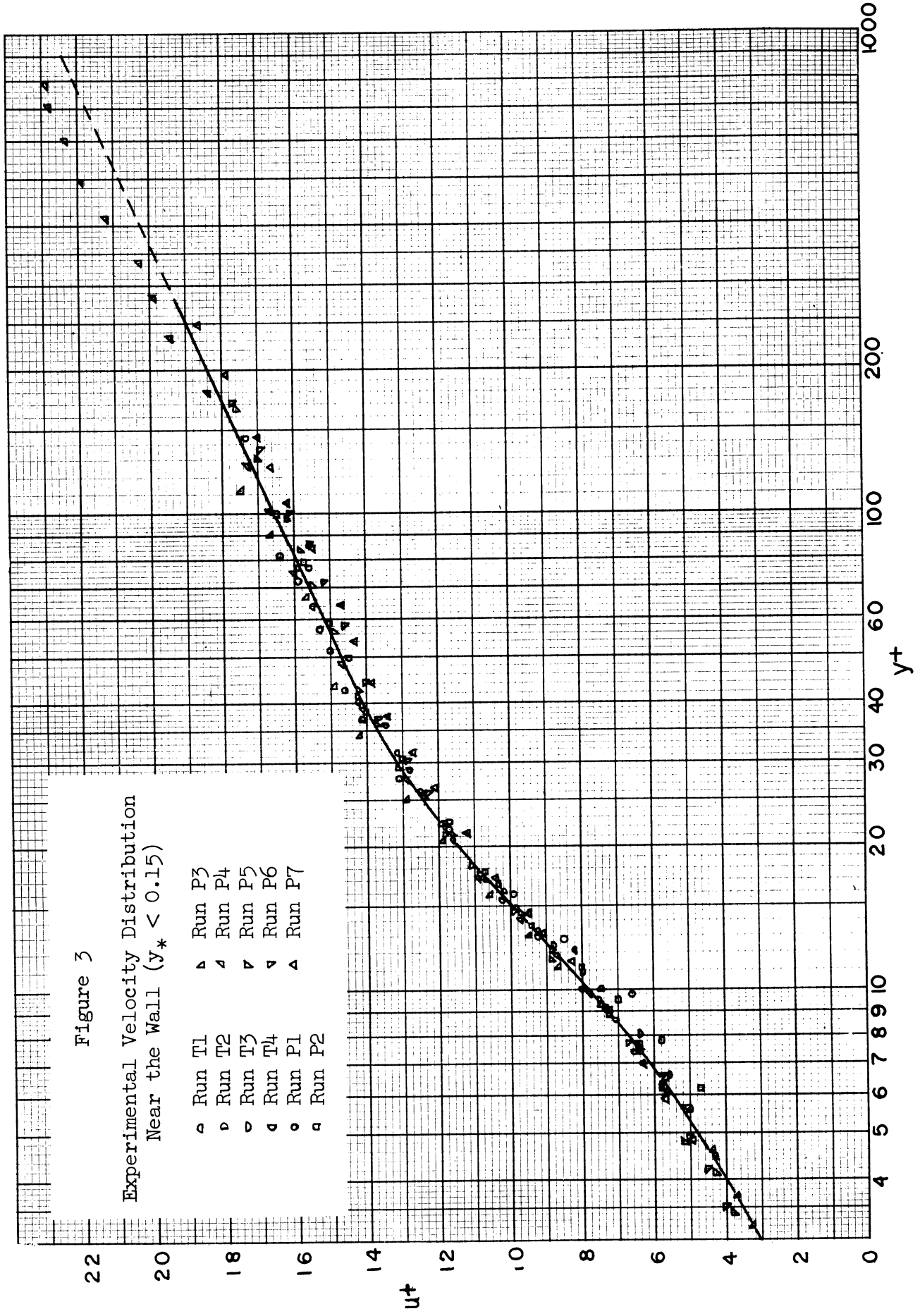
Figure 3
Experimental Velocity Distribution
Near the Wall ($y_* < 0.15$)
Run T1
Run T2
Run T3
Run T4
Run P1
Run P2
Run P3
Run P4
Run P5
Run P6
Run P7
u+
y+
0
2
4
6
8
10
12
14
16
18
20
22
4
5
6
7
8
9
10
20
30
40
60
100
200
1000

Figure 4 shows the results of several investigations including the present. Each of the lines is a mean through the data points of the author except the line labeled "Reichardt-Nikuradse," which is a mean line through the points of Nikuradse, Reichardt-Motzfeld, and Reichardt-Schuh as reported by Reichardt (42). All of the lines except Laufer's are in very close agreement. Yet on reading Laufer's report one finds that he took extreme care in his experimental work. He worked in a larger pipe than the others, which means that the boundary layer is thicker but velocities are lower for the same Reynolds number. His report is frequently cited, as for example by Van Driest (58), not only because of the care with which he worked, but also because he reports detailed measurements of the turbulent energy spectrum. Indeed, his report is the most thorough investigation of the hydrodynamics of fully developed pipe flow ever written. Yet this author is forced to conclude that Laufer's data cannot necessarily be considered the best representation of mean velocity near a wall in turbulent pipe flow. It should be mentioned, however, that the equation of Van Driest (58), discussed on page 16, fits Laufer's data better than the others. That is, no combination of the two constants in Van Driest's equation will make the equation fit the other data nearly as well as it fits Laufer's.

Figure 5 is a plot of $(u_{max} - u)/U_\tau$ vs. y_* for the region $y_* > .15$. A mean line is drawn through the points. It should be mentioned that this plot is quite sensitive to error since it involves the difference $u_{max} - u$.

Figure 6 is a comparison of the velocity distribution at the entrance of the test section (after 50 diameters of straight pipe) with that at the

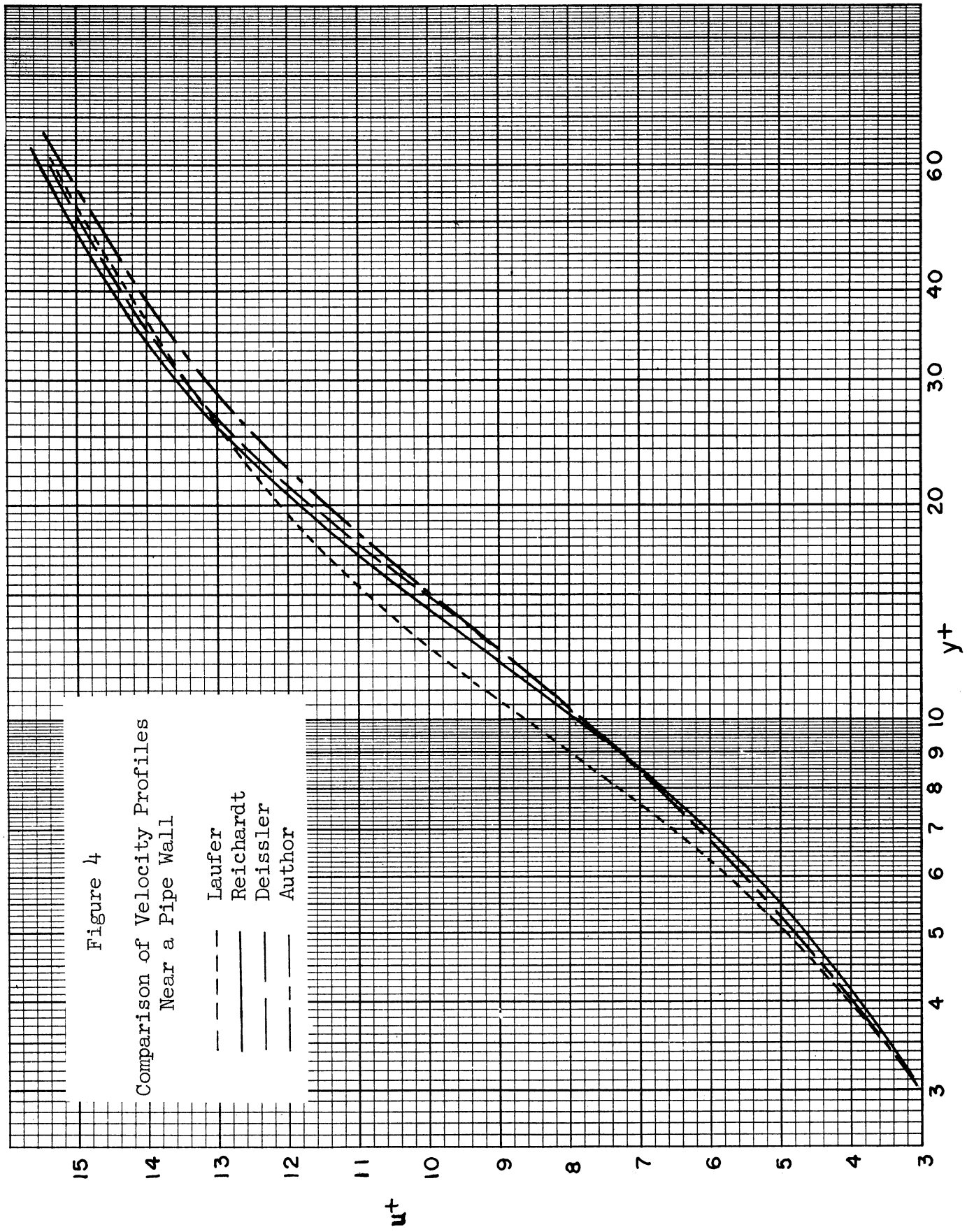
Figure 4
Comparison of Velocity Profiles
Near a Pipe Wall
Laufer
Reichardt
Deissler
Author
u+
y+
3
4
5
6
7
8
9
10
11
12
13
14
15
20
30
40
60

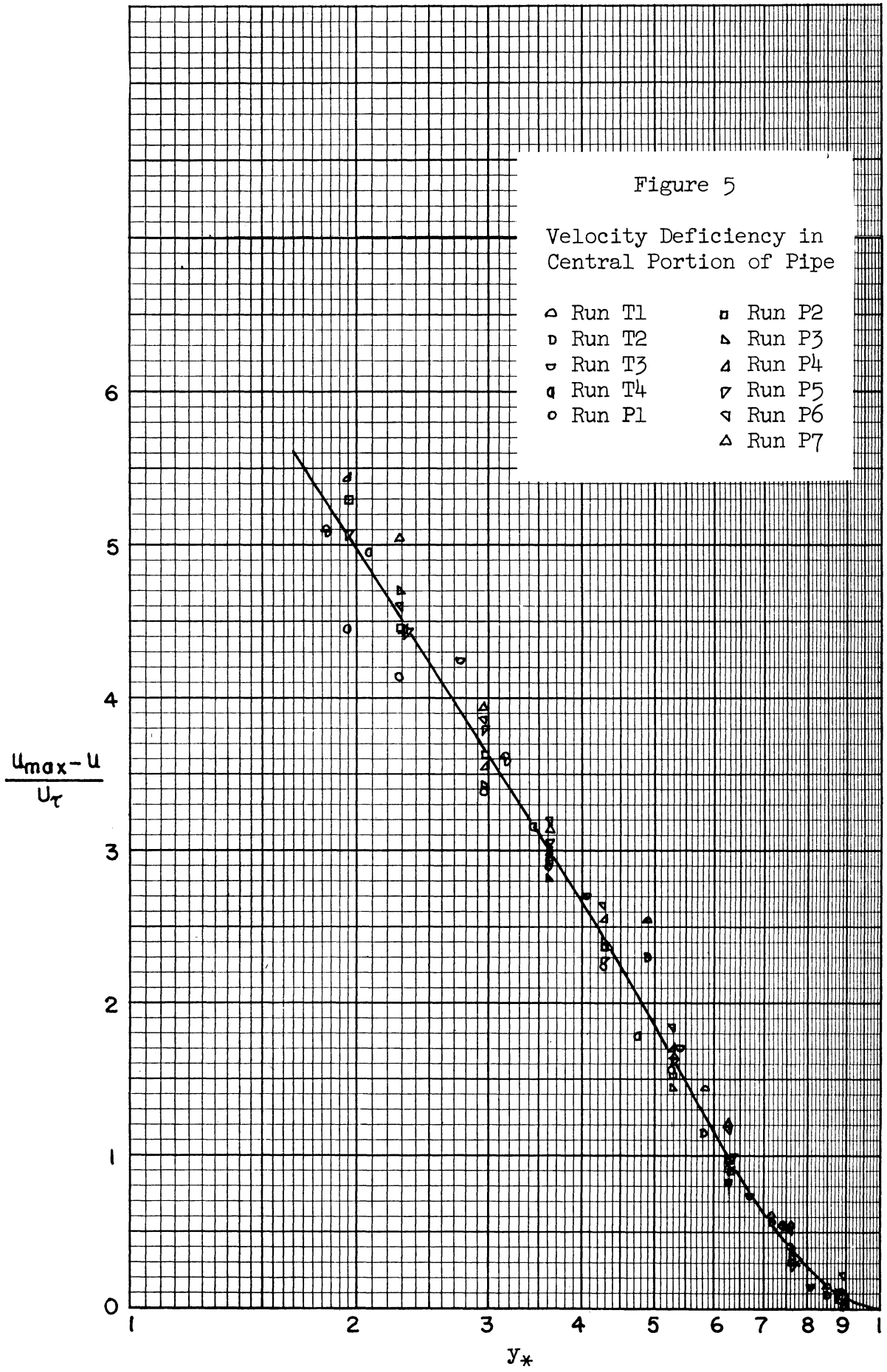
Figure 5
Velocity Deficiency in Central Portion of Pipe
Run T1
Run T2
Run T3
Run T4
Run P1
Run P2
Run P3
Run P4
Run P5
Run P6
Run P7
$\frac{u_{max}-u}{u_\tau}$
y_*
0
1
2
3
4
5
6
7
8
9

Figure 6

Velocity Profiles at Calorimeters A and C
Re = 24,000

– – – Cal. A, after 50 diameters of pipe
——— Cal. C, after 81 diameters of pipe

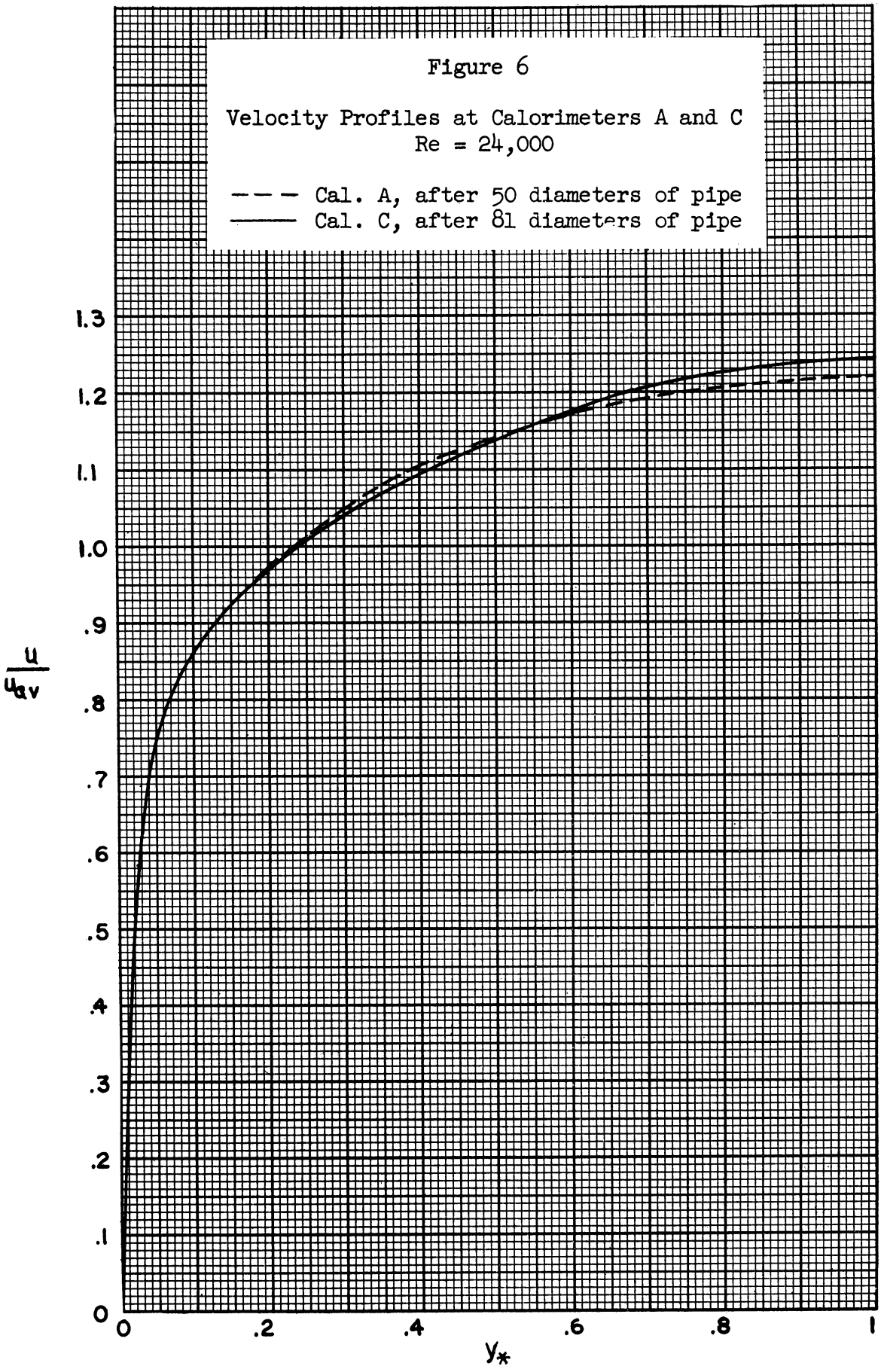

end of the test section (after 81 diameters of straight pipe). The figure shows that at the test section entrance, the velocity distribution was still developing slightly near the center of the pipe, an observation which is in agreement with Deissler (8). For a considerable distance from the wall, however, the velocity distribution had become established. Since this is the most critical region for heat transfer (that is, the region over which most of the temperature drop takes place), little experimental error is introduced by the difference in profiles shown.

One velocity profile was taken following a wall-temperature gradient of about 15°F in a foot of pipe. This profile and other velocity measurements made during heat transfer runs showed no effect of temperature. This was to be expected since temperature differences were relatively small, i.e., less than 20°F.

The ratio of mean to maximum velocity agreed very closely with the data of Nikuradse, being only slightly below his data at Reynolds numbers less than 20,000. Further details are given in Appendix C.

Friction factors were calculated from pressure drop measurements and agreed very closely with the accepted values of Moody (62). There was some scatter in the data at Reynolds numbers below about 15,000, and this was one of the considerations in deciding to take no heat transfer data below this Reynolds number. See Appendix C for details.

Gross Results of Heat-Transfer Runs

Table II gives the important variables and gross results for the heat transfer runs. The heat balances were calculated by determining the heat input in the following two ways: (a) integration of the velocity-temperature profiles at the end of the test section and (b) electrical energy to the heating coils. The latter is believed to be the more inaccurate

TABLE II

SUMMARY OF GROSS VALUES FOR HEAT-TRANSFER RUNS

Run No.	Reynolds Number	Inlet Temp, °F	Wall Temp, °F	Nu at A	Nu at B	Nu at C	Heat Balance, %
5	38,600	79.77	98.30	183	91	94	4.0
5B	38,400	81.01	99.56	183	92	95	6.0
7	23,900	80.15	94.30	141	66	72*	5.4
8	24,000	80.35	100.55	147	67	66	4.0
9	14,800	78.06	97.88	102	45	46	4.0
10	14,200	78.28	98.97	102	45	46	2.7
12	80,500	80.10	92.27	298	164	165	4.4
13	80,100	80.03	92.19	293	163	163	9.1

*Believed to be in error.

Heat balances are 100 $\frac{Q_a - Q_e}{Q_a}$ where Q_e is electrical input and Q_a is heat input to air from temperature-velocity profiles.

for two reasons. First, a correction had to be applied for heat transfer to the surroundings. This correction was determined by heating the test section with no air flow and measuring the heat losses as a function of wall-to-room temperature difference. The correction amounted to 5 - 15%. The second reason probably accounts for more of the error and has to do with the way the input wattage was measured to the 8-in. and 36-in. pipe sections. In order to maintain uniform wall temperature, some of the current at various positions had to be by-passed by shunting resistors across the taps provided on the windings. These resistors were, of course, placed outside of the insulation, and their magnitude was in the range two to fifty times the resistance of the winding shunted. Because of the by-passed current, it was necessary to measure the voltage drop separately across every set of taps to which an external resistor was connected. Input energy to the test section was then computed from these voltages and

the measured resistances of the windings. Unfortunately, however, an accurate but low-impedance A.C. voltmeter was used. This necessitated an elaborate network calculation to determine the heat input for each run. In every case the heat input calculated in this way was lower than that from flow and temperature measurements by the percentage shown in Table II. In this connection, it should be mentioned that several different temperature probes were used in the various runs and that each probe was calibrated before and after each run throughout the range of measurement. As mentioned previously, the absolute accuracy of the probe temperature measurements were about $\pm$ 0.2°F or 1 to 1.5% of the wall-to-inlet temperature differences.

The average Nusselt number of the first 0.6 in. of pipe (L/D = 0.40) is seen to be far higher than tha asymptotic value at Calorimeter C. There are two errors in this measurement that are in opposite directions but whose magnitudes are difficult to assess. The calculated Nusselt number is higher because of some leakage of heat into the adjoining plastic. Because of this leak and the very high initial heat transfer coefficient, however, the upstream edge of the calorimeter was lower in temperature than the downstream edge (by .3 to .5°F, depending on Reynolds number), and the incoming air had already been slightly heated by the plastic. These latter effects caused the Nusselt number to be lower than the case of a discontinuous jump in wall temperature.

The Nusselt number at Calorimeter C was calculated from the measured electrical input and the mean temperature of the air as determined from velocity-temperature profiles. The precision of measurement of the Nusselt number is 2-3% and agrees within this figure with the Dittus-Boelter equation (34).

The Nusselt number at Calorimeter B located between 8.60 and 9.60 inches downstream (L/D = 5.71 to 6.38) is the same as at Calorimeter C within the precision of measurement. The calculated values are actually slightly lower than at C, whereas they should be about 2% higher according to later calculations. The explanation is that the mean temperature at B was calculated from the electrical input up to B. As shown above, however, this calculation was subject to error. Had the calculated electrical input been higher, as the heat balances indicated it should be, the mean temperature of the air would have been higher, thus raising the Nusselt number, i.e.,

$$Nu = \frac{qD}{k(t_w - t_{mm})}$$

The precision of measurement of the Nusselt number at B is about 5%.

Eddy Conductivity Distribution

Eddy conductivities were calculated from the temperature distribution by the equations on page 14. To use these equations, it is necessary to show that the temperature profile is fully established at Calorimeter C, 31 diameters downstream, where all temperature profiles were taken. The constancy of the Nusselt number is some indication of this since it involves the mean temperature. On this basis the data of Boelter, et al. (4) and the analysis of Berry (3) indicate that the profile is established much sooner than 31 diameters. Deissler (10) calculated the growth of the thermal boundary layer, and he reports that the distance necessary for a fully developed temperature distribution increases with Reynolds number and is $18\frac{x}{D}$ for the highest Reynolds number employed here. Finally, temperature measurements at the center of the pipe at Calorimeter C had increased by at the least 15% of the difference between the inlet and wall temperatures.

The differentiation of the temperature profiles was done numerically by the Douglass-Avakian method (52). This method employs a fourth-degree polynomial which is fitted to seven equidistant points by the method of least squares. The actual experimental points were used except where interpolation was necessary because of a change in point spacing along the tube radius.

Figure 7 shows the calculated values of ϵ_c/ν plotted vs. y^+ on semi-log coordinates for the region close to the wall. The solid line is a mean line through the points. The other line is a plot of ϵ_ν/ν calculated from the mean curve of Figure 3. Over the range shown, the ϵ_ν/ν is almost identical to the expression given by Van Driest (58).

Figure 8 shows the calculated values of ϵ_c/ν for the center region of the pipe. There is some evidence of a slight decrease in ϵ_c/ν at the center, but the drop is not as large as that reported by Schlinger, et al. (47), or Corcoran, et al. (7), for uniform flow between flat plates.

The ratio $\alpha = \epsilon_c/\epsilon_\nu$ is plotted in Figure 9 for each of the four Reynolds numbers used. The values of ϵ_ν/ν for the region close to the wall was taken from Figure 7, and the equation of Van Driest (58) was used of the region $y^+ > 40$, $y_* < 0.20$ because the equation fit the present data quite well. The ratio increases near the wall as reported by Corcoran, et al. (7), but then seems to level off again very close to the wall. The calculated values of both ϵ_c and ϵ_ν are, of course, rather inaccurate very near the wall and near the center of the pipe as well.

Analog Computer Results

In Table III are given the eigenvalues and constants for the analog computer solutions of the two cases for which exact solutions are available (5,18,28,51). The values for the first three modes check the known

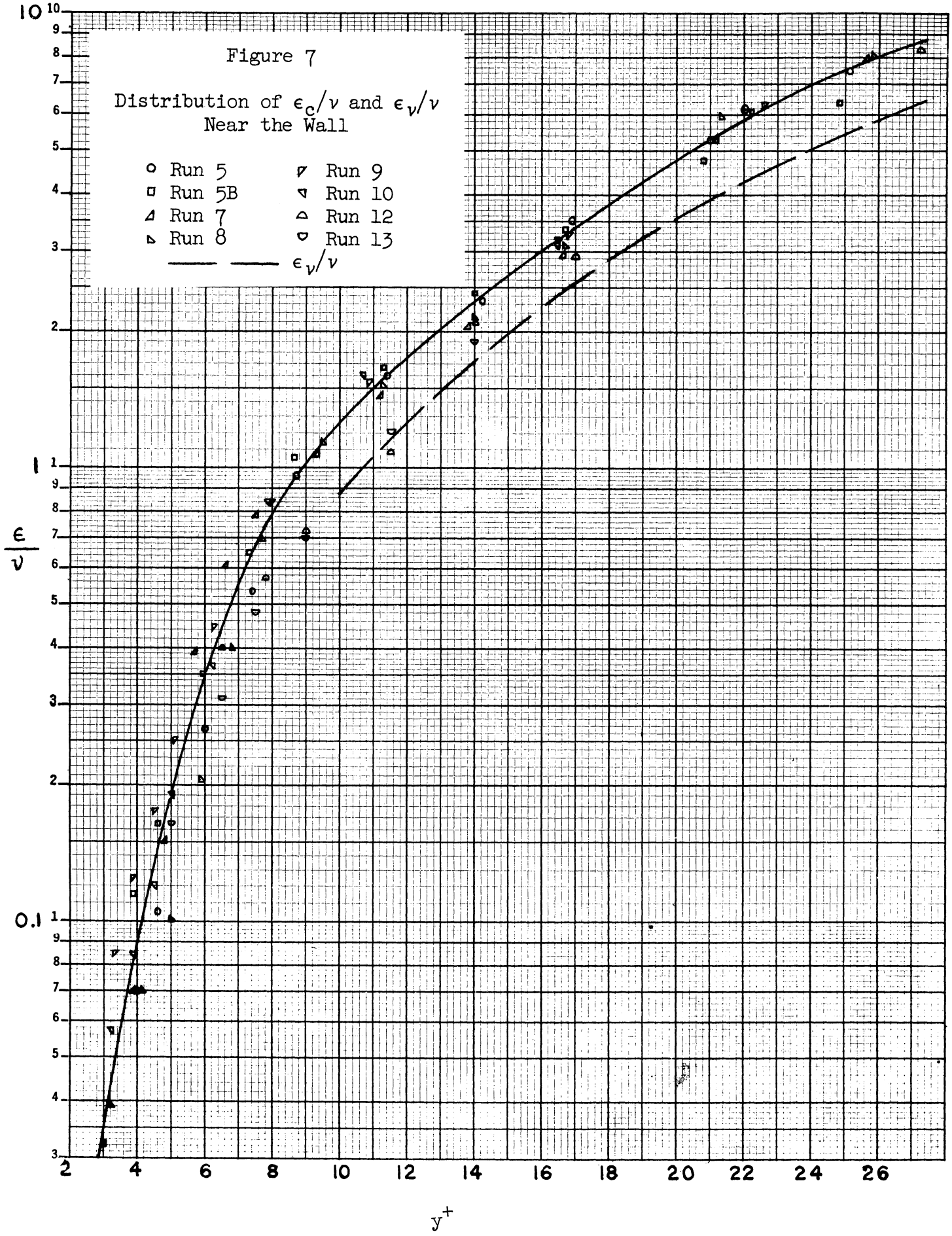
Figure 7
Distribution of ϵ_c/ν and ϵ_ν/ν Near the Wall
Run 5
Run 5B
Run 7
Run 8
Run 9
Run 10
Run 12
Run 13
ϵ_ν/ν
$\frac{\epsilon}{\nu}$
y^+
10
1
0.1
2
4
6
8
10
12
14
16
18
20
22
24
26

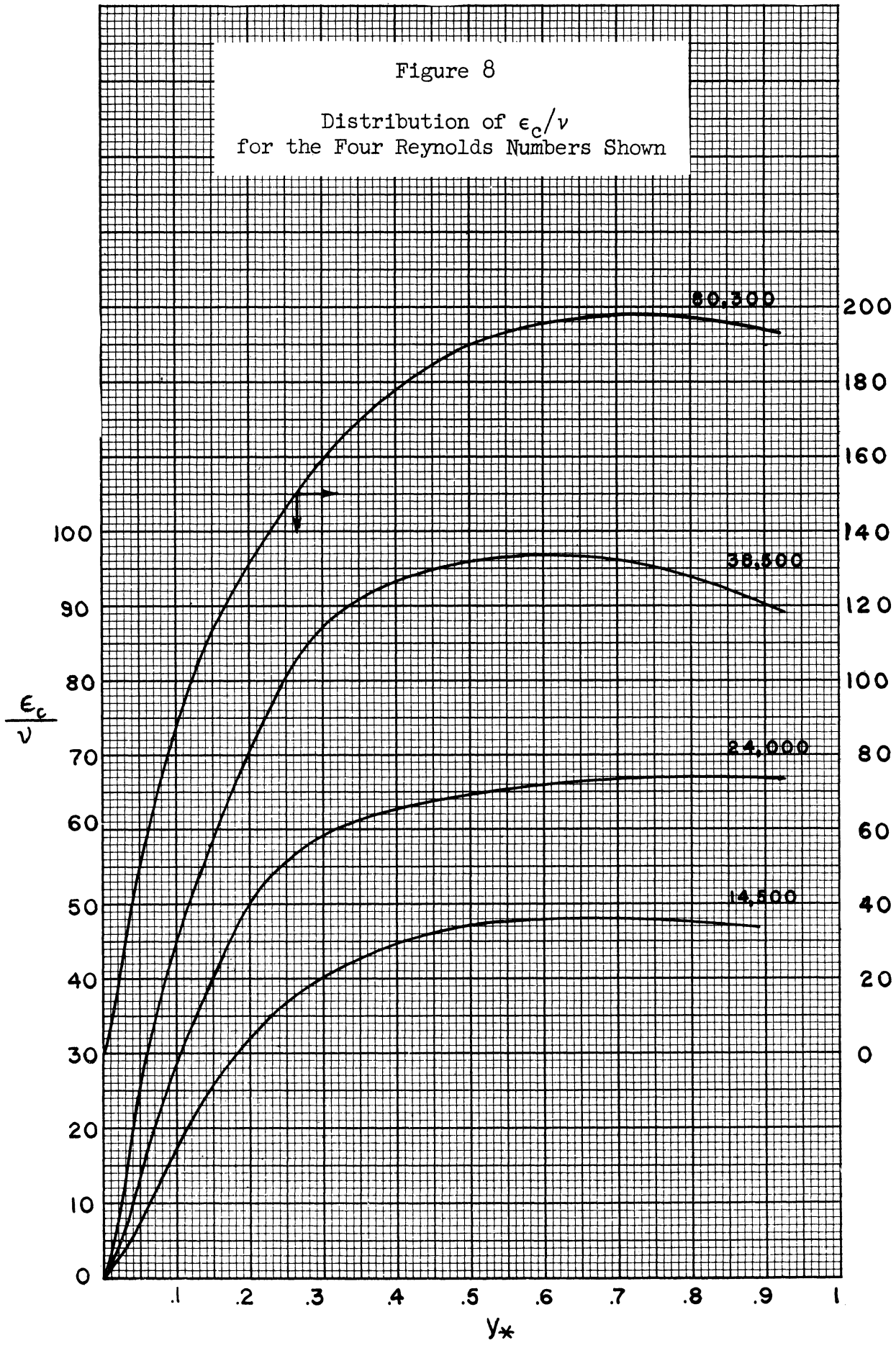

Figure 8

Distribution of ϵ_c/ν
for the Four Reynolds Numbers Shown

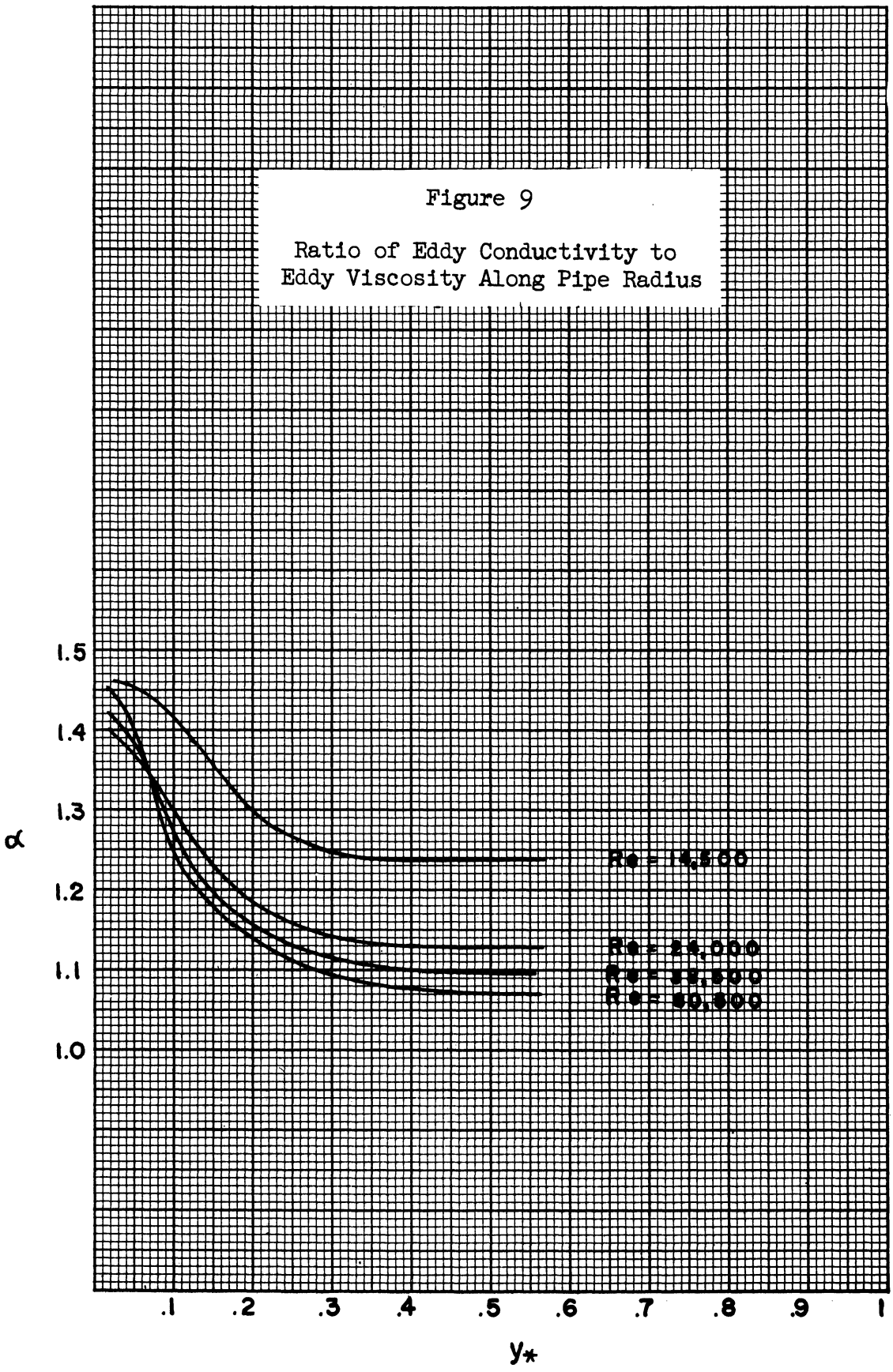

Figure 9

Ratio of Eddy Conductivity to
Eddy Viscosity Along Pipe Radius

TABLE III

EIGENVALUES AND CONSTANTS DETERMINED BY ANALOG COMPUTER

FOR PREVIOUSLY KNOWN SOLUTIONS

		Analog Value	Accepted Value (5,28)	Percent Deviation
Laminar Flow	λ_0^2	7.32	7.3135	0
	λ_1^2	44.4	44.60	-0.4
	λ_2^2	113.0	113.80	-0.7
	λ_3^2	212	215.1	-1.4
	λ_4^2	339	348.5	-2.7
The Graetz Solution	C_0	1.485	1.466	1.3
	C_1	-.817	-.802	1.9
	C_2	.607	.587	3.4
	C_3	-.514	-.475	8.2
	C_4	.466	.404	15.4
	A_0	.748	.749	-0.1
	A_1	.537	.544	-1.3
	A_2	.458	.462	-0.9
	A_3	.401	.415	-3.4
	A_4	.361	.382	-5.5
Slug Flow	λ_1^2	11.54	11.566	-0.2
	λ_2^2	60.8	60.94	-0.2
	λ_3^2	148.6	149.78	-0.8
	C_1	1.595	1.605	-0.6
	C_2	-1.076	-1.065	-1.0
	C_3	.876	.852	2.8
	A_n	.990	1	-1.0

values very well. The errors are no doubt smaller than the uncertainties of the input function $g(r_*) = 1 + Pr\ \epsilon_c/\nu$ for the turbulent cases.

It should be remarked that an internal check is possible from the measurements made. The eigenvalues were calculated both from resistances in the circuit (see page 30) and from

$$\lambda_n^2 = \frac{2R_n'}{\int_0^1 fr_* R_n dr_*}$$

which is a direct consequence of equation (5). If these methods gave results which differed by more than 1% for the first mode, 2% for the second mode, or 4% for the third mode, a search for the trouble was made. The agreement was considerably better than these figures except for the runs at Pr = 7.5.

Table IV contains the constants for the turbulent cases. These results are plotted with interpolated values in Figures 10-18. It is now possible to use these results to make comparisons with experiment, calculate thermal entry length and to make certain other calculations.

Comparison of Experimental and Predicted Temperature Distribution

Figure 19 is a comparison of experimental temperature distribution of Run 5 with the temperature distribution predicted from equation (4) and the eigenfunctions tabulated in Appendix C. It was to be expected, of course, that the prediction be good since the experimental run was used to determine the analog input functions.

Figure 20 shows the wall-temperature distribution of Run 6. The temperature distribution in the flowing air was calculated with the methods of Tribus and Klein (57) by assuming that wall temperature followed the straight line approximations shown. This calculation is carried out in

TABLE IV

EIGENVALUES AND CONSTANTS FOR TURBULENT FLOW

Reynolds Number	λ_0^2	λ_1^2	λ_2^2	C_0	$-C_1$	C_2	A_0	A_1	A_2
				Prandtl Number = 0					
8,000	9.84	53.8	134.0	1.570	.982	.777	.910	.800	.744
24,000	9.96	54.4	134.4	1.564	1.000	.797	.915	.835	.790
80,300	10.10	55.2	136.0	1.570	1.015	.811	.919	.860	.820
500,000	10.22	55.6	137.0	1.560	1.020	.814	.922	.874	.839
				Prandtl Number = .01					
8,000	10.12	55.6	139.0	1.550	.973	.750	.925	.815	.735
14,500	10.60	57.8	145.2	1.560	.985	.765	.980	.866	.797
24,000	11.00	60.4	150.4	1.552	.967	.768	1.020	.895	.840
38,500	11.30	62.6	156.4	1.560	.982	.770	1.055	.937	.859
80,300	12.48	69.6	176	1.545	.945	.746	1.185	.988	.907
150,000	14.92	83.6	215	1.522	.935	.721	1.445	1.135	.997
500,000	28.5	175.0	454	1.462	.775	.578	3.01	1.790	1.418
				Prandtl Number = .024					
8,000	10.62	58.8	147.6	1.538	.948	.740	.985	.840	.757
14,500	11.44	63.6	159.6	1.537	.944	.742	1.072	.906	.835
24,000	12.66	70.2	178.8	1.530	.940	.726	1.200	.995	.895
38,500	14.96	84.4	215	1.543	.933	.710	1.465	1.157	1.010
80,300	19.5	117.2	304	1.475	.829	.641	1.990	1.335	1.160
150,000	26.1	156.8	410	1.460	.800	.600	2.70	1.71	1.388
500,000	62.6	442	1,182	1.370	.620	.456	6.99	2.99	2.28
				Prandtl Number = .10					
8,000	17.66	108.8	285	1.455	.763	.546	1.807	1.12	.894
14,500	22.6	143.6	380	1.430	.733	.526	2.37	1.39	1.138
24,000	30.2	197	520	1.420	.686	.497	3.31	1.725	1.423
38,500	36.6	264	712	1.400	.633	.471	4.16	1.930	1.730
80,300	62.6	454	1,230	1.380	.568	.436	7.23	2.76	2.22
150,000	93.6	714	1,980	1.345	.558	.381	10.90	4.01	2.83
500,000	240	2,000	5,900	1.270	.428	.298	28.8	7.66	5.35
				Prandtl Number = .718					
8,000	59.4	700	1,995	1.228	.322	.216	7.20	1.48	1.105
14,500	92.6	1,108	3,200	1.185	.321	.203	11.25	2.39	1.705
24,000	133	1,540	4,320	1.220	.332	.215	16.42	3.30	2.16
38,500	193.6	2,170	6,210	1.214	.334	.217	23.8	4.81	3.12
80,300	339	3,820	11,080	1.200	.324	.202	41.6	7.94	5.01
150,000	546	6,030	16,860	1.210	.343	.212	66.8	14.86	9.20
500,000	1,468	17,700	50,800	1.185	.292	.178	179	30.5	17.68
				Prandtl Number = 7.5					
8,000	122	2,080		1.060	.109		14.95	1.03	
14,500	192	7,100		1.060	.0995		23.8	3.04	
38,500	434	15,400		1.060	.0974		54.3	3.01	
80,300	776	26,600		1.061	.0965		97.1	5.12	
150,000	1,260	46,400		1.053	.0878		158	7.51	
500,000	3,250	139,600		1.045	.0731		408	15.95	

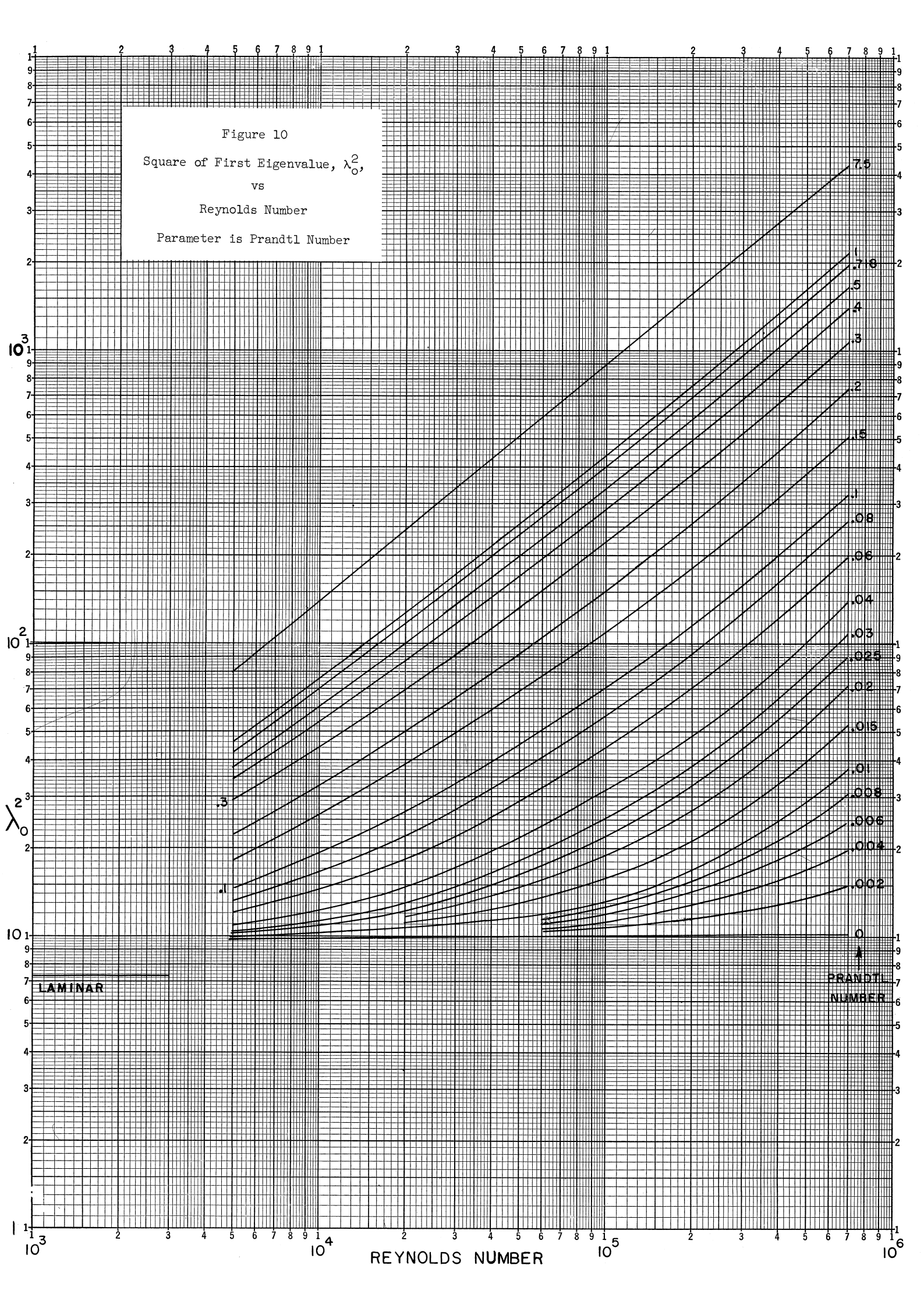
Figure 10
Square of First Eigenvalue, λ_o^2,
vs
Reynolds Number
Parameter is Prandtl Number
7.5
1
.7 & .8
.5
.4
.3
.2
.15
.1
.08
.06
.04
.03
.025
.02
.015
.01
.008
.006
.004
.002
0
PRANDTL NUMBER
LAMINAR
λ_o^2
REYNOLDS NUMBER
10^3
10^4
10^5
10^6

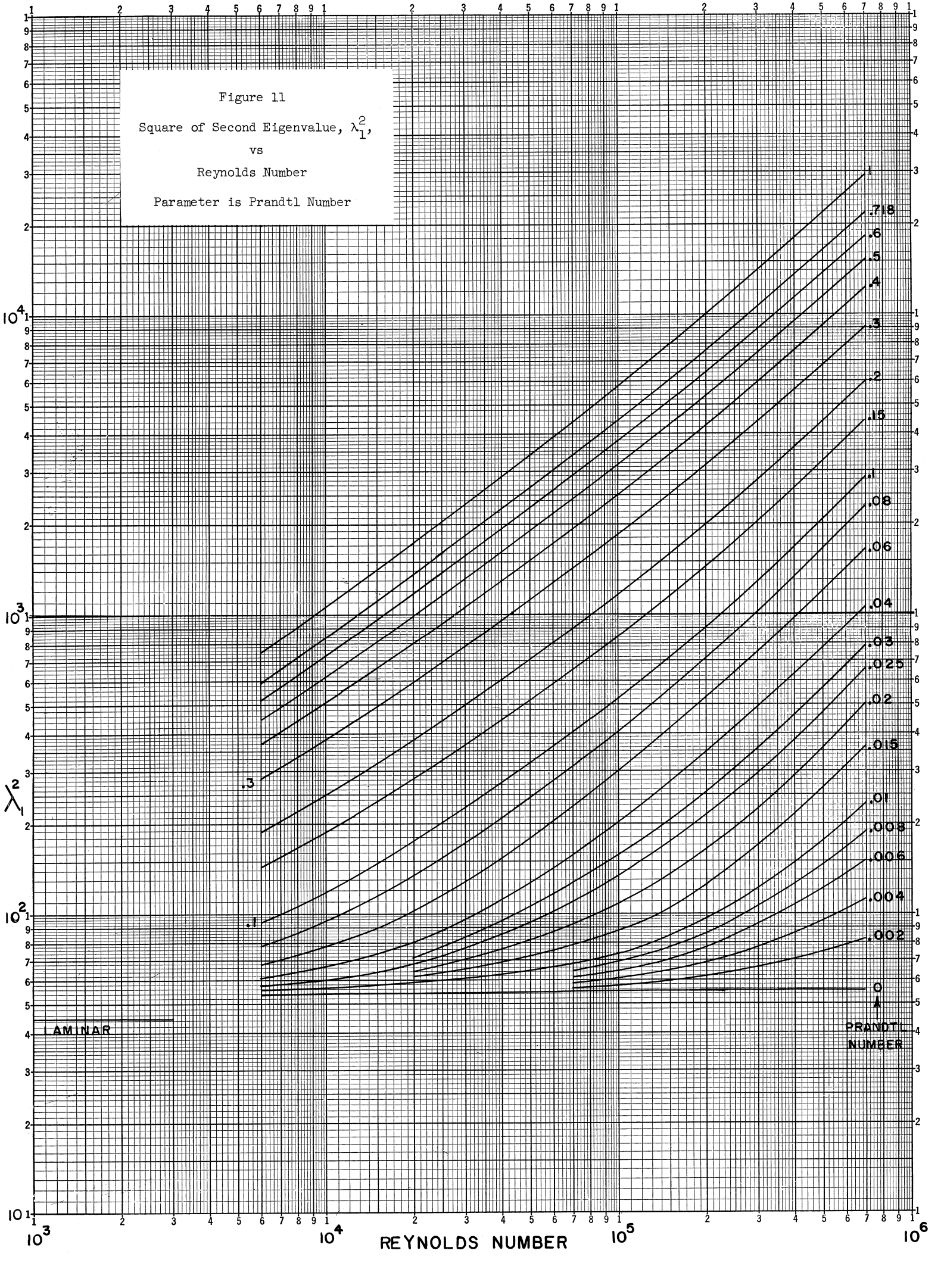
Figure 11
Square of Second Eigenvalue, λ_1^2,
vs
Reynolds Number
Parameter is Prandtl Number
1
.718
.6
.5
.4
.3
.2
.15
.1
.08
.06
.04
.03
.025
.02
.015
.01
.008
.006
.004
.002
0
PRANDTL NUMBER
LAMINAR
λ_1^2
REYNOLDS NUMBER
10^1
10^2
10^3
10^4
10^5
10^6

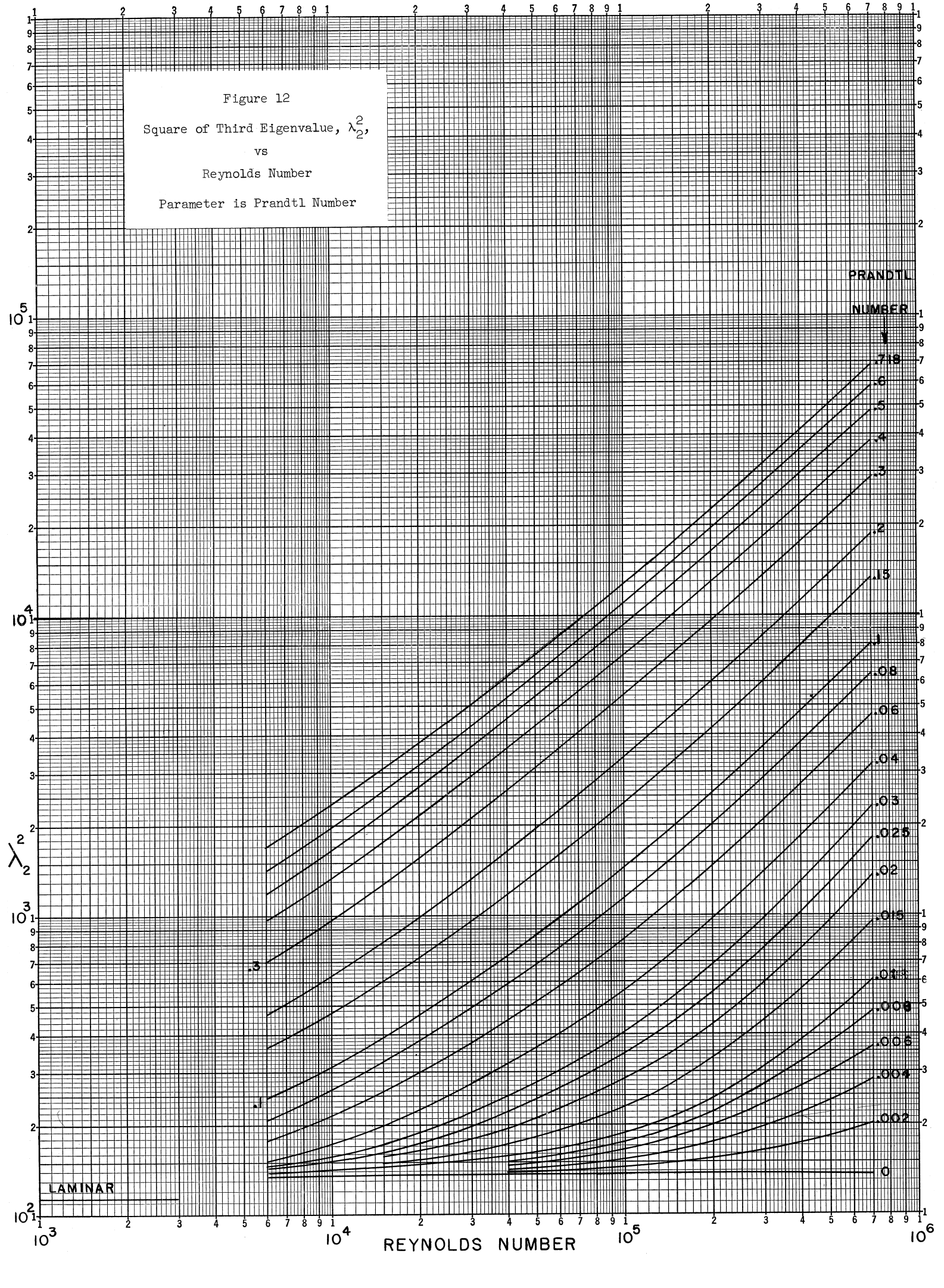
Figure 12
Square of Third Eigenvalue, λ_2^2,
vs
Reynolds Number
Parameter is Prandtl Number
PRANDTL NUMBER
1
.719
.6
.5
.4
.3
.2
.15
.1
.08
.06
.04
.03
.025
.02
.015
.01
.008
.006
.004
.002
0
LAMINAR
λ_2^2
REYNOLDS NUMBER
10^1
10^2
10^3
10^4
10^5
10^6

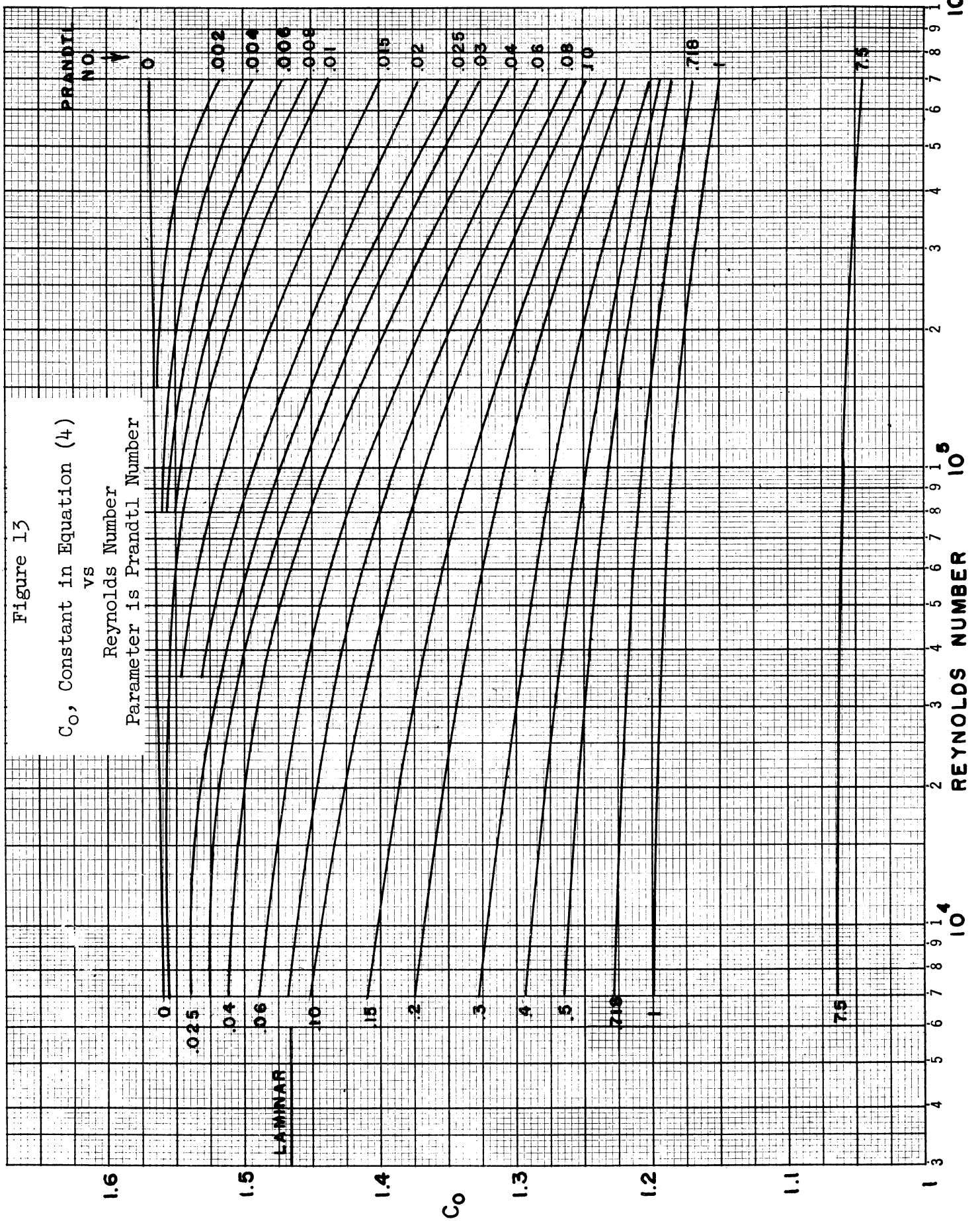

Figure 13

C_o, Constant in Equation (4)
vs
Reynolds Number
Parameter is Prandtl Number

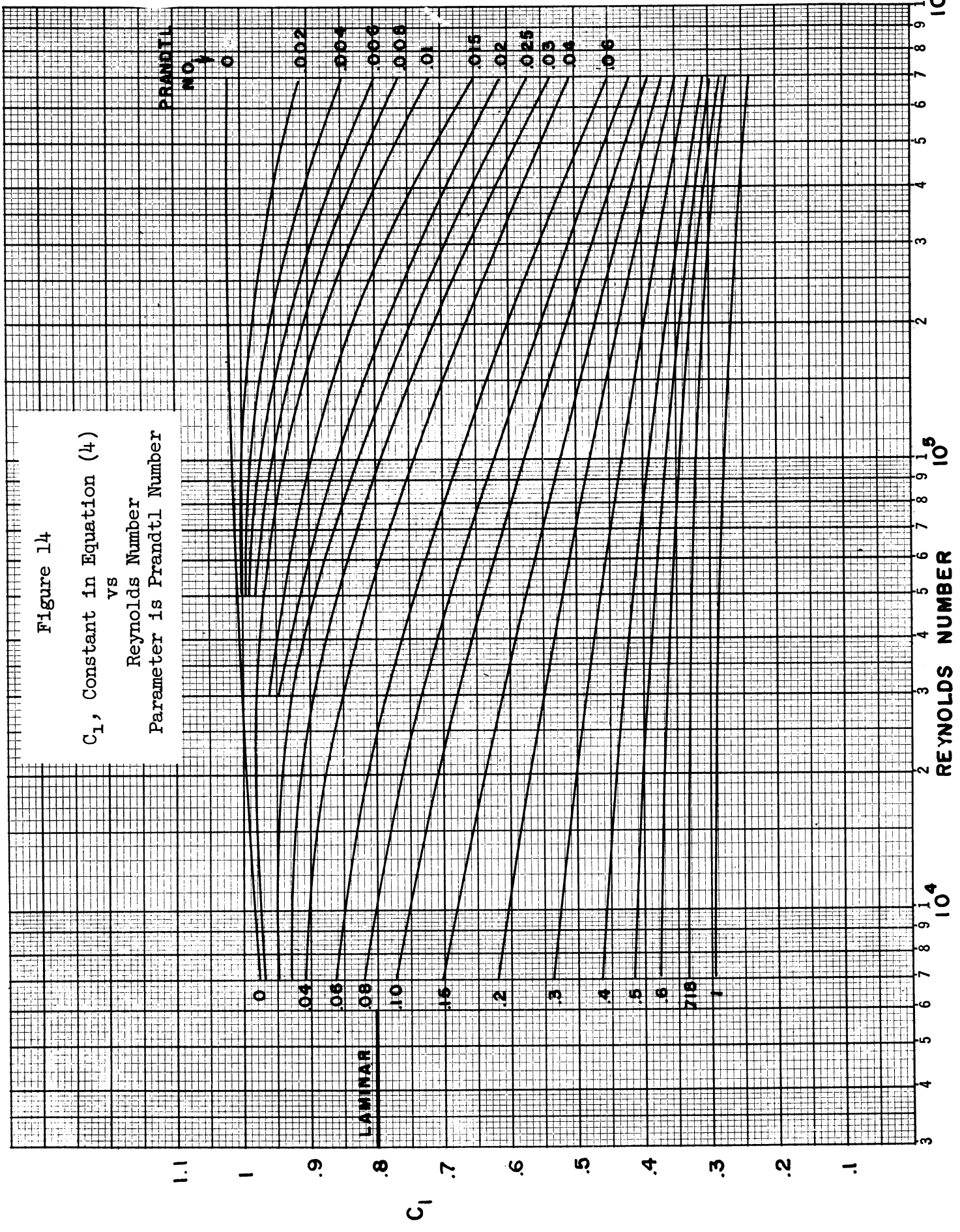

Figure 14

C_1, Constant in Equation (4)
vs
Reynolds Number
Parameter is Prandtl Number

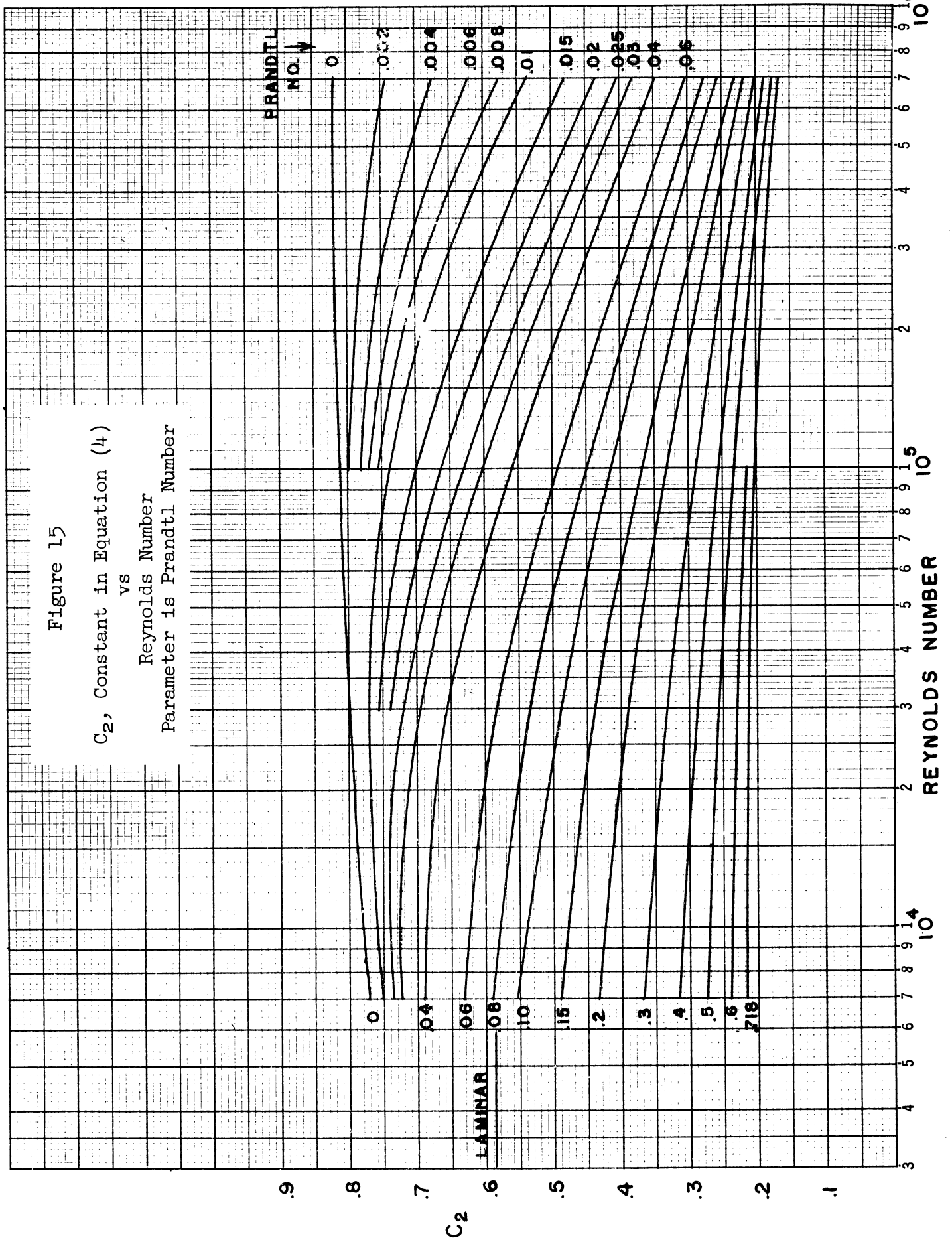

Figure 15

C_2, Constant in Equation (4)
vs
Reynolds Number
Parameter is Prandtl Number

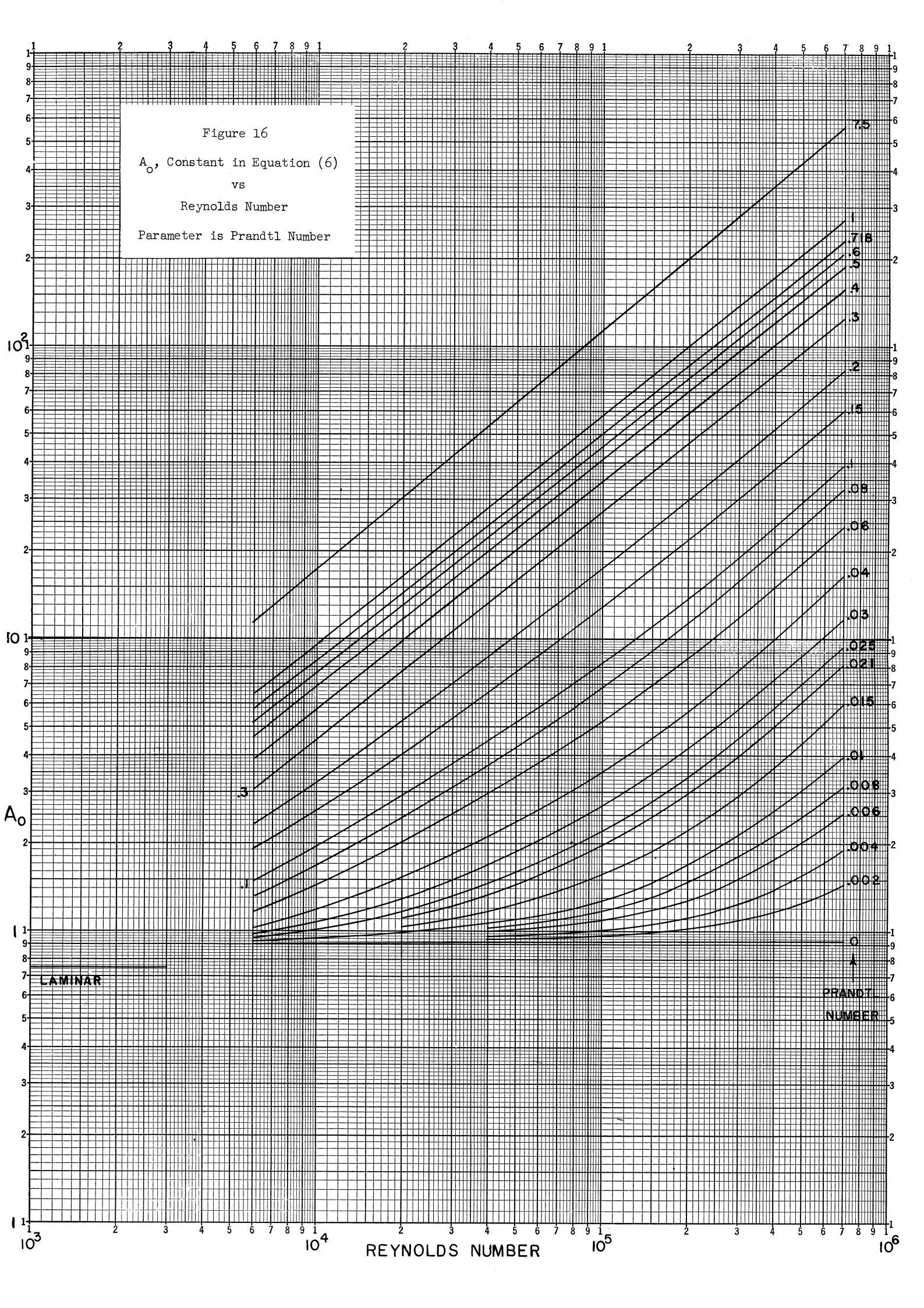
Figure 16
A_o, Constant in Equation (6)
vs
Reynolds Number
Parameter is Prandtl Number
7.5
1
.718
.6
.5
.4
.3
.2
.15
.1
.08
.06
.04
.03
.025
.021
.015
.01
.008
.006
.004
.002
0
PRANDTL NUMBER
LAMINAR
A_o
REYNOLDS NUMBER
10^3
10^4
10^5
10^6
10^2
10 1
1

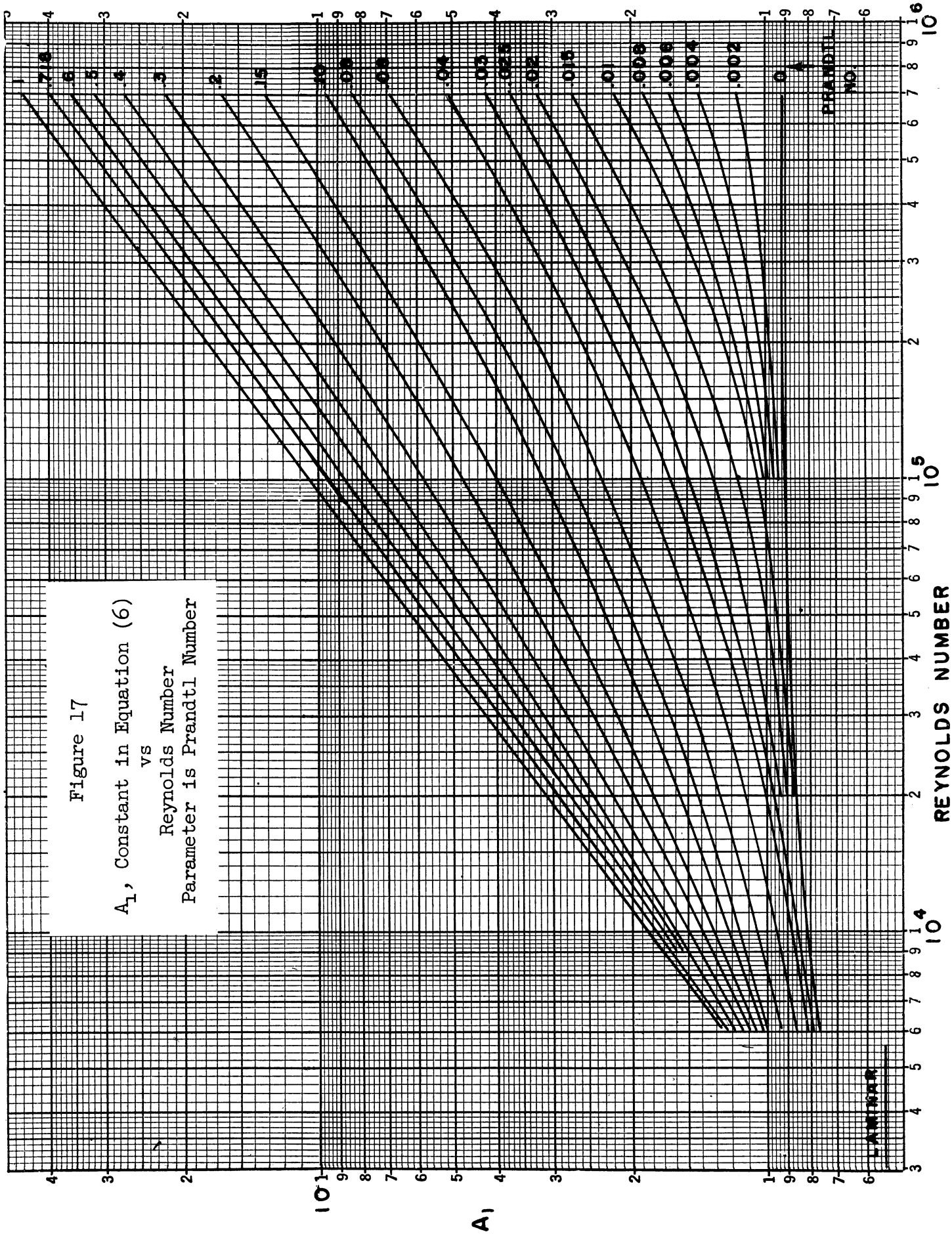
Figure 17
A_1, Constant in Equation (6)
vs
Reynolds Number
Parameter is Prandtl Number
A_1
REYNOLDS NUMBER
LAMINAR
PRANDTL NO.
7.0
6
5
4
3
2
1.5
1.0
.9
.8
.7
.6
.5
.4
.3
.2
.15
.1
.08
.06
.04
.03
.025
.02
.015
.01
.008
.006
.004
.002
.1

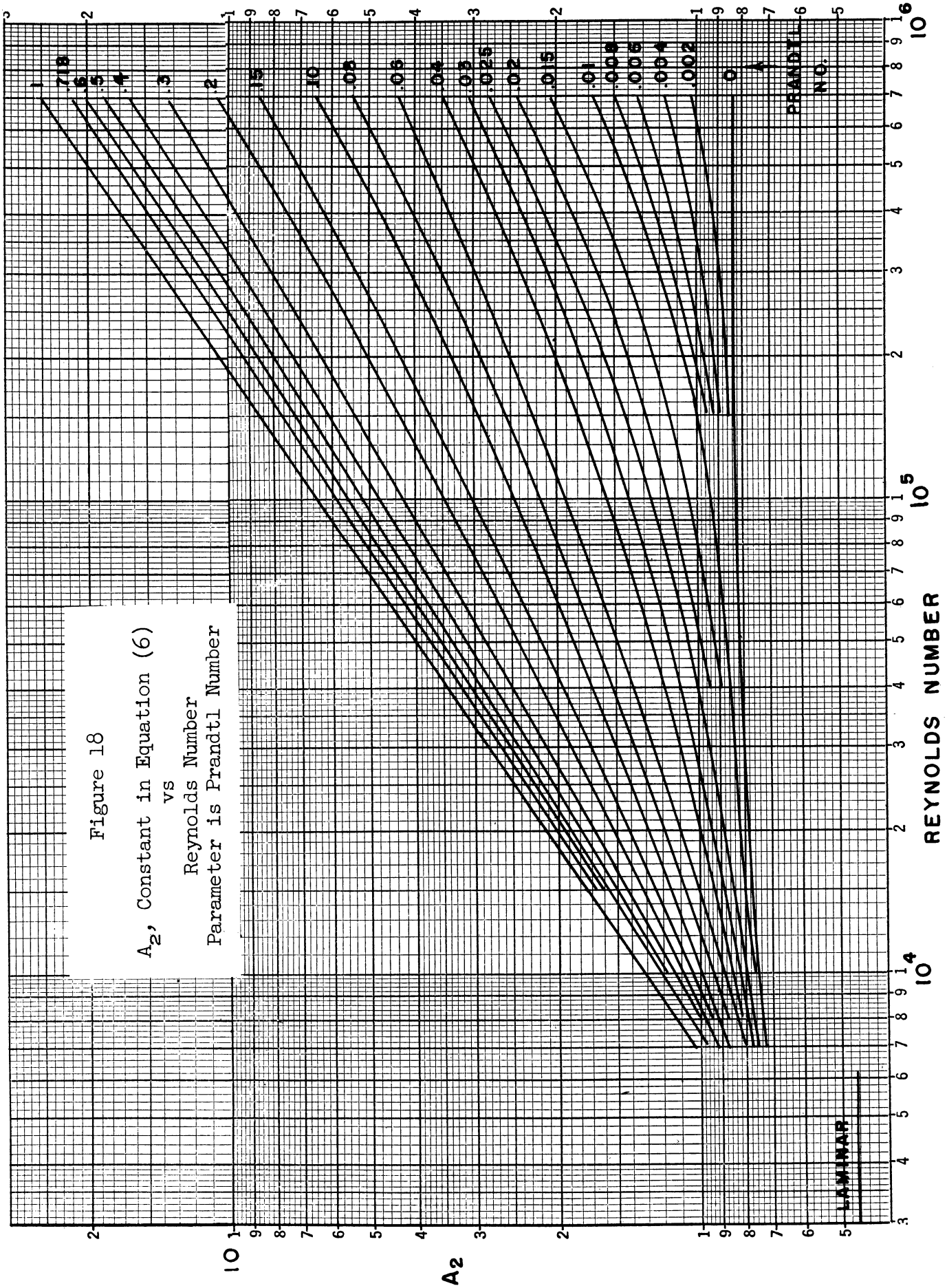
Figure 18
A_2, Constant in Equation (6)
vs
Reynolds Number
Parameter is Prandtl Number
A_2
REYNOLDS NUMBER
PRANDTL NO.
LAMINAR
10
10^4
10^5
10^6
.718
.6
.5
.4
.3
.2
15
10
.08
.06
.05
.04
.03
.025
.02
.015
.01
.008
.006
.004
.002
0

Figure 19

Experimental and Predicted Temperature Profile for Run 5

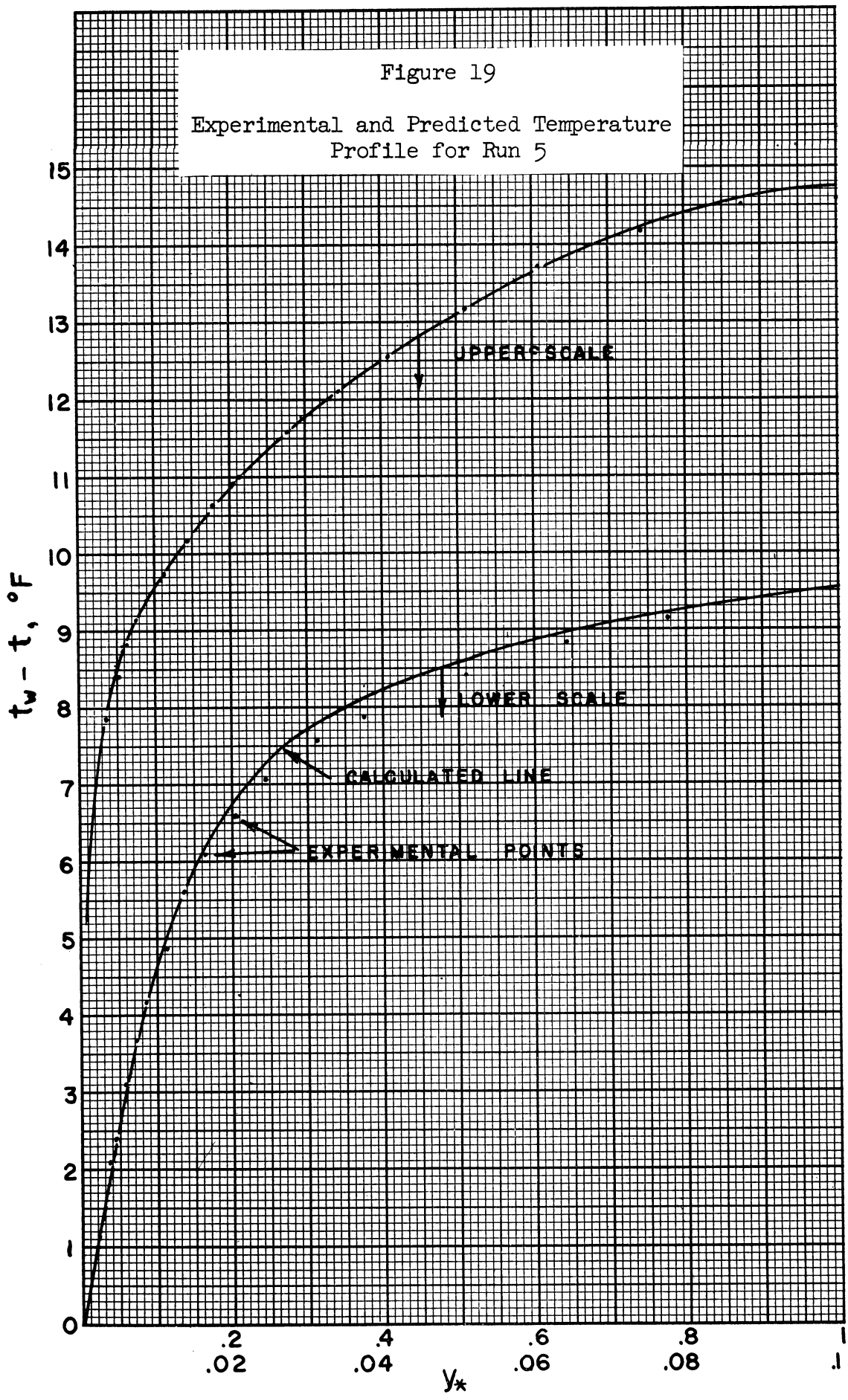

Figure 20

Wall-Temperature Distribution of Run 6

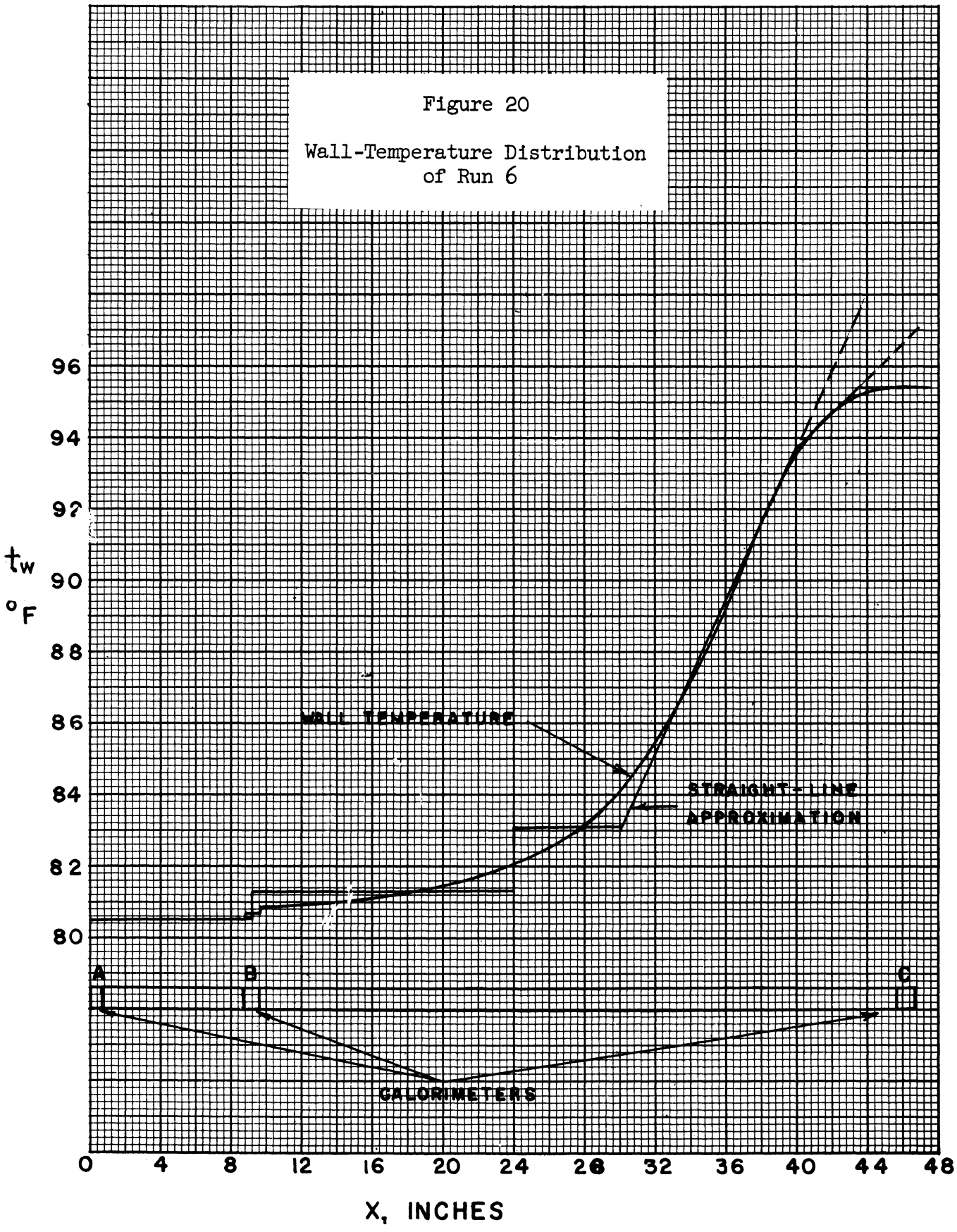

detail in Appendix D. The experimental and calculated Nusselt numbers are 101 whereas the asymptotic, uniform wall-temperature Nusselt number is 96. The temperature distribution in the fluid is shown in Figure 21 together with the predicted temperature. The figure shows that the methods employed here enable the prediction of temperature distribution in a fluid under conditions of wall-temperature distribution widely different from the uniform wall-temperature case for which experimental and analog data were compiled.

Asymptotic Nusselt Number for Uniform Wall Temperature and Uniform Heat Flux

For fluid flowing in a pipe at uniform wall temperature, it is shown in Appendix D that the asymptotic Nusselt number is

$$Nu_a = \frac{\lambda_0^2}{2} \tag{31}$$

Thus, the Nusselt number for this case can be easily determined from Figure 10. For liquid metals the Nusselt number is often correlated against Peclet number as an independent variable. This is done in Figure 22. Shown also is a line through the data of Gilliland, Musser, and Page (12) after being corrected for thermal entrance error. These authors used a uniform wall-temperature system, but the tube had a length-to-diameter ratio of 45, which is sufficiently short that the average Nusselt number was 8 to 12% higher than the asymptotic value. The correction to their data was made by multiplying their Nusselt numbers by the ratio Nu_{av}/Nu_a as determined from the data and methods presented here. The prediction is seen to be in fair agreement with their data. The predictions of Figure 22 may be represented within 10% by

$$Nu_a = 4.8 + 0.0056\ Pe^{.9} \tag{32}$$

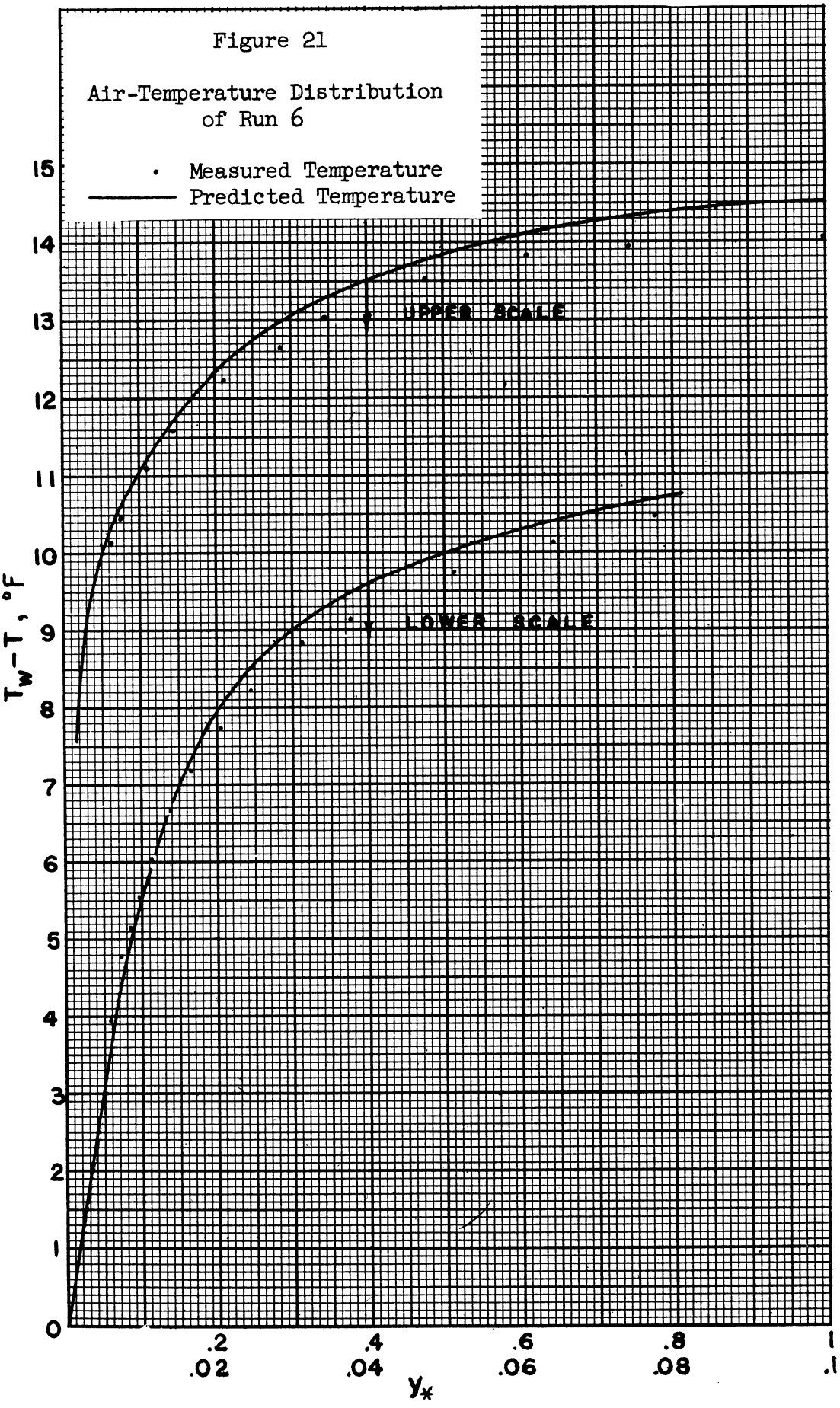
Figure 21
Air-Temperature Distribution of Run 6
• Measured Temperature
——— Predicted Temperature
UPPER SCALE
LOWER SCALE
$T_w - T$, °F
0
1
2
3
4
5
6
7
8
9
10
11
12
13
14
15
.2
.02
.4
.04
.6
.06
.8
.08
y_*

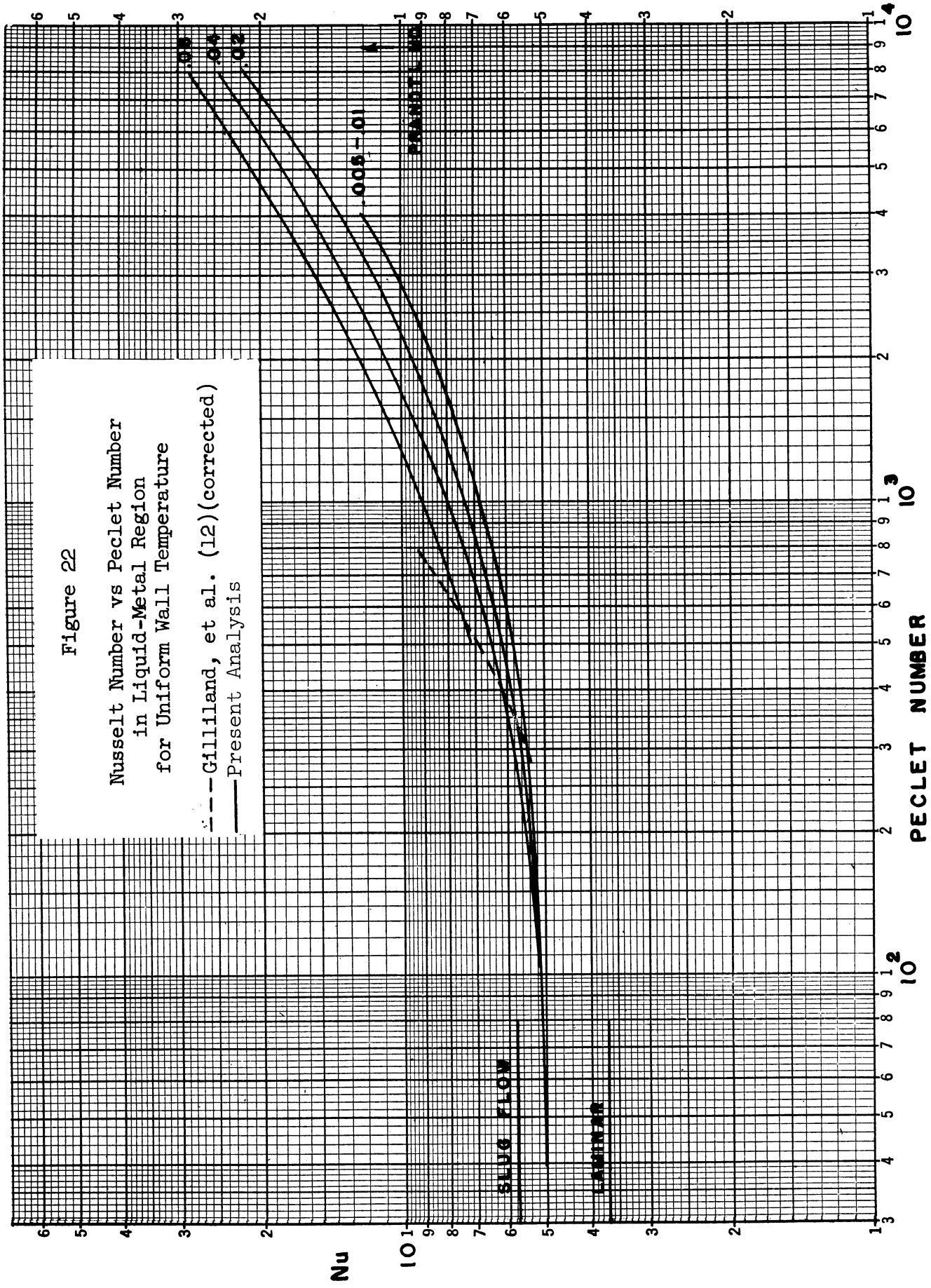
Figure 22
Nusselt Number vs Peclet Number
in Liquid-Metal Region
for Uniform Wall Temperature
---Gilliland, et al. (12)(corrected)
——Present Analysis
.08
.04
.02
.005-.01
1
Nu
PECLET NUMBER
SLUG FLOW
LAMINAR

This equation is recommended for the asymptotic Nusselt number for heat transfer to liquid metals in a pipe at uniform wall temperature.

If the wall-heat flux is uniform, it is shown in Appendix D that the asymptotic Nusselt number is

$$Nu_a = \frac{1}{16 \sum \frac{A_n}{\lambda_n^4}} \tag{33}$$

This series converges extremely rapidly. For example, for the laminar case, which converges more slowly than the turbulent ones, the first two terms of the series give 4.379 whereas the exact value is 48/11 = 4.364.

Figure 23 is a plot of equation (33) vs Peclet number for the liquid-metal region. Shown also are mean lines through the data of several experimental investigations. Johnson, et al. (20), took data with lead-bismuth eutectic at four Prandtl numbers. Lines are shown for two of these. The others were not drawn because of lack of space on the figure. The prediction agrees with all four sets of Johnson's data within 4% over the entire range.

The agreement with the data of Isakoff and Drew (17) is not nearly as good. The discrepancy between Isakoff's results and others could be accounted for, however, by waviness of the inside wall temperature. Isakoff and Drew believe that such waviness was reduced to a negligible degree, yet their apparatus was in this respect inferior to that of Johnson, et al. Isakoff wrapped a stainless steel tube with heating ribbon whereas Johnson had a 1/4-in. aluminum jacket between the inside steel pipe and the heating wires.

The data of Trefethen (55) are not shown, but his data are nearly

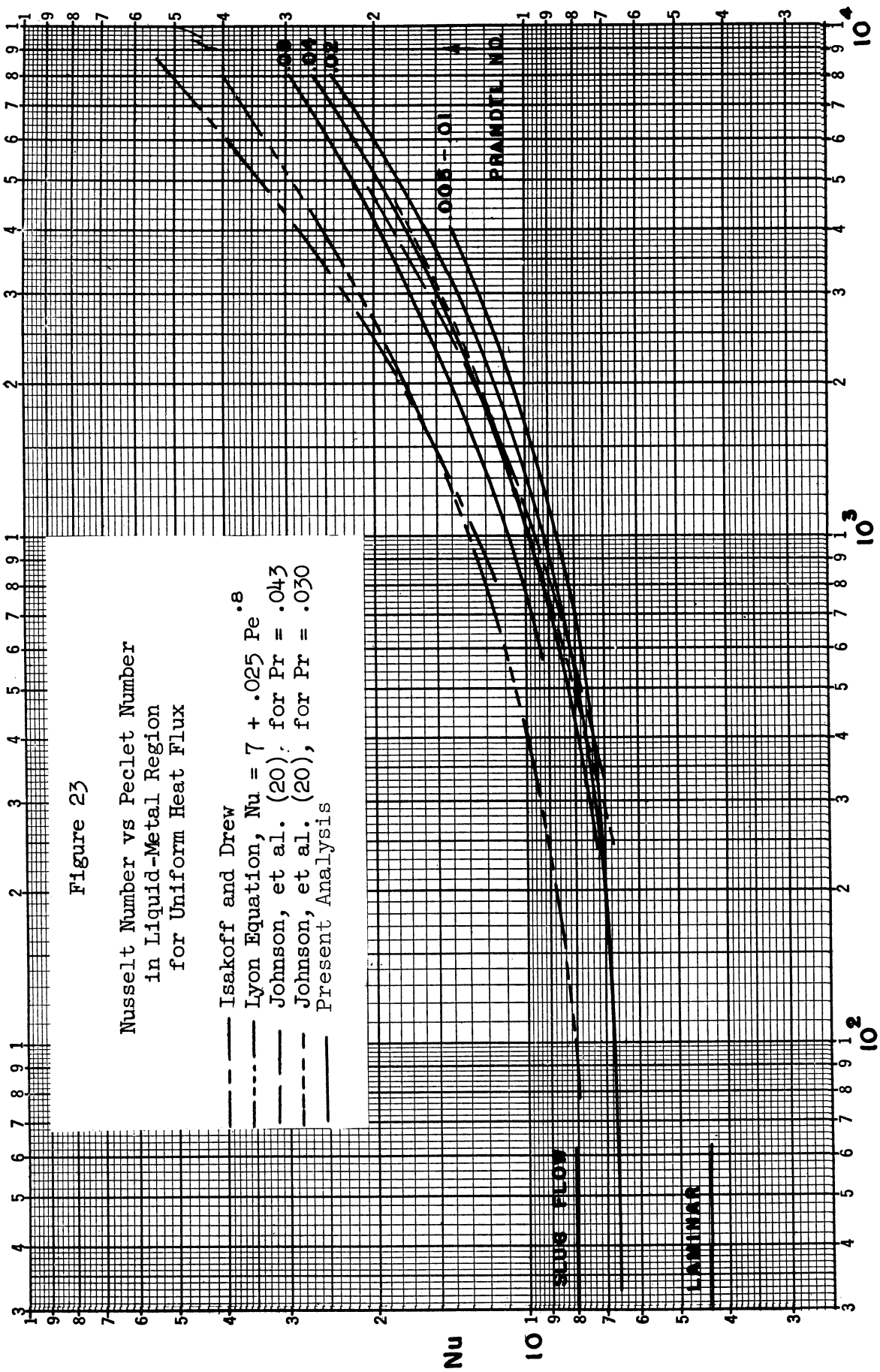
Figure 23
Nusselt Number vs Peclet Number
in Liquid-Metal Region
for Uniform Heat Flux
Isakoff and Drew
Lyon Equation, Nu = 7 + .025 Pe^.8
Johnson, et al. (20), for Pr = .043
Johnson, et al. (20), for Pr = .030
Present Analysis
PRANDTL NO.
.005 - .01
.02
.04
.06
SLUG FLOW
LAMINAR
Nu
PECLET NUMBER

identical to the data of Johnson when compared at the same Prandtl number. The prediction agrees with Trefethen's data within 4% except at his lowest Peclet numbers, where the prediction is about 10% higher.

The data of Werner, King, and Tidball (60) are above the prediction but they used a double-pipe, "Figure of Eight" system in which a large part of both annulus and tube side were in the thermal entrance region. Their data are, therefore, not expected to fit the present correlation.

Other data have been reported for heat transfer to liquid metals at uniform heat flux, but the most reliable ones have been discussed above. In general the agreement of the present prediction with the data is better than the Lyon-Martinelli prediction thus confirming the suggestion of Jenkins (19) and others that for liquid metals the eddy conductivity is lower than the eddy viscosity.

The predictions of Figure 23 can be represented within 10% by

$$Nu = 6.3 + 0.0060\ Pe^{.9} \qquad (34)$$

This equation is recommended for the asymptotic Nusselt number for liquid metals in a pipe at uniform heat flux.

The ratio of the asymptotic Nusselt number at uniform heat flux to that at uniform wall temperature is shown in Figure 24, and confirms similar results by Seban and Shimazaki (50). The figure illustrates the important fact that wall-temperature distribution strongly affects the heat-transfer coefficient at low Peclet numbers.

Thermal Entry Length

Figure 25 contains the result of thermal-entry-length calculations for a pipe at constant wall temperature. The thermal entry length is defined here as the number of diameters downstream from the beginning of

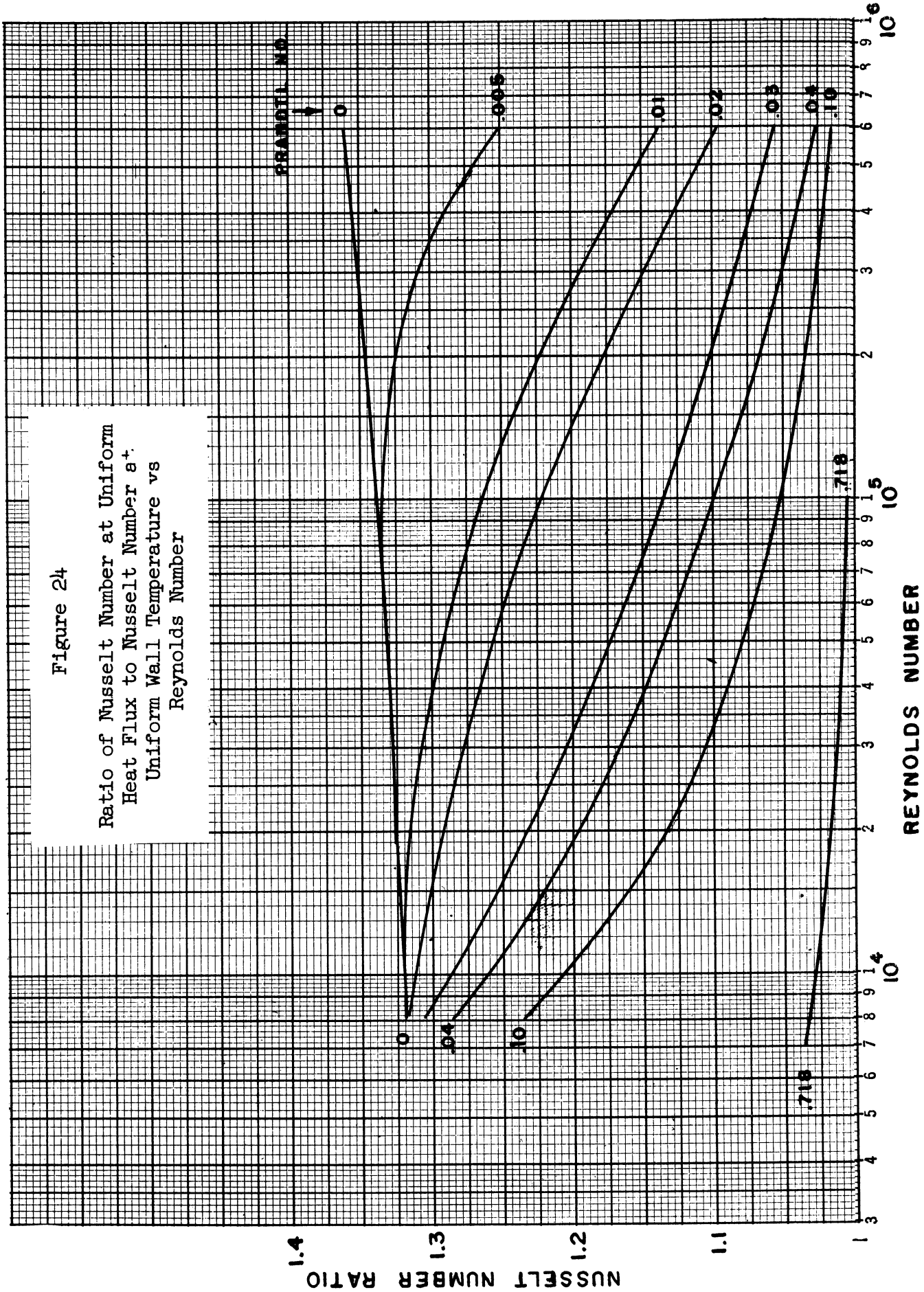

Figure 24

Ratio of Nusselt Number at Uniform Heat Flux to Nusselt Number at Uniform Wall Temperature vs Reynolds Number

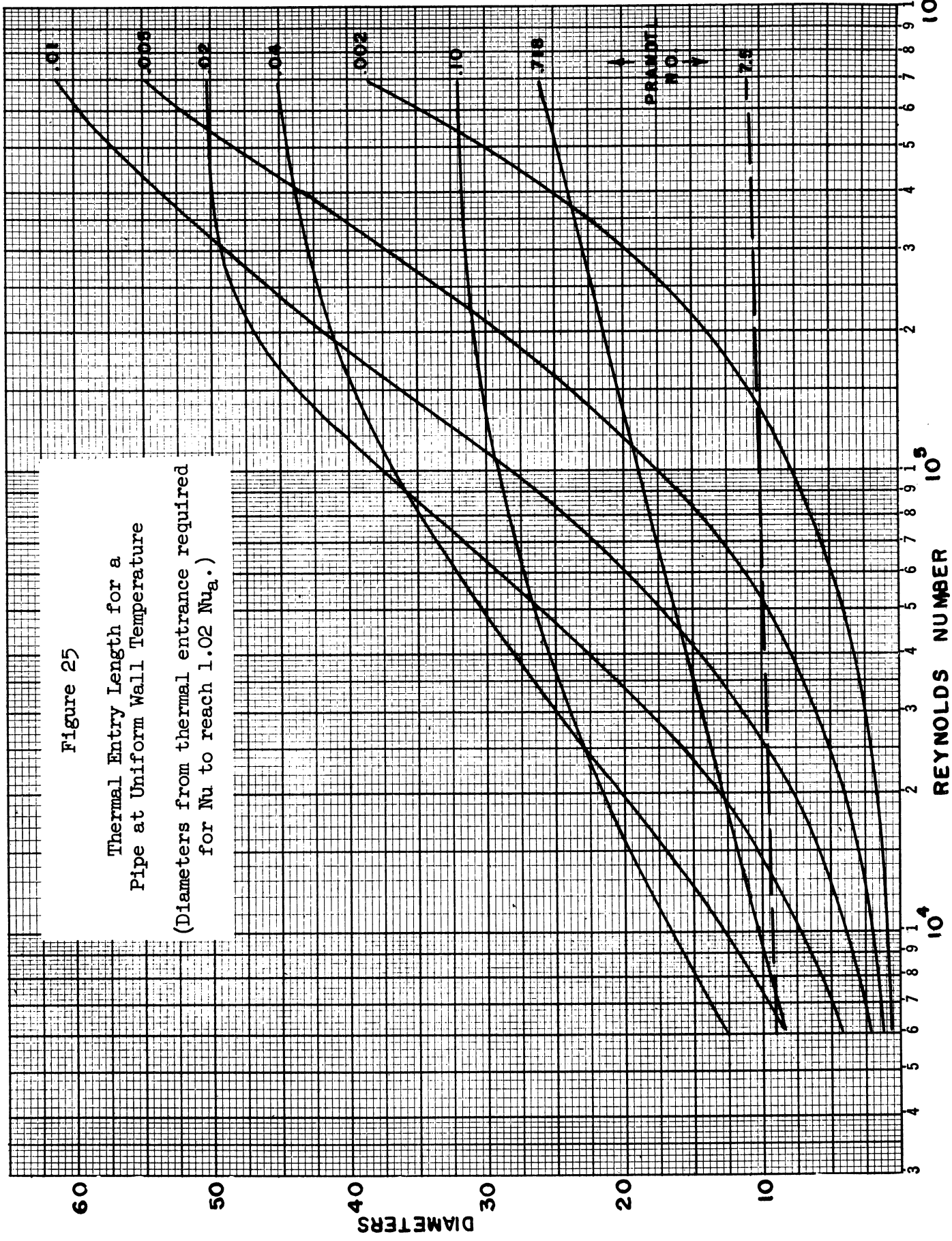

Figure 25

Thermal Entry Length for a Pipe at Uniform Wall Temperature

(Diameters from thermal entrance required for Nu to reach 1.02 Nu_a.)

heating at which the Nusselt number is within 2% of its asymptotic value. Other authors have used a 1% criterion for entry length, but that figure is somewhat severe for heat transfer data. The lengths do not differ greatly, however, because of the exponential nature of the variation with distance. The entry length was calculated from the equation (Appendix D)

$$Nu = \frac{2A_o e^{-\lambda_o^2 x_*} + 2A_1 e^{-\lambda_1^2 x_*}}{\frac{4A_o e^{-\lambda_o^2 x_*}}{\lambda_o^2} + \frac{4A_1 e^{-\lambda_1^2 x_*}}{\lambda_1^2}}$$

The line for water (Prandtl number 7.5) is shown dotted because there is some doubt about its accuracy. In order to obtain the correct value for the asymptotic Nusselt number for water, it was necessary to use values of the eddy conductivity much lower than had been expected. In calculating the eddy conductivity for water, it was assumed that $\epsilon_c = \epsilon_\nu$ in the central portion of the pipe. Near the wall the equation of Deissler (17)

$$\frac{\epsilon_c}{\nu} = \alpha \frac{\epsilon_c}{\nu} = 0.0154\alpha u^+ y^+ \left[1 - e^{-.0154\ u^+ y^+}\right]$$

was used, and α was varied until the asymptotic Nusselt number agreed with the correlation in McAdams (34). The values used varied from 0.4 to 0.6 depending on Reynolds number. The reason for such low values of α is not certain, but it is possibly caused by the limitations of the function generator used with the analog computer. In order to obtain good accuracy, the solutions of the equation near the wall had to be expanded as described in Section III. Two time-constant changes were made during the solution of the equations for a Prandtl number of 7.5, but this technique may have been insufficient to give an accurate solution of the eigenfunctions.

It is curious that the thermal entry length at first increases with increasing Prandtl number and then begins to decrease. This variation is contrary to the prediction of Berry (3), but his results at high Prandtl number are considerably higher than the experimental entry-length determinations of Hartnett (14) for oil and water. Both Hartnett's data and the predictions of Berry and Levy (27) indicate that as the Prandtl number increases above about ten, there is very little increase in entry length at a given Reynolds number. Thus, the dotted line in Figure 25 is the prediction for all Prandtl numbers above 7.5.

Table V summarizes the results of previous investigations and compares them to the present results at two Reynolds numbers. This table is similar to one reported by Hartnett except that a 2% entry length is used here whereas Hartnett apparently used 1% in determining the entry length of Boelter, Latzko and Deissler.

The entry lengths calculated in this investigation for air are somewhat higher than the analytical results of Latzko and Deissler. The experimental results of Boelter fall about halfway between the earlier analyses and the present. For higher Prandtl numbers the present results agree very well with the data of Hartnett for oil and water, which were taken, however, at uniform heat flux. This agreement and the fact that the entry lengths for air at uniform heat flux and uniform wall temperature calculated by Deissler are nearly equal indicate that the entry lengths for the two cases are in fact about the same for Prandtl numbers above one. This observation disagrees with the prediction of Levy (27) that the entry lengths for the two cases differ by a factor of 3.6. Levy's analysis is oversimplified, however, in that it assumes a sublayer of a calculated thickness in which there is no eddy diffusion bounded by a

TABLE V

SUMMARY OF THERMAL-ENTRY-LENGTH INVESTIGATIONS

Investigator	Type of Investigation	Boundary Condition	Prandtl Number	Thermal Entry Length x/D	
				$Re = 10^4$	$Re = 10^5$
Present Results	Analytical	Uniform Wall Temp	7.5	9	11
Deissler (10)	Analytical	Uniform Heat Flux	10	2-3	2-3
Berry* (3)	Analytical	Uniform Wall Temp	10	13	17
Hartnett (14)	Experimental	Uniform Wall Flux	7-200	10	15
Present Results	Analytical	Uniform Wall Temp	.718	10	19
Deissler (10)	Analytical	Uniform Wall Temp	.73	2	7
Deissler (10)	Analytical	Uniform Heat Flux	.73	3	7
Latzko (24)	Analytical	Uniform Wall Temp	1	6	11
Berry* (3)	Analytical	Uniform Wall Temp	1	12	17
Boelter, et al. (4) (extrapolated)	Experimental	Uniform Wall Temp	.72	8	15

*Berry used a 1% instead of a 2% entry-length criterion. A factor of about 0.7 would convert his results to a 2% entry length.

well-stirred fluid in which the eddy diffusivity is infinite.

The entry lengths reported by Aladyev (1) for water are as high as 40 x/D. Since this is so much higher than all other data and predictions, it can be concluded that his results are in error.

At low Prandtl numbers the calculated entry length is in general agreement with Johnson, et al. (20), who estimate from their experimental data that for Prandtl numbers of .020 to .045 and Reynolds numbers of 10,000 to 100,000 the thermal entry length is about 30. Their data were taken at uniform heat flux. In this region the uniform heat flux and uniform wall-temperature entry lengths probably differ more but not much more than at higher Prandtl numbers. Entry length calculations in Appendix D for a fluid of Prandtl number 0.025 flowing in a pipe at a Reynolds number of 120,000 give the following results:

entry length at uniform wall temperature	40
entry length at uniform heat flux	44
entry length at linear wall temperature	195

Heat Transfer in the Entry Region

In Figure 26 are plotted the experimental values of Nu/Nu_a at two Reynolds numbers taken from Boelter, et al. (4), and the corresponding computed line. The short line running from the ordinate to $x/D = 0.4$ is an estimate based on the data given in Table II for the heat transfer in Calorimeter A. It is a mean value for x/D between zero and 0.4. There is some scatter in the data, but the line follows the data fairly well out to about $x/D = 4$. For the region closer than that more eigenvalues and constants are needed for the case of air. That close to the entrance the boundary layer calculations of Deissler (10) undoubtedly give more accurate results. A quite good estimate of this region could be made with the present technique, however, by observing the lengths at which

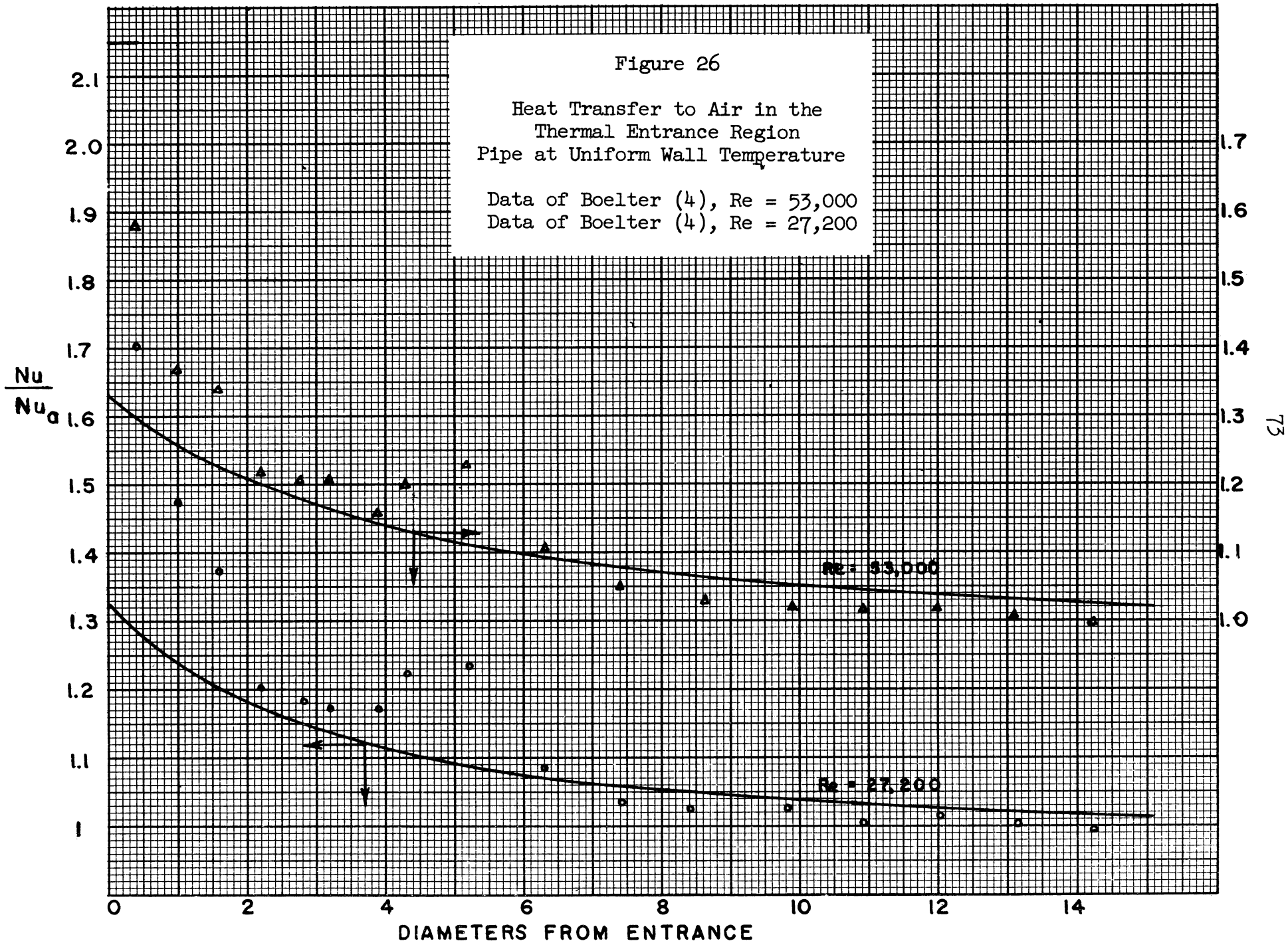
Figure 26
Heat Transfer to Air in the Thermal Entrance Region Pipe at Uniform Wall Temperature
Data of Boelter (4), Re = 53,000
Data of Boelter (4), Re = 27,200
Nu / Nu_a
DIAMETERS FROM ENTRANCE
Re = 53,000
Re = 27,200
2.1
2.0
1.9
1.8
1.7
1.6
1.5
1.4
1.3
1.2
1.1
1
1.7
1.6
1.5
1.4
1.3
1.2
1.1
1.0
0
2
4
6
8
10
12
14

the second and third eigenvalues begin to have appreciable effect. The length at which the fourth eigenvalue would begin to be significant could then be estimated, and from there a line could be drawn asymptotic to the ordinate.

Summary of Equations for Estimating Heat Transfer

Below are listed equations for computing the temperature distribution, rate of heat transfer, mixed-mean temperature and Nusselt number for three wall-temperature conditions. These equations are derived in Appendix D. With the aid of these equations and the constants given in Figures 10-18, it is a simple matter to calculate heat transfer in a pipe for any of the three cases.

Uniform Wall Temperature

$$\frac{t - t_w}{t_o - t_w} = \sum_n C_n R_n e^{-\lambda_n^2 x_*} \tag{4}$$

$$q(x_*) = \frac{-4k(t_o - t_w)}{D} \sum_n A_n e^{-\lambda_n^2 x_*} \tag{6}$$

$$t_{mm} = t_w - 8(t_w - t_o) \sum_n \frac{A_n}{\lambda_n^2} e^{-\lambda_n^2 x_*} \tag{35}$$

$$Nu(x_*) = \frac{2 \sum_n A_n e^{-\lambda_n^2 x_*}}{4 \sum_n \frac{A_n}{\lambda_n^2} e^{-\lambda_n^2 x_*}} \tag{36}$$

After only the first exponential is important, equation (36) reduces to the asymptotic Nusselt number

$$Nu_a = \frac{\lambda_o^2}{2} \tag{31}$$

Linear Wall Temperature

If

$$t_w(x_*) - t_o = Bx_* \tag{37}$$

$$t(x_*,r_*) - t_o = Bx_* - B\sum_n \frac{C_nR_n}{\lambda_n^2} + B\sum_n \frac{C_nR_n}{\lambda_n^2} e^{-\lambda_n^2 x_*} \tag{38}$$

$$q(x_*) = \frac{Bk}{2D} + \frac{4Bk}{D}\sum_n \frac{A_n}{\lambda_n^2} e^{-\lambda_n^2 x_*} \tag{39}$$

$$t_{mm} - t_o = Bx_* + 8B\sum_n \frac{A_n}{\lambda_n^4}\left(e^{-\lambda_n^2 x_*} - 1\right) \tag{40}$$

$$Nu(x) = \frac{1 + 8\sum_n \frac{A_n}{\lambda_n^2} e^{-\lambda_n^2 x_*}}{16\sum_n \frac{A_n}{\lambda_n^4}\left(1 - e^{-\lambda_n^2 x_*}\right)} \tag{41}$$

For the asymptotic Nusselt number, equation (41) reduces to

$$Nu_a = \frac{1}{16\sum_n \frac{A_n}{\lambda_n^4}} \tag{33}$$

Uniform Heat Flux at the Wall

The method of deriving these equations is explained by Tribus and Klein (57) and Sellars, Tribus, and Klein (51). Those references should be consulted for further details.

Let

$$H(s) = 2\sum_n \frac{A_n}{s + \lambda_n^2} \tag{42}$$

Then

$$H'(s) = -2\sum_n \frac{A_n}{(s + \lambda_n^2)^2} \tag{43}$$

Now let γ_m^2 be the values satisfying $H(-\gamma_m^2) = 0$. The temperature distribution is then given by

$$t(x_*,r_*) - t_o = \frac{qD}{2k}\left[4x_* + 32\sum_n \frac{A_n}{\lambda_n^4} + \sum_n \frac{e^{-\gamma_m^2 x_*}}{\gamma_m^4 H'(-\gamma_m^2)} - \sum_n C_n R_n \sum_n \frac{1 - e^{-\gamma_m^2 x_*}}{\gamma_m^2(\lambda_m^2 - \gamma_m^2)}\right] \tag{44}$$

The first summation in the brackets is equal to

$$-\sum_m \frac{1}{\gamma_m^4 H'(-\gamma_m^2)}$$

given by Sellars, Tribus and Klein. It converges much faster than their expression above, however. The proof of the equality is given in Appendix D.

Remaining expressions of importance for uniform heat flux are

$$t_{mm} - t_o = \frac{2qD}{k} x_*$$

$$Nu(x_*) = \frac{1}{16\sum_n \frac{A_n}{\lambda_n^4} + \frac{1}{2}\sum_m \frac{e^{-\gamma_m^2 x_*}}{\gamma_m^4 H'(-\gamma_m^2)}} \tag{45}$$

V. CONCLUSIONS

1. For the flow of air in a pipe the ratio of eddy conductivity to eddy viscosity varies with radial position and Reynolds number. The range of variation is 1.1 to 1.5.

2. A method is developed by means of which it is an easy matter to calculate heat transfer and temperature distribtuion in a fluid in turbulent flow in a pipe whose wall-temperature distribution is arbitrary.

3. The effects of wall-temperature distribution on heat transfer in a pipe are most marked in the liquid metal region.

4. For heat transfer to liquid metals the thermal entry length is large, and failure to consider this accounts for some scatter in previous correlations.

5. The eddy conductivity of liquid metals is significantly lower than the eddy viscosity.

6. The asymptotic Nusselt number for turbulent flow of liquid metals in pipes at uniform wall temperature can be correlated within 10% by

$$Nu = 6.3 + 0.0060\ Pe^{.9}$$

7. The asymptotic Nusselt number for turbulent flow of liquid metals in pipes at uniform heat flux can be correlated within 10% by

$$Nu = 4.8 + 0.0056\ Pe^{.9}$$

VI. APPENDICES

APPENDIX A

DETAILS OF APPARATUS

The apparatus has been briefly described in Section III, and this appendix presents further details, some of which are repeated to make this description complete.

The Air Circulation System

The blower for moving the air was firmly bolted to the concrete floor and the connections to the piping were made of soft rubber. With this arrangement vibration was not a problem. From the blower air could be recirculated through a double-pipe cooler or sent to the test section. All piping except the test and inlet sections was 2-1/2-in. galvanized steel. The relative flow rates through the two paths were controlled by gate valves. In practice the gate valve in the double-pipe heat exchanger circuit was left wide open except for runs at the highest flow rates. This recirculated air served to remove heat from the blower.

The air for the test section first entered an entrance section whose purpose was to provide to the test section air with an established velocity profile and a controllable, known temperature. To achieve these ends, the air first entered a heat exchanger whose purpose was to cool the warm air from the blower down to room temperature. This exchanger consisted of about twenty-one short lengths of 5/8-in. finned tubing stacked in a 4 x 4-in. channel two feet long. Cooling water passed through the tubes in four passes. The water for this and the double-pipe cooler was supplied from a constant-head tank in order to assure a steady flow rate.

Across the outlet of the finned-tube cooler were two layers of baffles consisting of 1/2 x 1/8-in. steel strips. Just above these baffles

was a small heater consisting of a plastic disk criss-crossed with 40-gage copper wire in three layers. Electric current to this heater was controlled by a Variac. The heater was used for fine and rapid control of the inlet air temperature. The capacity of the heater was sufficient to raise the air temperature about 1°F at the highest flow rate used.

The wire heater was located in the bottom of a 2-1/2-in. pipe tee. It was held down by a piece of 2-in. pipe which extended to the plug at the top of the tee. This 2-in. pipe was drilled with a number of 1/4-in. holes facing the branch of the tee. This served to provide more mixing and to prevent large swirls from forming. Piping from the branch of the tee enlarged to a piece of 4-in. pipe 9 inches long which contained straightening vanes made of a honeycomb of 1-in. pieces of 3/8-in. copper tubing. Just downstream of the honeycomb was the thermocouple well for measuring the inlet air temperature. This well was a piece of 3/32-in. stainless steel tubing 3 in. long. At the downstream end of the 4-in. pipe were two screens of 1/16-in. mesh held between flanges, and after the flanges was a reducer which changed the inside diameter from 4 to 1.5 in. in a length of about 5 in. The last 2 in. of the reducer had a diameter of 1.50 in.

At the junction of the reducer and the following pipe was a rubber gasket 1/16 in. thick which protruded into the air stream about 1/16 in. Its purpose was to trip any laminar boundary layer that would form. Following the gasket were 66 in. of straight copper pipe with an inside diameter of 1.50 in. and wall thickness 0.20 in. and finally 6 in. of Lucite pipe. This entire entrance section was covered with 1 in. of 85% magnesia insulation and 3 in. of glass wool. The insulation and the fact that the inlet air temperature was within 3°F of ambient temperature for all runs

assured a negligible temperature change throughout the length of the entrance section.

After the test section, which is described later, the air passed through a bed of silica gel contained between two screens in a steel box whose inside dimensions were 12 x 12 x 12 in. The silica gel was tested once during the course of the runs and following the runs. It still retained most of its absorptive capacity at the completion of the work, thus assuring that the air was dry throughout the investigation. The fact that the silica gel was not saturated was to be expected since careful testing revealed no leaks in the system. From the dryer the air passed again to the blower.

The Test Section

The five pieces of the test section were 0.606, 8.00, 1.003, 36.0, and 1.002 in. in length, respectively. The three short pieces served as calorimeters by means of which the heat flux at the wall could be determined as an average over their length. The manner in which the pieces were fitted together and other details of the calorimeters can be seen in Figure 27, which is a detail of Calorimeter B.

The other calorimeters were identical except that Calorimeter A was shorter, and there was no copper ring or face on the upstream side of the guard heater of Calorimeter A. The bottom half of the cross section shows the Chromel pins which kept the pieces from sliding. Bolts through the flange holes held the pieces together. The pieces were separated by polyethylene gaskets 0.01 in. thick. These were slightly undercut to be certain that they did not protrude into the stream. The gaskets, the Chromel pins of low thermal conductivity, and the operation of the equipment at uniform wall temperature meant that there could be very little longitudinal

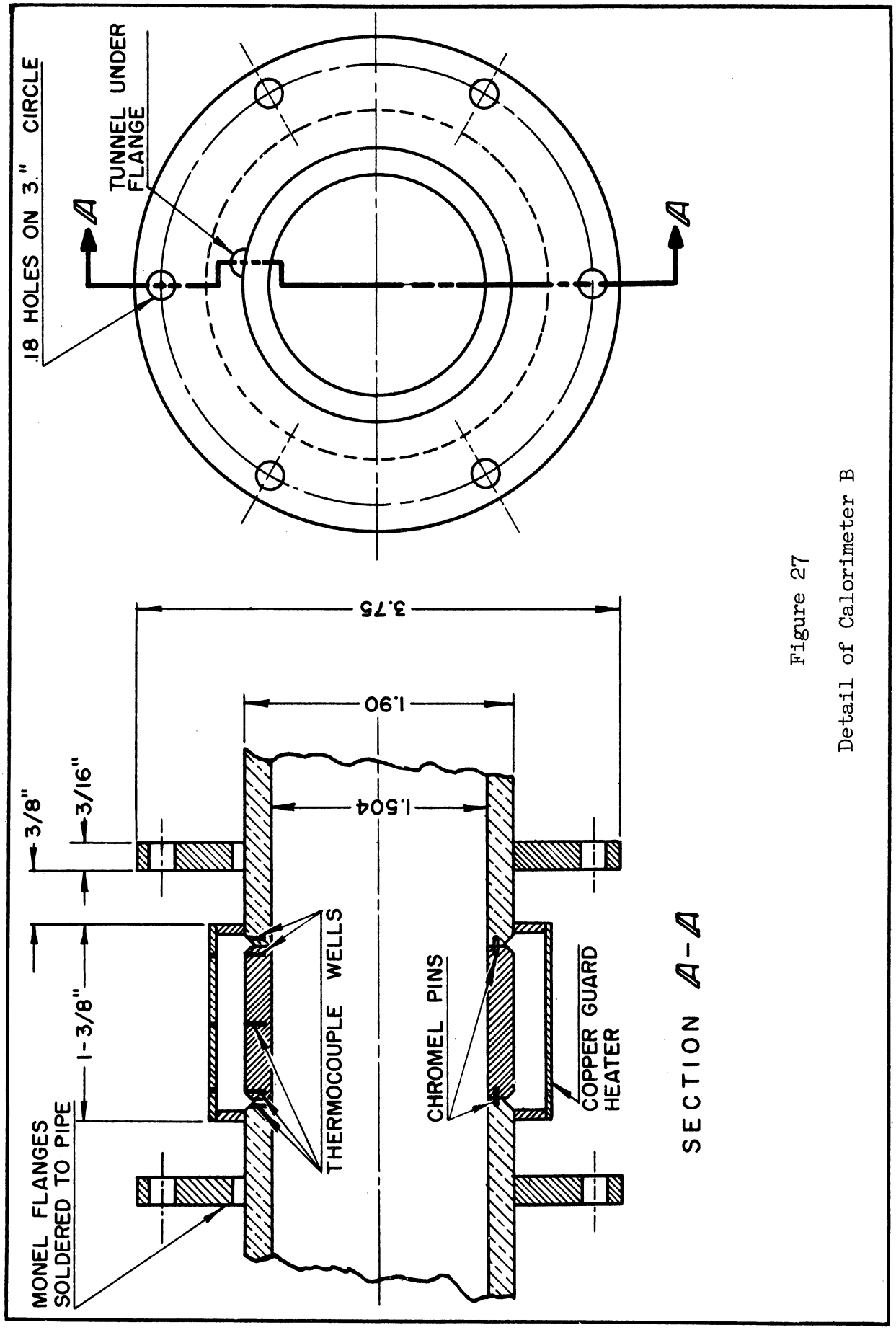

Figure 27

Detail of Calorimeter B

heat flow to or from the calorimeters.

The steps in wall surface at the junction of the sections were estimated to be 0.002 in. at the most, and these were removed by honing of the test and entrance sections in two assembled pieces. One piece consisted of the test section and the 6-in. plastic pieces at either end. The 66-in. entrance section and the attached reducer were honed separately to the same diameter, 1.504 in. from the original 1.496 in. The two-piece operation meant that there could have been a small step at the junction of the two assemblies 6 in. upstream of the thermal entrance at Calorimeter A. This step was not greater than 0.001 in. or 6000 step-heights downstream and thus had a negligible effect on the velocity distribution. The wall roughness after honing was about 30 microinches (36).

The axial location of the most important thermocouple wells can also be seen in Figure 27. Calorimeter A had four such wells, one at the upstream edge, one in the center, and two 60° apart at the downstream edge. Opposite these two in the neighboring 8-in. length of pipe were two more wells. Calorimeter B had three wells along one line, but the downstream thermocouple failed to operate. Calorimeter C had three wells, two upstream and one in the center. In addition to thermocouples in the wells mentioned above, thermocouples were located in the following places: (1) One was in the entrance section as previously described. (2) One was placed in a V groove in the downstream edge of the Lucite section upstream and adjacent to Calorimeter A. Its bead was about 0.01 in. in diameter, and the top of the bead was about 0.005 in. from the pipe surface. Since it was upstream of the gasket, it was 0.01 in. upstream of Calorimeter A. This thermocouple was located in a region of steep temperature gradients and was, therefore, not expected to give a reading which could be quanti-

tatively interpreted, but rather its purpose was to give an indication of the order of magnitude of the gradient in the plastic section. (3) One thermocouple was near the downstream end of the long copper pipe of the entrance section and was placed adjacent to the pipe wall under the insulation. It thus recorded essentially inlet temperature. (4) Thermocouples were placed in wells every two inches along the 8-in. and 36-in. sections. (5) One thermocouple was located on the outside surface of each calorimeter guard. All of the above thermocouples were of 36-gage Chromel-Constantan wire which were fused with a small flame. The beads were then cut to a length of less than 0.02 in., lacquered, and placed in the 0.020-in. diameter wells. All thermocouples were calibrated with air flowing in the apparatus under adiabatic conditions against a Bureau of Standards thermometer. The axial position of the thermocouple can be read from Table VII.

To return to the construction of the calorimeters—Figure 27 shows clearly the cross section of the calorimeter guards or guard heaters. Each guard was split axially into two 180° segments. When the thermocouples and heating coil were in place on the calorimeters, the guards were padded with fluffy cotton and clamped over the calorimeter. Heating wire of 36-gage Chromel wire was wrapped tightly around the outside of the guard, which was first coated with lacquer and a layer of tissue paper over the wet lacquer. In practice the guard served not only as a guard heater but also to give fine control of the temperature of the ends of the pipe adjacent to the calorimeters. Because of this latter function the temperature of the outside ring of the guard was always slightly above the calorimeter temperature. A correction was applied for this added heat, but the corrections were always less than 2%.

The calorimeters were heated with Chromel ribbon 1/8 x 0.0126 in., which was wrapped evenly around the calorimeters in coils about 1/16 in. apart. Grounding was prevented by a sprayed coat of lacquer and a layer of tissue paper. The leads to the Chromel coil were of 1/8 x 0.01-in. copper strips which were silver-soldered to the Chromel coil at the surface of the calorimeter. The copper strips were wrapped flush with the outside of the guard for about 1/2 in. before passing through the thermal insulation. Conduction from the leads was negligible.

The 8-in. and 36-in. sections were also sprayed with lacquer and covered with a layer of tissue paper before the heating coils were wrapped on the pipe. The 8-in. section was wrapped with 3/16-in. and the 36-in. section with 1/4-in.-wide Chromel ribbon 0.002 in. thick. These coils were tightly wrapped and spaced not greater than 1/8 in. apart except at the flanges. The coils were brought up close to the flanges and a copper lead went under the flange through a hole so that one coil could be placed on the other side of the flange between the flange and guard heater. Taps were provided at every second winding so that some of the current could be by-passed at arbitrary intervals. In this way the wall-temperature distribution could be controlled. It was possible, for example, to pass more current through the coils on either side of the flanges to make up for the wider coil spacing there. The flanges were 3/16 in. wide and made of low-thermal-conductivity Monel metal. They were slightly heated at their edges by a continuation of the guard heater coils. Since they were well insulated and constructed as described above, the ripples in surface temperature beneath the flanges were less than 0.2% of the difference between the mixed-mean temperature of the air and the wall temperature.

Four pressure taps were located 4, 45, 65, and 110 in. upstream of

Calorimeter C. The tap holes were 0.030 in. in diameter and were made free from burrs by the honing. Over the holes were soldered 1/8-in. stainless steel tubing 3/8 in. long to which was attached 1/8 in. inside diameter Tygon tubing. The tubing lengths differed by less than a ratio of two to one.

The entire test section except Calorimeter C was placed in a box made of 3/4-in. wood of inside dimensions 4 x 4 in. The box was then filled with vermiculite (exploded mica) insulation. Calorimeter C was outside the box but was thoroughly insulated with cotton as can be seen in Figure 28.

The Temperature-Velocity Probe and Traversing Mechanism

Temperature and velocity traverses were made only inside Calorimeter C except that after completion of the heat transfer runs the test section was dismantled and velocity traverses were made inside Calorimeter A. It was believed traverses elsewhere would be of little utility and would only serve to place an undesirable disturbance in the stream or pipe wall. The traversing mechanism is photographed in Figure 28, which shows the mechanism itself and the cotton insulation surrounding Calorimeter C on the right. The construction of the device was very simple. It consisted of a micrometer barrel rigidly mounted on supports fixed to the Lucite pipe downstream of Calorimeter C. The barrel bore down on a 3/8-in. ball bearing fixed to the top of the probe. The probe was held up against the micrometer by a small steel cable on each side which ran over pulleys and on which weights were hung.

The probe itself is photographed in Figure 29. It consisted of a piece of 1/8-in. stainless-steel tubing of 1/32-in. wall thickness bent to the shape shown. Its bearing was a 1/8-in., close pipe nipple which

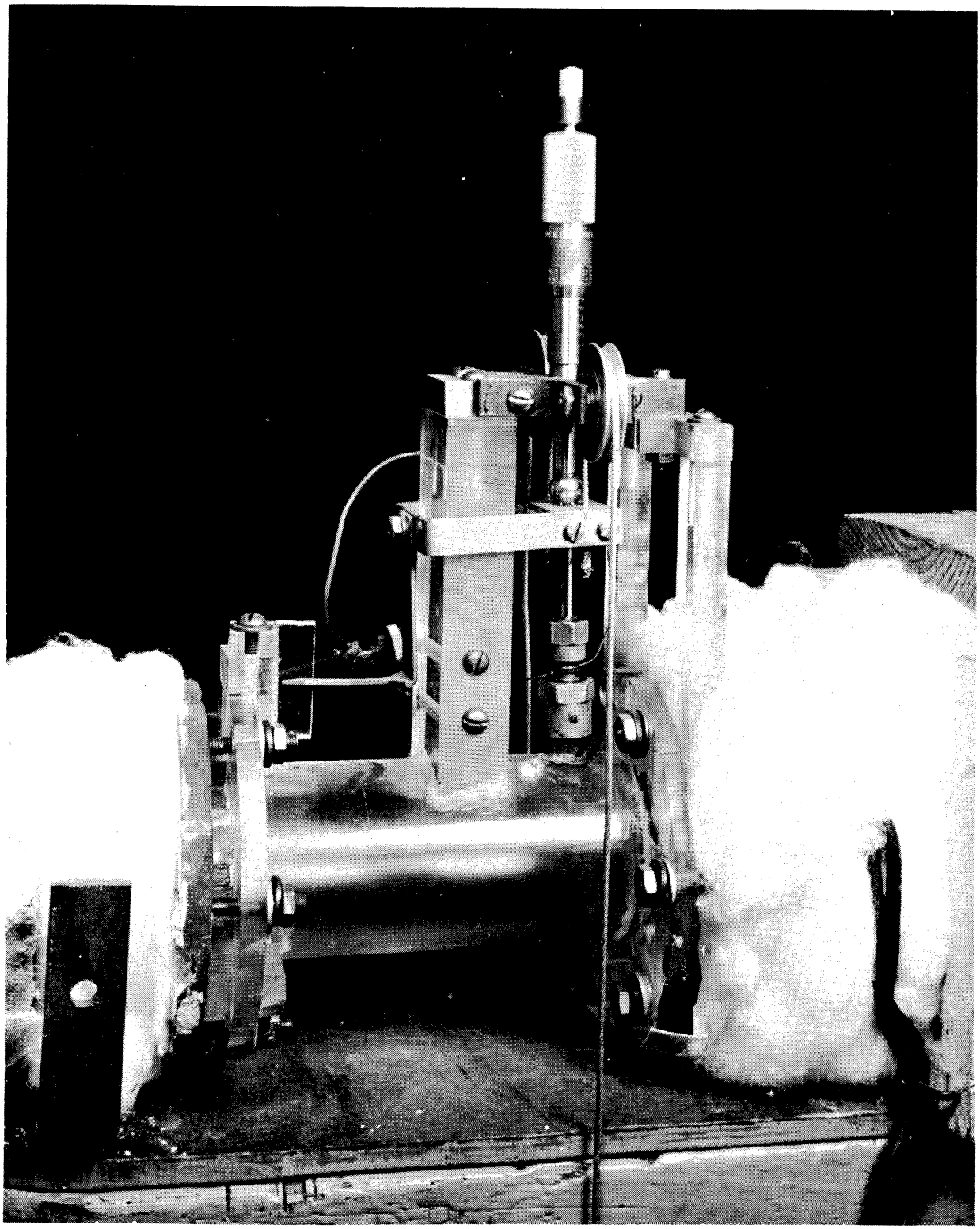

Figure 28. Traversing Mechanism

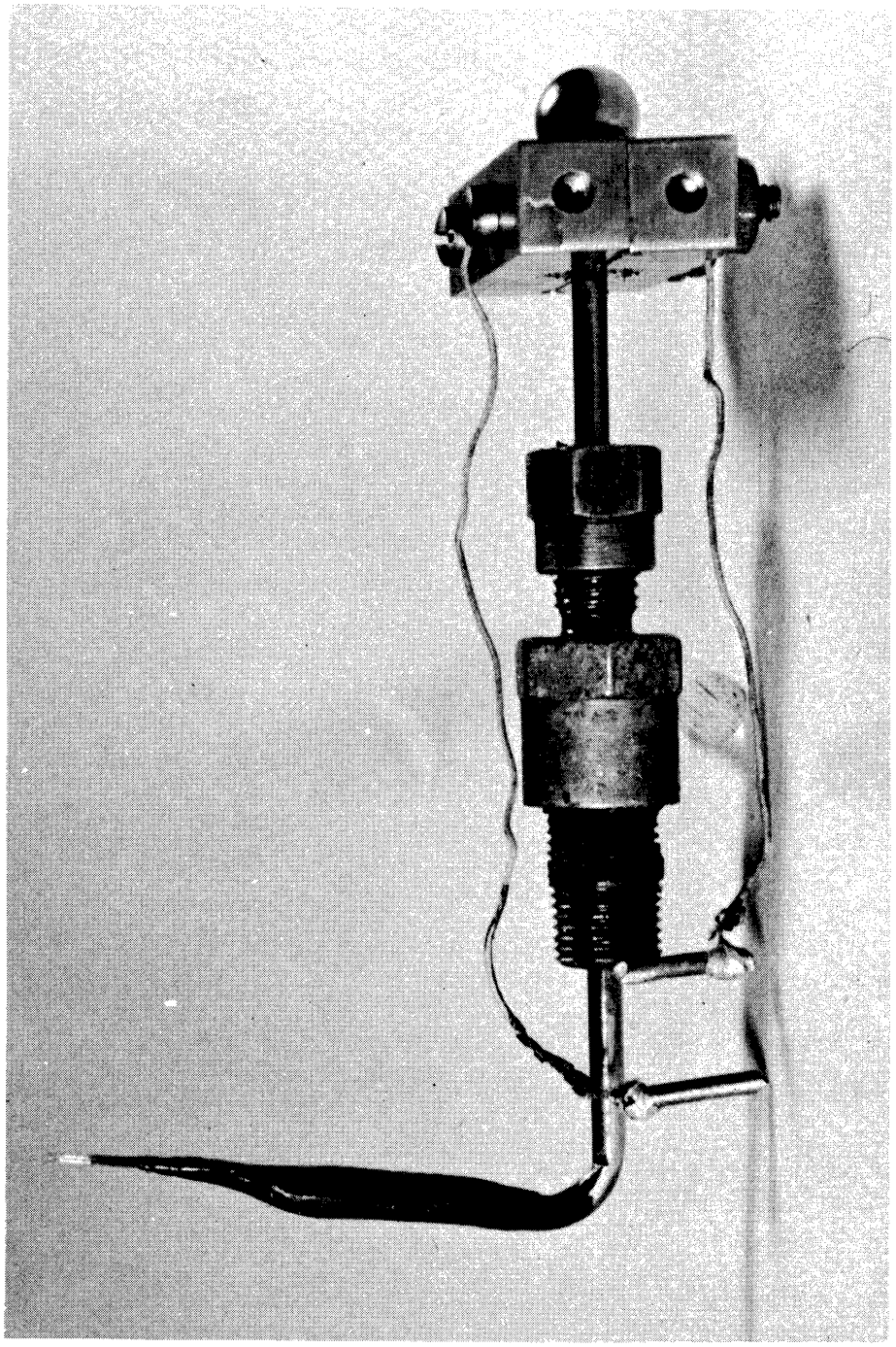

Figure 29. Velocity-Temperature Probe.

had been filled with brass and then carefully drilled out to a tight fit. The nipple was screwed into a high pressure tubing-to-pipe connector, the top of which was filled with graphite-string packing and which served as a packing gland. The bottom of the probe projected forward and slightly up and supported the steel needles.

Two copper wires were passed through the tube and soldered to the steel needles. The needles were then lacquered except at the tips, bound with thread to the tubing, covered with successive layers of Sauereisen cement, and finally lacquered. The final result was a streamlined and very stiff probe.

The fine platinum wires were placed across the tip of the probe by conventional techniques. That is, platinum wire 0.00016 or 0.00020 in. in diameter is procured imbedded in the center of silver wire 0.003 in. in diameter (Wollaston process). A short piece of this wire is bent into a semicircle and soldered to the needle tips in the stages shown in the following sketch.

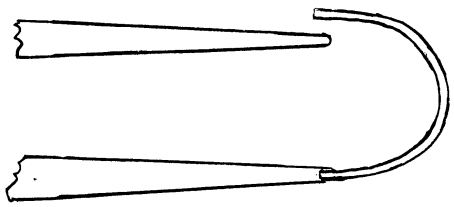

Step 1

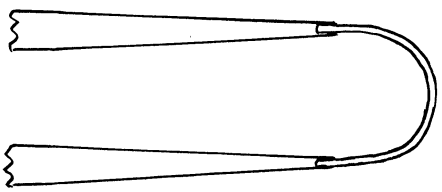

Step 2

The silver is then etched off the center of the arc with a jet of weak electrolyte through which a current is passed. As the silver is removed the two remaining wire stubs spring apart slightly because of the slight tension under which it is soldered, the tension being caused

by the gap between the wire and the needle shown in step 1 of the sketch. The amount of tension is quite critical because too much would snap the platinum wire and not enough would leave it bent in an arc. Enlarged photographs of the probe tip are shown in Figure 30. In the photographs the platinum wire is missing and the silver wires are bent slightly out of shape.

Two other considerations are important in the tip construction. The platinum wire must be at right angles to the traversing diameter, and the silver wire at the junction of the platinum must be that part of the probe tip which is closest to the pipe wall. With all of the foregoing restrictions, it is clear that the making of the probe tip is a very painstaking process.

One final consideration in the design of the probe was the possible generation of thermal E.M.F.'s caused by junctions of dissimilar metals at different temperatures. The whole probe was as symetrical as it could be made, and so thermal E.M.F. was not a problem. It was measured by placing the probe near a wall during a heat transfer run with no current flowing through the wire and found to be less than one microvolt for the entire circuit including the galvanometer. This E.M.F. was fairly constant and was little more than the reproducibility of voltage drop across the probe. Furthermore, the E.M.F. was not a function of probe location, so the very slight error it might have caused was constant throughout a traverse.

Instrumentation and Control

Most of the instrumentation and control methods have been adequately described in Section III. More detail is warranted, however, on the thermocouple circuitry. All of the thermocouple leads and the cold junction

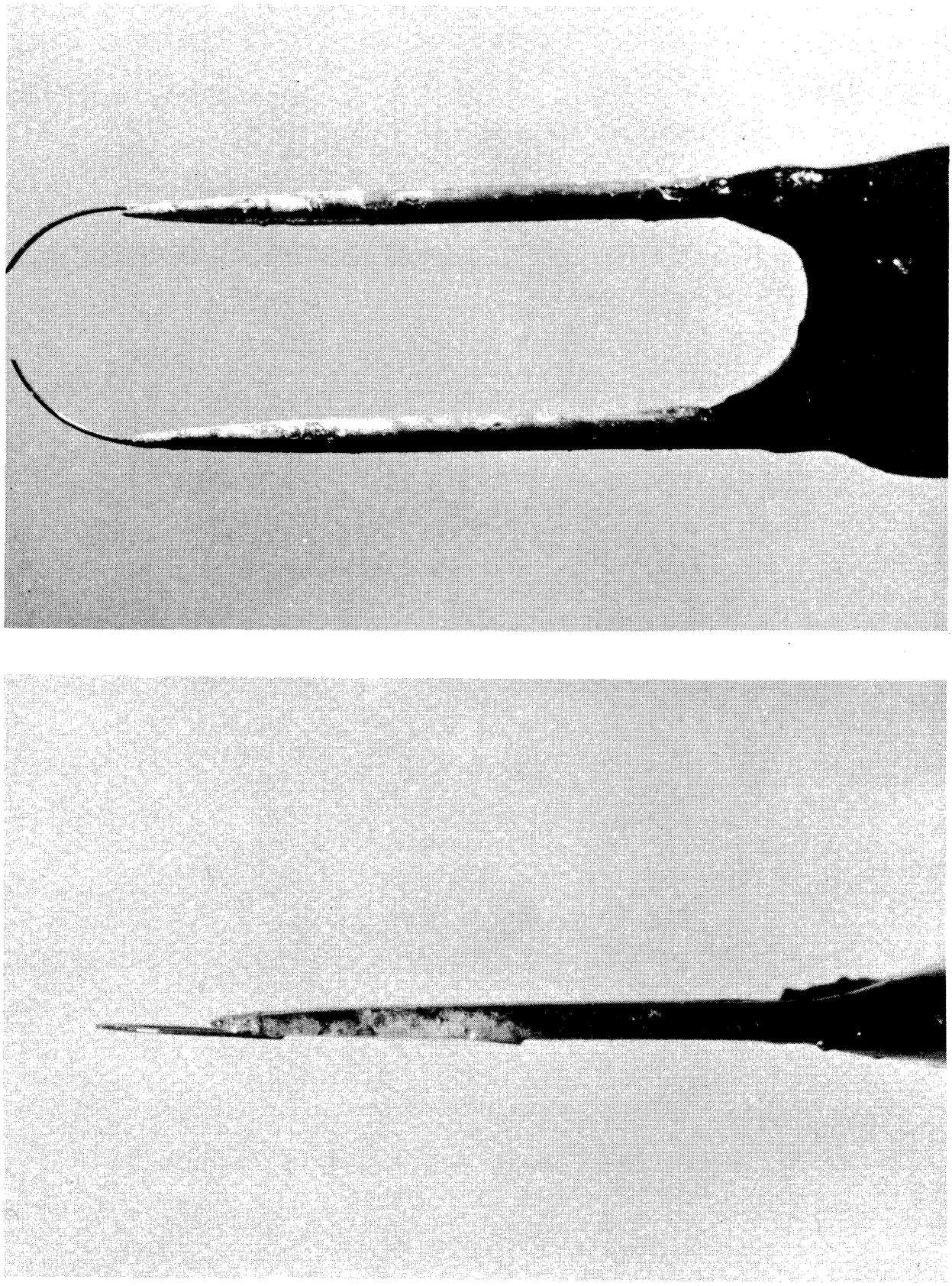

Figure 30. Probe Tips.

leads entered a well-insulated wooden box which was lined with copper to assure its being isothermal. The box housed four Leeds and Northrup 2-pole, 12-position selector switch, type 31-3. Copper wires connected the switches to the K-2 potentiometer.

The cold junction was immersed in purified kerosene in a small glass tube which was placed in melting ice in a well-insulated thermos bottle. Frozen distilled water was used at first, but the commercial crushed ice available in the Chemical Engineering Laboratory was used later since no difference in melting temperature could be detected between the two.

APPENDIX B

DETAILS OF PROCEDURE

In this appendix are some details of procedure not fully described in Section III. These details include some calculation procedures used to convert voltage readings to velocity or temperature.

Determination of Probe Location

The platinum wire at the probe tip was placed under a microscope with a traveling, calibrated hair line. The hair line was placed parallel to and on top of the wire and was then moved up to the uppermost edge of the supporting silver wire adjacent to the platinum wire. It was this edge that would make first contact with the pipe wall, and its distance from the platinum wire could be read directly on the dial of the hair line.

The probe circuit was so arranged that an ammeter with a full-scale deflection of 1.6 milliamps could be placed in series with the probe, a 16,000-ohm resistance, and a 24-volt storage battery. This circuit could be broken and one side grounded to the pipe so that contact of the probe tip with the pipe would close the circuit and deflect the ammeter. Very slight contact with the wall was sufficient to give nearly full-scale deflection of the meter because of the large series resistance. For example, even if the contact resistance were 16,000 ohms, a half-scale deflection of the needle would have resulted. In practice the device was extremely sensitive, and the contact reading could be reproduced to $\pm$ 0.0002 in. provided that temperature remained constant. The contact position was always read before and immediately after each traverse.

In order to assure that the platinum wire was parallel to the wall,

the tip was rotated about its axis so that first one side of the probe tip touched the wall and then the other. The angular position of the probe could be read on an attached pointer outside of the pipe. The probe was then raised slightly and the touching repeated until the angular position of the probe was found that would result in both sides of the probe touching the wall simultaneously as the probe was raised. The probe was then left at this angular position during a traverse. The position was maintained by keeping the pointer against an adjustable barrier. It should be emphasized that extreme care had to be taken in "touching" the probe tip to the wall. Any but the gentlest contact might have broken the platinum wire.

Calculation of Velocity

Measurement of instantaneous as well as mean velocity can be made with hot-wire anemometers, and the techniques are covered in a number of articles including Willis (61) and Kovásznay (23). The procedure adopted here was fairly simple. The mean velocity at the center of the tube was measured with a carefully made pitot tube (total-head tube) which was permanently mounted in the pipe at right angles to the hot-wire probe. This pitot tube was made of .08-in. stainless steel tubing and could be moved close to the wall. Its tip extended about 1-1/2 in. upstream into Calorimeter C about 1/4 in. downstream of the platinum wire. For calibration the probe was moved near the wall and the pitot placed at the center, at which time the pressure difference between the pitot tube and a wall pressure tap 4 in. upstream was measured. This pressure difference, after being corrected for the pressure drop between the static hole and the impact tube opening, was used to calculate the center velocity with the assumption that the pitot tube coefficient was unity. The pitot tube was

then moved to about 1/4 in. from the wall and the probe was moved to the center. At that position a constant current of about 40 milliamps was passed through the wire and the voltage drop across the probe and the standard, 10-ohm series resistance were measured with the K-2 potentiometer. The current was then reduced to 1.5 milliamps and the voltage readings again taken. These readings were used to calculate the hot resistance of the probe, R_p, and its cold resistance, R_p', measured with the 1.5 mil current.

The above procedure was repeated with the same current for velocities ranging from 7 to 120 ft/sec. Corresponding precisions were about 5 and 0.5%, respectively. The results were plotted as $\sqrt{u}$ vs $R_p/(R_p-R_p')$, which according to elementary theory (61) gives a straight line. In this case the line was straight except at velocities below about 20 ft/sec, where its slope was slightly greater. This plot was then used to calculate velocity from voltage readings with the probe at other positions.

When the hot-wire anemometer is used near the wall, two sources of error may lead to erroneous results. Very close to the wall, the wall acts as a heat sink, thus cooling the wire and raising the apparent velocity. In fact, this effect may cause the velocity to appear to increase near the wall. The effect was noticed with some 0.005-in.-diameter tungsten wires tried in the early experimental stages, but it was not observed with the 0.0002-in. platinum wires at distances greater than 0.0025 in. and velocities above 7 ft/sec, the minimum experimental conditions.

A second source of error is caused by the large velocity fluctuations near the wall and the fact that the behavior of the wire is nonlinear. A proper correction for this nonlinearity would require a knowledge of the voltage fluctuation across the wire. These data require much more elaborate

equipment than was on hand, and the procurement of more equipment was hardly merited by this aspect of the investigation. Furthermore, an approximate correction can be applied by making use of the measurements of velocity fluctuations reported by Laufer (26). The correction is derived as follows.

Time averages of voltage and velocity are measured and a plot made of $\sqrt{u}$ vs. $R_p/(R_p-R_p')$ or more precisely

$$\psi\left(\frac{R_p}{R_p - R_p'}\right) = \overline{\sqrt{u + u_x + v_y + w_z}} = \sqrt{u_1} \qquad (46)$$

where u_1 is the uncorrected value of the mean velocity, u, and u_x, v_y and w_z are the instantaneous values of the velocity fluctuations.

Neglecting the relatively small values of v_y and w_z

$$\sqrt{u_1} = \overline{\sqrt{u + u_x}} = \frac{1}{\Delta t'} \int_o^{\Delta t'} \sqrt{u + u_x}\, dt'$$

$$= \frac{\sqrt{u}}{\Delta t'} \int_o^{t'} \left(1 + \frac{u_x}{u}\right)^{1/2} dt'$$

$$= \frac{\sqrt{u}}{\Delta t'} \int_o^{t'} \left[1 + \frac{1}{2}\,\frac{u_x}{u} - \frac{1}{8}\left(\frac{u_x}{u}\right)^2 + \ldots . \, dt'\right]$$

where t' is time. The second term in the brackets integrates to zero and the third to the square of the root-mean-square, u'/u. Thus neglecting higher terms

$$\sqrt{u_1} = \sqrt{u}\left[1 - \frac{1}{8}\left(\frac{u'}{u}\right)^2\right]$$

or

$$u = \frac{u_1}{\left[1 - \frac{1}{8}\left(\frac{u'}{u}\right)^2\right]^2} \qquad (47)$$

The values of u' can be calculated from Laufer's data, and the above correction was applied to all velocity readings. The correction raised the velocity in the region $5 < y^+ < 20$, but the maximum correction was 4%.

Calculation of Temperature

Temperatures in the air stream were measured by using the platinum hot-wire anemometer as a resistance thermometer. This technique has been described in detail by Schlinger, et al. (48) and only the essentials will be covered here. To determine air temperature, the resistance of the platinum wire is measured by passing as small a current as possible through the wire. The resistance of the wire is a function of temperature, so the wire temperature can be calculated from its resistance after calibration. The air temperature is calculated from the wire temperature by applying three corrections which are functions of velocity. One correction is for aerodynamic heating of the wire: The total or stagnation temperature of flowing stream of a perfect gas is given by

$$t = t_g + \frac{u^2}{2g_c J C_p} \tag{48}$$

where t_g is the stream or static temperature. The wire with no current (adiabatic) actually comes to a temperature somewhat less than t given by

$$t_a = t_g + \gamma \frac{u^2}{2g_c J C_p} \tag{49}$$

where γ is the experimentally determined "recovery factor." The commonly accepted value of the recovery factor in the range of variables used is 0.66, reported by Hottel and Kalitinsky (16). This value was used here. With the above equations t_g and t can be computed from t_a.

The second correction is for heating of the wire caused by the current

used to measure its resistance. This correction can be determined in two ways: (a) by calculation from generalized correlations for the heat-transfer coefficient of cylinders at right angles to gas streams or (b) by measuring the resistance under given conditions with a series of currents and extrapolating to zero current. Both methods were employed here, and the agreement was excellent, as will be shown after a discussion of the third correction.

The third correction is for cooling of the wire at the ends. The fine wire is heated by the current, but the heavier supporting silver wires may be assumed to be close to t_a, the temperature assumed by an adiabatic wire. Some heat is, therefore, conducted from the platinum wire at its ends. Thus, this correction is really a correction to the electric heating correction. The correction is unimportant if length-to-diameter ratio of the wire is very large and high velocities are used. The ratio employed here was approximately 220, and at the lowest velocities used the correction to the electric heating was about 20%.

The latter two corrections can be combined, and they are derived as follows: The differential equation describing the temperature of a wire with uniform heat generation per unit length, Q; uniform heat-transfer coefficient, h, along its length axis, x; and ends and surroundings at $t = 0$ is

$$\frac{d^2t}{dx^2} - \frac{4h}{k_w D} t + \frac{4Q}{k_w \pi D^2} = 0$$

$$t(0) = 0$$

$$t(\infty) = \text{finite}$$

The solution of the equation is

$$t = \frac{Q}{\pi k_a Nu}\left[1 - e^{-\phi \frac{x}{D}}\right] \qquad (50)$$

where

$$\phi = 2\sqrt{Nu \frac{k_a}{k_w}}$$

and k_a and k_w are the thermal conductivities of the air and wire.

The average temperature can be determined by integration of (50) over the wire length, L, yielding

$$t_{av} = \frac{Q}{\pi k_a Nu}\left[1 + \frac{e^{-\phi \frac{L}{D}}}{\phi\ L/D} - \frac{1}{\phi\ L/D}\right] \qquad (51)$$

The term in brackets is the correction factor to be applied to account for the conduction cooling.

Radiation corrections were found to be less than 0.002°F and, therefore, negligible.

Schlinger, et al. (48), observed that very close to the wall the temperature corrections were not single-valued functions of point velocity but depended also on distance from the wall. With the wire used here, this effect amounted to less than 0.02°F at velocities greater than 4 ft/sec and was therefore neglected.

Figure 31 shows the individual and total corrections. The solid lines were calculated from equation (51) using Nusselt numbers that were averages of the values reported by McAdams (35) and those calculated from the data of Schlinger, et al. (48). Schlinger's results are about 10% lower than McAdams. The circles are experimental points for 1.475 milliamps determined by extrapolation to zero current.

The maximum error in temperature measurement was not caused by the

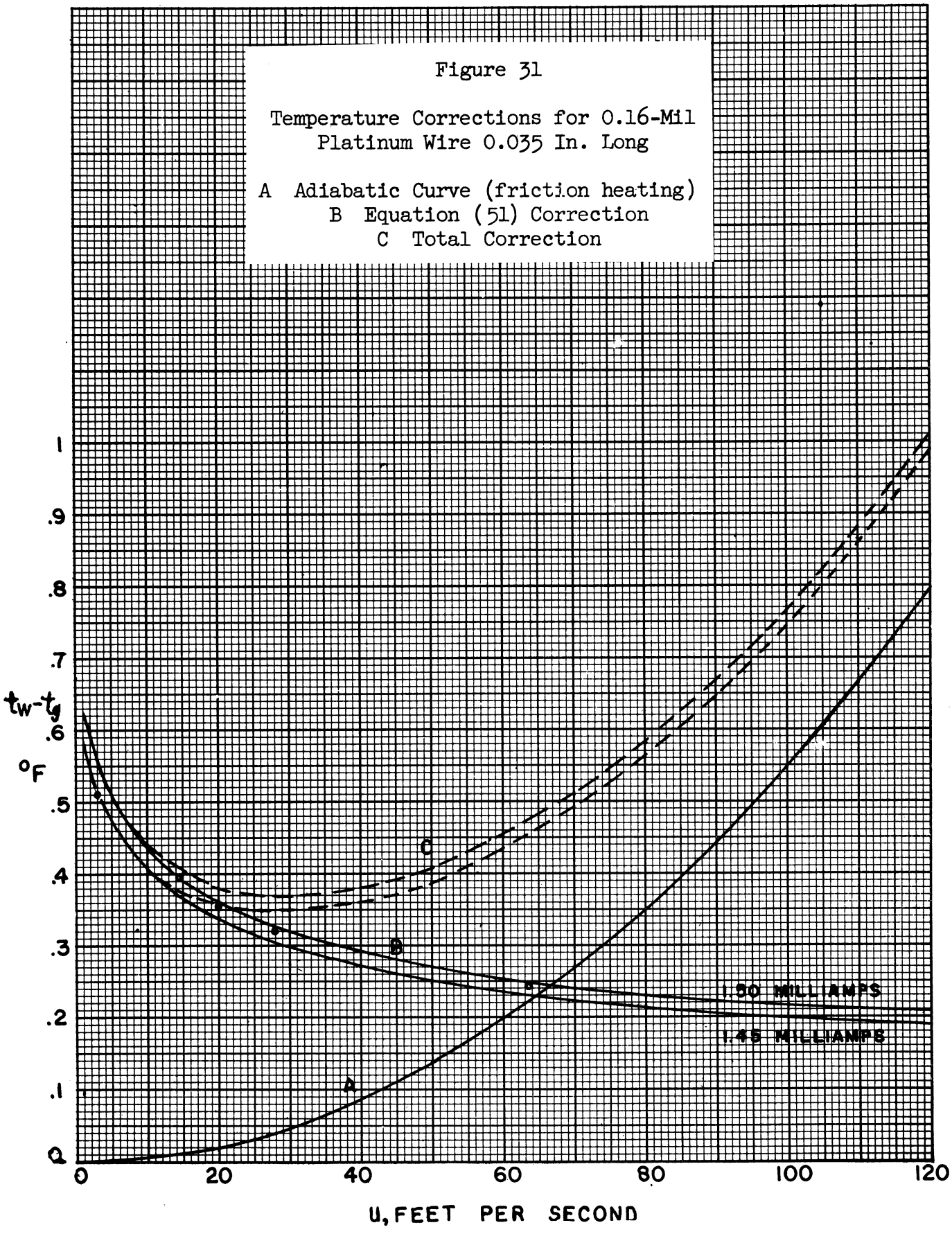
Figure 31
Temperature Corrections for 0.16-Mil Platinum Wire 0.035 In. Long
A Adiabatic Curve (friction heating)
B Equation (51) Correction
C Total Correction
$t_w - t_g$ °F
1
.9
.8
.7
.6
.5
.4
.3
.2
.1
0
0
20
40
60
80
100
120
U, FEET PER SECOND
A
B
C
1.50 MILLIAMPS
1.45 MILLIAMPS

above correction except perhaps at velocities above about 100 ft/sec and below about 10 ft/sec. Most of the error was due to limitations in the measuring equipment. The fine wires employed responded to the rapid, turbulent fluctuations in temperature, which caused oscillation of the electronic galvanometer despite the fact that a D.C. amplifier was used in order to observe the mean D.C. component of voltage. The K-2 potentiometer setting was determined by estimating by eye whether or not the mean reading of the galvanometer was zero. The reproducibility of the readings depended upon radial position of the probe, i.e., upon degree of turbulent fluctuation. The fluctuations were small in the center of the pipe, reached a maximum in the vicinity of $8 < y^+ < 15$, and then decreased closer to the wall. The reproducibilities were $\pm$ 0.25 microvolts over most of the range. Since the resistance of the probe was about 9 ohms and a 10-ohm standard resistance was used, the voltage drops caused by the 1.5- (approximate) milliamp current were 1.35 $\pm$ .00025 millivolts and 1.500 $\pm$ .0001 millivolts (no fluctuation), respectively. The resistance and its maximum error was thus 9.00 $\pm$ 0.025%. This error in resistance corresponded to a maximum error of about $\pm$ 0.07°F.

The temperature probe was calibrated against a thermocouple under isothermal conditions in the center of the pipe over a wider range of temperature than was employed in the test runs. It was calibrated before each run and two or more points were checked after each run. This procedure was necessary because the wire sometimes changed calibration very suddenly. The explanation is that a very small particle in the air stream collided with the wire and stretched it. This happened four times in the course of hundreds of hours of operation. The resistance of the wire always increased, the increase being of the order of 0.02%. On several

other occasions, wires were broken while in use.

It should be mentioned that fine tungsten wire proved unsatisfactory for temperature measurement because of apparent instability. Sometimes readings spaced a few minutes apart varied by as much as 1°F. Tungsten wire has the advantage of being much stronger than platinum wire, however.

APPENDIX C

SUMMARY OF DATA AND CALCULATED VALUES

On Figure 32 is plotted the experimental friction-factor data determined from measured pressure drop in the pipe and integrated velocity profiles. Some data on the plot were taken in the early experimental stages, and these data are not included in the tabulated velocity profiles that follow. Except for the scatter at low Reynolds numbers, the data are in excellent agreement with the chart of Moody (62).

Figure 33 shows the experimental ratio of mean velocity to maximum velocity. Also plotted is a mean line through the experimental points of Nikuradse (37) for comparison.

Following Figure 33 are tabulations of the principal data of this investigation in Tables VI, VII, VIII, and IX.

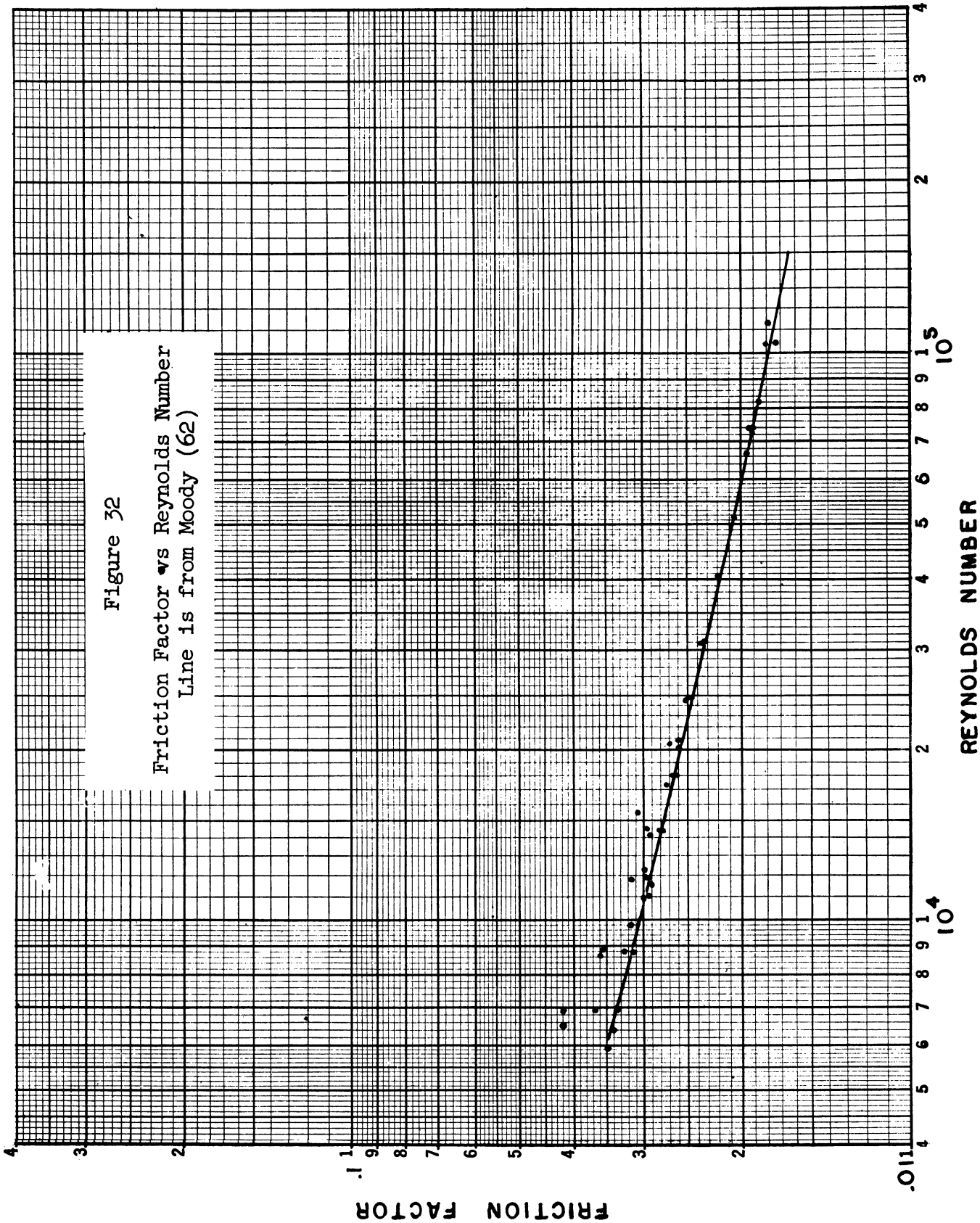

Figure 32

Friction Factor vs Reynolds Number
Line is from Moody (62)

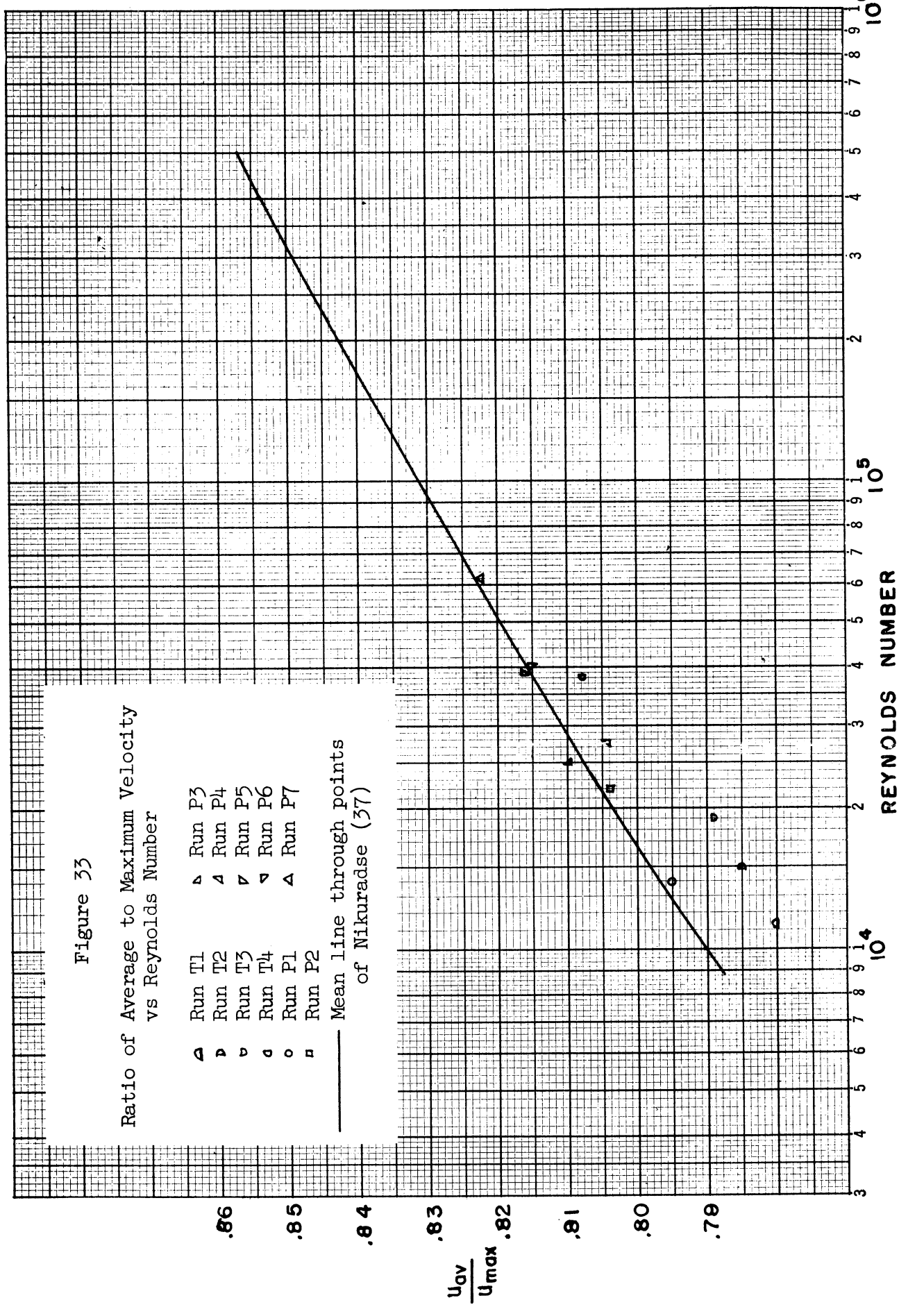
Figure 33
Ratio of Average to Maximum Velocity vs Reynolds Number
Run T1
Run T2
Run T3
Run T4
Run P1
Run P2
Run P3
Run P4
Run P5
Run P6
Run P7
Mean line through points of Nikuradse (37)
$\frac{u_{av}}{u_{max}}$
.86
.85
.84
.83
.82
.81
.80
.79
10^4
10^5
10^6
REYNOLDS NUMBER

TABLE VI

EXPERIMENTAL VELOCITY DISTRIBUTION

T Runs with Tungsten Probe
P Runs with Platinum Probe

Run T1

Re = 11,300 u_{av}/u_{max} = .780
u_{av} = 15.3 ft/sec f = .0296
u_{max} = 19.6 ft/sec

y, in.	$\frac{y}{a}$	y^+	u, ft/sec	u^+	$\frac{u_{max}-u}{U_\tau}$
.746	1.	349	19.6	20.5	0.
.636	.849	297	19.45	20.4	.16
.536	.715	251	19.0	20.0	.62
.436	.581	204	18.25	19.2	1.44
.336	.448	157	17.2	18.1	2.54
.236	.315	110	16.15	17.0	3.62
.136	.181	63.5	14.75	15.5	5.10
.086		40.1	13.45	14.2	
.066		30.8	12.5	13.1	
.046		21.5	11.15	11.7	
.036		16.8	9.8	10.3	
.031		14.5	9.0	9.45	
.026		12.1	7.8	8.2	

Run T2

Re = 15,100 u_{av}/u_{max} = .785
u_{av} = 20.4 ft/sec f = .0277
u_{max} = 26.0 ft/sec

y, in.	$\frac{y}{a}$	y^+	u, ft/sec	u^+	$\frac{u_{max}-u}{U_\tau}$
.748	1.	445	26.0	21.4	0.
.638	.851	380	25.9	21.35	.1
.537	.716	320	25.3	20.85	.58
.437	.583	261	24.7	20.3	1.16
.337	.450	201	23.2	14.1	2.30
.237	.316	141	21.7	17.9	3.6
.137	.183	81.5	19.9	16.4	5.1
.087		51.8	18.2	15.0	
.062		37.0	17.2	14.2	
.037		22.0	14.4	11.9	
.027		16.1	12.35	10.2	
.022		13.1	11.15	9.2	
.017		10.1	9.14	7.5	

TABLE VI (Continued)

Run T3

Re = 19,000 u_{av}/u_{max} = .789
u_{av} = 25.7 ft/sec f = .0262
u_{max} = 32.6 ft/sec

y, in.	$\frac{y}{a}$	y^+	u, ft/sec	u^+	$\frac{u_{max}-u}{U_\tau}$
.750	1.	548	32.6	22.0	0.
.605	.806	442	32.4	21.9	.13
.505	.672	369	31.5	21.2	.74
.405	.540	296	30.1	20.3	1.70
.305	.406	223	28.7	19.4	2.70
.205	.273	150	26.4	17.8	4.25
.105	.140	76.7	23.5	15.9	6.2
.055		40.2	21.0	14.2	
.035		25.8	18.6	12.5	
.025		18.3	16.4	11.1	
.020		14.6	14.5	9.8	
.017		12.4	13.0	8.8	
.015		11.0	11.9	8.0	
.013		9.50	11.2	7.55	
.011		8.05	9.5	6.4	
.009		6.6	8.25	5.6	

Run T4

Re = 39,000 u_{av}/u_{max} = .808
u_{av} = 51.9 ft/sec f = .0221
u_{max} = 64.2 ft/sec

y, in.	$\frac{y}{a}$	y^+	u, ft/sec	u^+	$\frac{u_{max}-u}{U_\tau}$
.750	1.	1,025	64.2	23.3	0.
.557	.741	760	62.7	22.8	.55
.357	.475	488	59.3	21.5	1.78
.257	.342	351	55.5	20.2	3.16
.157	.209	215	50.6	18.4	4.95
.1065	.142	145	47.7	17.3	6.00
.0565		77	42.9	15.6	
.0365		50	40.0	14.5	
.0265		36	37.0	13.5	
.0215		29	35.2	12.8	
.0165		22.5	32.3	11.7	
.0115		15.5	28.2	10.2	
.0095		13	25.4	9.2	
.0075		10	22.0	8.0	
.0065		8.9	20.0	7.3	
.0055		7.5	18.0	6.5	
.0045		6.2	15.9	5.8	

TABLE VI (Continued)

Run P1

Re = 14,800 u_{av}/u_{max} = .794
u_{av} = 20.15 ft/sec f = .0278
u_{max} = 25.4 ft/sec

y, in.	$\frac{y}{a}$	y^+	u, ft/sec	u^+	$\frac{u_{max}-u}{U_\tau}$
.7535	1.	448	25.4		0.
.6715	.893	400	25.3		.08
.5715	.760	340	24.9		.41
.4715	.627	281	24.3		.91
.3965	.527	236	23.5		1.57
.3215	.427	190	22.7		2.23
.2715	.361	161.5	21.9		2.90
.2215	.296	132	21.3		3.39
.1715	.228	102	20.4		4.13
.1465	.195	87.2	19.9	16.4	4.45
.1215		72.3	19.3	15.9	
.0965		57.4	18.5	15.3	
.0715		42.5	17.6	14.6	
.0465		27.7	15.8	13.1	
.0365		21.7	14.2	11.7	
.0265		15.8	12.0	9.95	
.0215		12.8	10.3	8.5	
.0165		9.8	7.95	6.6	

Run P2

Re = 21,800 u_{av}/u_{max} = .804
u_{av} = 29.5 ft/sec f = .0253
u_{max} = 36.7 ft/sec

y, in.	$\frac{y}{a}$	y^+	u, ft/sec	u^+	$\frac{u_{max}-u}{U_\tau}$
.7535	1.0	621	36.7		0.
.6715	.893	554	36.7		0.
.5715	.760	472	36.2		.30
.4715	.627	389	35.3		.83
.3965	.527	327	34.1		1.55
.3215	.427	265	32.7		2.38
.2715	.361	224	31.8		2.92
.2215	.296	183	30.6		3.63
.1715	.228	141	29.2		4.46
.1215	.195	100	27.8	16.5	5.30
.0965		79.5	26.5	15.75	
.0715		59.0	25.2	15.0	
.0465		38.4	23.5	14.0	
.0365		30.1	21.9	13.0	
.0265		21.9	19.9	11.8	
.0215		17.7	17.9	10.7	
.0165		13.6	15.8	9.4	
.0135		11.1	13.4	8.0	
.0115		9.5	11.7	7.0	
.0095		7.8	9.8	5.8	
.0075		6.2	7.9	4.7	

TABLE VI (Continued)

Run P3

Re = 25,100 u_{av}/u_{max} = .810
u_{av} = 34.1 ft/sec f = .0245
u_{max} = 42.1 ft/sec

y, in.	$\frac{y}{a}$	y^+	u, ft/sec	u^+	$\frac{u_{max}-u}{U_\tau}$
.754	1.0	700	42.1		0.
.672	.893	624	41.9		.10
.572	.760	531	41.5		.32
.472	.627	438	40.3		.96
.397	.528	369	39.4		1.44
.322	.428	299	37.6		2.40
.272	.362	252	36.8		2.82
.222	.295	206	35.7		3.41
.172	.229	160	34.2		4.70
.122		113	32.7	17.5	
.097		90	31.2	16.7	
.072		67	29.4	15.7	
.047		43.6	27.8	14.9	
.037		34.4	26.6	14.2	
.027		25.1	24.1	12.9	
.022		20.4	22.6	11.9	
.017		15.8	19.9	10.6	
.014		13.0	17.8	9.5	
.012		11.1	16.2	8.7	
.010		9.3	14.1	7.5	
.0080		7.4	11.9	6.4	
.0070		6.5	10.7	5.7	
.0060		5.6	9.4	5.0	
.0050		4.6	8.2	4.4	
.0040		3.7	6.9	3.7	
.0035		3.2	6.2	3.3	

TABLE VI (Continued)

Run P4

Re = 28,500 u_{av}/u_{max} = .804
u_{av} = 38.8 ft/sec f = .0237
u_{max} = 48.3 ft/sec

y, in.	$\frac{y}{a}$	y^+	u, ft/sec	u^+	$\frac{u_{max}-u}{U_\tau}$
.7533	1.0	790	48.3	22.8	0.
.6713	.893	705	48.3	22.8	.05
.5713	.760	600	47.3	22.35	.47
.4713	.627	495	46.4	21.9	.90
.3963	.527	415	44.7	21.2	1.70
.3213	.427	337	42.9	20.3	2.55
.2713	.361	285	42.0	19.9	2.97
.2213	.296	232	40.8	19.4	3.54
.1713	.228	180	38.9	18.4	4.44
.1213	.195	127	36.7	17.3	5.47
.0963		101	35.3	16.7	
.0713		74.8	33.8	16.0	
.0463		48.6	31.2	14.7	
.0363		38.1	29.6	14.0	
.0263		27.6	27.4	12.9	
.0213		22.4	25.1	11.8	
.0163		17.1	23.1	10.9	
.0133		14.0	20.6	9.7	
.0113		11.9	18.5	8.7	
.0093		9.8	16.45	7.8	
.0073		7.7	13.6	6.4	
.0063		6.6	12.1	5.7	
.0053		5.6	10.8	5.1	
.0043		4.5	9.0	4.3	

TABLE VI (Continued)

Run P5

Re = 39,100 u_{av}/u_{max} = .816
u_{av} = 51.9 ft/sec f = .0221
u_{max} = 63.5 ft/sec

y, in.	$\frac{y}{a}$	y^+	u, ft/sec	u^+	$\frac{u_{max}-u}{U_\tau}$
.7535	1.0	1,030	63.5		0.
.6715	.893		63.2		.11
.5715	.760		62.7		.29
.4715	.627		60.8		.99
.3965	.527		59.1		1.61
.3215	.427		57.3		2.26
.2715	.361		55.2		3.04
.2215	.296		53.1		3.80
.1715	.228		50.8		4.64
.1465	.195	201	49.6	18.0	5.08
.1215		166	48.2	17.6	
.0965		132	46.6	17.0	
.0715		98	44.5	16.2	
.0615		84.2	43.3	15.8	
.0515		70.5	42.5	15.5	
.0415		56.8	40.8	14.9	
.0315		43.1	38.9	14.2	
.0265		36.3	37.6	13.7	
.0215		29.4	35.8	13.1	
.0185		25.3	33.9	12.4	
.0155		21.2	31.9	11.6	
.0125		17.1	29.3	10.7	
.0105		14.4	26.6	9.7	
.0085		11.6	24.0	8.8	
.0065		8.9	19.9	7.3	
.0055		7.5	17.6	6.4	
.0045		6.2	15.8	5.8	
.0035		4.8	14.15	5.2	
.0030		4.1	11.7	4.3	
.0025		3.4	10.3	3.8	

TABLE VI (Continued)

Run P6

Re = 40,000 u_{av}/u_{max} = .815
u_{av} = 52.8 ft/sec f = .02205
u_{max} = 64.9 ft/sec

y, in.	$\frac{y}{a}$	y^+	u, ft/sec	u^+	$\frac{u_{max}-u}{U_\tau}$
.7535	1.0	1,053	64.9		0.
.6715	.893		64.3		.22
.5715	.760		63.5		.51
.4715	.627		61.6		1.19
.3965	.527		59.8		1.84
.3215	.427		57.6		2.64
.2715	.361		56.0		3.20
.2215	.296		54.2		3.85
.1715	.228	240	52.1		4.60
.1465	.195	205	51.1	18.1	
.1215		170	49.8	17.7	
.0965		135	47.3	16.8	
.0715		100	45.2	16.1	
.0615		86	43.7	15.6	
.0515		72	42.8	15.2	
.0415		58	41.1	14.6	
.0315		44.1	39.4	14.0	
.0265		37.1	38.5	13.7	
.0215		30.1	36.4	12.9	
.0185		25.9	34.7	12.3	
.0155		21.7	32.9	11.7	
.0125		17.5	30.3	10.8	
.0105		14.7	27.9	9.9	
.0085		11.9	24.5	8.7	
.0065		9.1	20.8	7.4	
.0055		7.7	18.8	6.7	
.0045		6.3	16.4	5.8	
.0035		4.9	14.0	5.0	
.0030		4.2	12.6	4.5	
.0025		3.5	11.2	4.0	

TABLE VI (Concluded)

Run P7

Re = 60,000 u_{av}/u_{max} = .815
u_{av} = 83 ft/sec f = .0199
u_{max} = 102 ft/sec

y, in.	$\frac{y}{a}$	y^+	u, ft/sec	u^+	$\frac{u_{max}-u}{U_\tau}$
.7534	1.0		102		0.
.6714	.893		101.8		.05
.5714	.760		99.8		.53
.4714	.627		97.0		1.21
.3964	.527		95.2		1.64
.3214	.427		92.1		2.38
.2714	.361		88.9		3.16
.2214	.296		85.7		3.94
.1714	.288	351	81.9		5.06
.1464	.195	300	79.6	19.3	5.40
.1214		249	76.9	18.6	
.0964		197	74.0	17.9	
.0714		146	70.2	17.0	
.0614		126	68.6	16.6	
.0514		105	67.1	16.2	
.0414		85	64.3	15.5	
.0314		64.4	60.8	14.7	
.0264		54.1	59.1	14.3	
.0214		44.0	57.1	13.8	
.0184		37.7	55.4	13.4	
.0154		31.6	52.6	12.7	
.0124		25.4	50.0	12.1	
.0104		21.3	46.5	11.2	
.0084		17.2	43.0	10.4	
.0064		13.1	37.6	9.1	
.0054		11.5	34.2	8.3	
.0044		9.0	30.5	7.4	
.0034		7.0	26.2	6.3	
.0029		5.9	23.7	5.7	
.0024		4.9	21.2	5.1	

TABLE VII

APPARATUS TEMPERATURES

Location	Distance from Thermal Distance, in.	Total Temperature, °F								
		Run 5	Run 5B	Run 6	Run 7	Run 8	Run 9	Run 10	Run 12	Run 13
Room		79.5	80.1	78.5	79.1	78.2	76.9	78.4	81.2	78.1
Inlet Air	-90	79.77	81.01	80.41	80.10	80.35	78.03	78.19	80.10	80.04
Inlet Pipe	-12	79.72	80.98	80.36	80.26	80.35	78.08	78.31	79.98	79.89
Inlet Plastic	- .010	89.98	91.26	80.41	88.6	92.37	90.78	91.66	85.89	85.89
Cal. A	.04	97.72	99.01		93.90	99.98	97.35	98.55	91.74	91.73
"	.30	97.98	99.28	80.44	94.00	100.22	97.52	98.76	91.97	91.96
"	.56	98.16	99.46		94.17	100.39	97.64	98.88	92.16	92.16
"	.56	98.33	99.61		94.26	100.51	97.74	98.99	92.34	92.34
Guard A		99.2	100.2		94.7	101.2	98.2	99.3	93.9	93.2
8" Section	.65	98.34	99.66		94.24	100.51	97.73	98.99	92.33	92.25
"	.65	98.21	99.52		94.17	100.40	97.65	98.92	92.36	92.10
"	2.6	98.28	99.60		94.23	100.45	97.68	98.95	92.25	92.16
"	4.6	98.34	99.67	80.53	94.26	100.46	97.68	98.98	92.19	92.17
"	6.6	98.40	99.73	80.54	94.27	100.48	97.68	98.98	92.24	92.22
"	8.58	98.34	99.70		94.23	100.46	98.67	98.96	92.19	92.17
Cal. B	8.67	98.28	99.63		94.24	100.49	97.70	98.88	92.19	92.19
"	9.13	98.30	99.64	80.62	94.26	100.51	97.71	98.88	92.21	92.20
"	9.59	-	-	-	-	-	-	-	-	-
Guard B		99.1	100.0		94.7	101.1	98.1	99.1	93.1	93.1
36" Section	9.68	98.27	99.61	80.82	94.23	100.49	97.77	98.85	92.25	92.23
"	11.6	98.30	99.66		94.27	100.52	97.83	98.88	92.28	92.25
"	13.6	98.30	99.67	80.95	94.27	100.52	97.85	98.90	92.25	92.19
"	15.6	98.31	99.67	81.05	94.27	100.52	97.85	98.88	92.22	92.11
"	17.6	98.39	99.76	81.20	94.31	100.58	97.91	97.42	92.31	92.22
"	19.6	98.33	99.70	81.36	94.30	100.54	97.85	98.85	92.22	92.14
"	21.6	98.31	99.67	81.64	94.29	100.54	97.86	98.85	92.27	92.17
"	23.6	98.28	99.64	81.98	94.27	100.52	97.85	98.81	92.31	92.20
"	25.6	98.25	99.61	82.46	94.27	100.54	97.86	98.82	92.27	92.14
"	27.6	98.24	99.61	83.10	94.26	100.54	97.88	98.82	92.24	92.13
"	29.6	98.24	99.60	83.95	94.27	100.57	97.91	98.84	92.25	92.13
"	31.6	98.22	99.57	85.11	94.24	100.57	97.91	98.84	92.24	92.08
"	33.6	98.24	99.57	86.67	94.24	100.55	97.91	98.84	92.24	92.08
"	35.6	98.27	99.57	88.74	94.26	100.58	97.92	98.87	92.30	92.13
"	37.6	98.22	99.52	91.31	94.22	100.57	97.89	98.85	92.27	92.10
"	39.6	98.22	99.51	93.27	94.22	100.57	97.91	98.88	92.28	92.10
"	41.6	98.24	99.51	94.52	94.24	100.57	97.92	98.93	92.33	92.10
"	43.6	98.34	99.58	95.27	94.34	100.60	97.96	98.93	92.37	92.22
"	45.59	98.27	99.49	95.18	94.26	100.52	97.94	98.93	92.31	92.14
Cal. C	45.68	98.29	99.54	95.27	94.26	100.52	97.92	98.96	92.29	92.19
"	45.68	98.27	99.51	95.25	94.26	100.51	97.91	98.95	92.27	92.16
"	46.14	98.30	99.56	95.28	94.30	100.57	97.94	98.98	92.25	92.19
Guard C		98.9	99.9	96.2	94.5	101.0	98.4	99.5	93.2	93.4

TABLE VIII

POINT VALUES OF TOTAL TEMPERATURE AND EDDY CONDUCTIVITY FOR HEAT-TRANSFER RUNS

Run 5

$Re = 38,600$
$t_o = 79.77°F$
$t_w = 80.30°F$

$\left(\frac{dt}{dy}\right)_w = -738°F/in.$

y, in.	y^+	t, °F	$\frac{\epsilon_c}{\nu}$
.7504	1022	83.71	
.6584	896	83.79	92
.5584	760	84.12	97.5
.4584	624	84.59	95
.3834	522	85.12	96
.3084	420	85.73	93
.2584	352	86.20	91
.2084	284	86.72	83.4
.1584	216	87.30	69.2
.1334	182	87.66	63.9
.1084	147.5	88.12	57.8
.0834	113.5	88.59	48.2
.0584	79.5	89.17	36.9
.0484	66.0	89.49	32.6
.0384	52.4	89.90	26.3
.0284	38.7	90.44	16.3
.0234	31.9	90.74	12.1
.0184	25.1	91.26	7.5
.0154	21.0	91.71	5.29
.0124	16.9	92.21	3.50
.0104	14.2	92.70	2.33
.0084	11.4	93.41	1.60
.0064	8.7	94.12	.96
.0054	7.4	94.62	.535
.0044	6.0	95.20	.265
.0034	4.6	95.90	.105
.0029	4.0	96.20	.070

TABLE VIII (Continued)

Run 5B

$Re = 38,400$
$t_o = 81.01°F$
$t_w = 99.56°F$
$\left(\frac{dt}{dy}\right)_w = -738°F/in.$

y, in.	y^+	t, °F	$\frac{\epsilon_c}{\nu}$
.7504		85.09	
.6584		85.18	91
.5584		85.50	94
.4584		86.03	95.5
.3834		86.51	94
.3084		87.15	93.5
.2584		87.58	90.5
.2084		88.08	84.4
.1584	214	88.70	72.3
.1334	180	89.03	65.5
.1084	147	89.47	55.7
.0834	112.5	89.96	43.9
.0584	78.7	90.57	36.0
.0484	65.4	90.80	31.6
.0384	51.9	91.25	25.5
.0284	38.3	91.71	17.3
.0234	31.6	92.14	11.5
.0184	24.8	92.55	6.39
.0154	20.8	93.03	4.78
.0124	16.7	93.64	3.37
.0104	14.0	94.07	2.41
.0084	11.3	94.73	1.66
.0064	8.65	95.50	1.05
.0054	7.3	95.93	.65
.0044	5.95	96.48	.35
.0034	4.6	97.11	.165
.0029	3.9	97.43	.115

TABLE VIII (Continued)

Run 7

$Re = 23,900$
$t_o = 80.15°F$
$t_w = 94.30°F$
$\left(\frac{dt}{dy}\right)_w = -370°F/in.$ (estimated)

y, in.	y^+	t, °F	$\frac{\epsilon_c}{\nu}$
.7503		83.81	
.6583		83.87	67.5
.5583		84.10	67
.4583		84.45	65.7
.3833		84.85	62.5
.3083		85.30	61.5
.2583		85.63	61.5
.2083		86.04	57
.1583	143.5	86.47	51.3
.1333	121	86.76	45.0
.1083	98	87.09	38.7
.0833	75.4	87.45	31.9
.0583	52.8	87.89	23.9
.0483	43.7	88.14	19.3
.0383	34.7	88.43	14.9
.0283	25.6	88.90	7.94
.0233	21.1	89.22	5.30
.0183	16.6	89.69	2.95
.0153	13.8	90.15	2.10
.0123	11.2	90.61	1.44
.0103	9.3	91.00	1.07
.0083	7.5	91.48	.78
.0073	6.6	91.70	.605
.0063	5.7	92.00	.39
.0053	4.8	92.31	.15
.0043	3.9	92.65	.070
.0033	3.0	93.03	.032

TABLE VIII (Continued)

Run 8

$Re = 24{,}000$
$t_o = 80.35°F$
$t_w = 100.55°F$
$\left(\frac{dt}{dy}\right)_w = -546°F/in.$

y, in.	y^+	t, °F	$\frac{\epsilon_c}{\nu}$
.7505		85.19	
.6585		85.26	66.5
.5585		85.59	66.5
.4585		86.16	65
.3835		86.69	63.5
.3085		87.36	62.5
.2585		87.86	61.5
.2085		88.42	60.3
.1585	143	89.03	52.6
.1335	121	89.42	47.9
.1085	98	89.85	38.8
.0835	75.5	90.35	30.1
.0585	53	91.14	21.1
.0485	43.9	91.43	17.8
.0385	34.8	91.84	14.0
.0285	25.8	92.56	8.04
.0235	21.3	93.04	5.97
.0185	16.7	93.70	3.09
.0155	14.0	94.33	2.15
.0125	11.3	95.03	1.51
.0105	9.5	95.62	1.13
.0085	7.7	96.28	.695
.0075	6.8	96.65	.40
.0065	5.9	97.12	.205
.0055	5.0	97.62	.10
.0045	4.1	98.12	.070
.0035	3.2	98.65	.039

TABLE VIII (Continued)

Run 9

$Re = 14,800$
$t_o = 78.06°F$
$t_w = 97.88°F$
$\left(\frac{dt}{dy}\right)_w = -358°F/in.$

y, in.	y^+	t, °F	$\frac{\epsilon_c}{\nu}$
.7507		83.46	
.6587		83.57	48
.5587		83.86	47.5
.4587		84.38	49
.3587		85.02	47
.2837		85.67	42.5
.2087		86.50	38.6
.1587	92.5	87.14	32.9
.1087	63.5	87.94	25.4
.0837	48.8	88.47	20.5
.0587	34.3	89.23	11.5
.0387	22.6	90.31	6.31
.0287	16.8	91.11	3.39
.0187	10.9	92.50	1.53
.0137	8.0	93.48	.84
.0107	6.25	94.25	.445
.0087	5.1	94.82	.25
.0077	4.5	95.18	.175
.0067	3.9	95.45	.125
.0057	3.3	95.82	.085

TABLE VIII (Continued)

Run 10

$Re = 14{,}200$
$t_o = 78.28°F$
$t_w = 98.97°F$
$\left(\frac{dt}{dy}\right)_w = -374°F/in.$

y, in.	y^+	t, °F	$\frac{\epsilon_c}{\nu}$
.7508		83.92	
.6588		83.99	47.5
.5588		84.31	48
.4588		84.89	47.5
.3588		85.55	46.5
.2838	162	86.26	44
.2088	120	87.07	40
.1588	90.8	87.68	34.7
.1088	62.3	88.55	26.0
.0838	48.0	89.10	19.6
.0588	33.6	89.91	12.4
.0388	22.2	90.98	6.04
.0288	16.5	91.92	3.19
.0188	10.7	93.38	1.60
.0138	7.9	94.35	.835
.0108	6.2	95.15	.365
.0088	5.0	95.80	.19
.0078	4.5	96.12	.12
.0068	3.9	96.50	.084
.0058	3.2	96.85	.057

TABLE VIII (Continued)

Run 12

$Re = 80,500$
$t_o = 80.10°F$
$t_w = 92.27°F$
$\left(\frac{dt}{dy}\right)_w = -924°F/in.$

y, in.	y^+	t, °F	$\frac{\epsilon_c}{\nu}$
.7535		81.90	
.6715		81.95	193
.5715		82.12	200
.4715		82.39	196
.3965		82.67	195
.3215		83.05	185
.2715		83.35	177
.2215		83.62	155
.1715	443	84.04	141
.1465	379	84.28	130
.1215	314	84.51	118
.0965	250	84.79	105
.0715	185	85.14	84.5
.0615	160	85.32	68
.0515	134	85.49	62.4
.0415	107	85.76	56.2
.0315	81.5	85.95	46.0
.0265	68.5	86.10	37.3
.0215	56.6	86.31	28.4
.0185	47.8	86.45	22.4
.0155	40.1	86.65	16.4
.0125	32.3	86.91	11.5
.0105	27.2	87.11	8.38
.0085	22	87.37	6.20
.0065	17	87.79	2.91
.0055	14	88.13	2.16
.0045	11.5	88.70	1.09
.0035	9	89.35	.72
.0030	7.8	89.70	.57
.0025	6.5	90.05	.40

TABLE VIII (Concluded)

Run 13

$Re = 80,100$
$t_o = 80.03°F$
$t_w = 92.19°F$
$\left(\frac{dt}{dy}\right)_w = -902°F/in.$

y, in.	y^+	t, °F	$\frac{\epsilon_c}{\nu}$
.7535		82.17	
.6715		82.19	199
.5715		82.42	198
.4715		82.62	194
.3965		82.93	188
.3215		83.28	180
.2715		83.55	170
.2215		83.88	156
.1715		84.25	137
.1465	376	84.52	130
.1215	312	84.73	119
.0965	248	85.01	105
.0715	184	85.34	79.5
.0615	158	85.47	71.3
.0515	132	85.71	63.5
.0415	106	85.91	55.1
.0315	81	86.13	44.5
.0265	68	86.41	29.7
.0215	55	86.57	25.8
.0185	47.5	86.75	21.6
.0155	40	86.93	17.6
.0125	32	87.20	13.4
.0105	27	87.38	10.6
.0085	22	87.65	6.15
.0065	16.5	88.07	3.19
.0055	14	88.36	1.90
.0045	11.5	88.84	1.21
.0035	9	89.37	.70
.0030	7.5	89.67	.48
.0025	6.5	90.00	.31
.0020	5	90.45	.165

TABLE IX

EIGENFUNCTIONS AND CONSTANTS

Laminar (Graetz)

		First Mode	Second Mode	Third Mode	Fourth Mode	Fifth Mode
λ^2		7.32	44.4	113	212	339
C		1.485	-.817	.607	-.514	.466
A		.748	.537	.458	.401	.361
R at r/a =	.0208	1.000	.992	.980	.964	.930
	.0625	.990	.942	.856	.740	.584
	.1042	.978	.866	.678	.440	.180
	.1458	.960	.760	.450	.120	-.164
	.1875	.934	.634	.206	-.160	-.338
	.229	.906	.486	-.020	-.328	-.310
	.271	.870	.332	-.206	-.366	-.130
	.3125	.830	.180	-.332	-.284	.086
	.354	.788	.036	-.386	-.126	.232
	.396	.740	-.096	-.374	.050	.258
	.4375	.692	-.208	-.306	.200	.160
	.479	.640	-.296	-.200	.274	.000
	.521	.588	-.364	-.070	.274	-.146
	.5625	.530	-.400	.060	.200	-.222
	.604	.476	-.420	.170	.086	-.210
	.646	.420	-.416	.254	-.040	-.120
	.6875	.368	-.396	.302	-.150	.000
	.729	.312	-.360	.320	-.228	.116
	.771	.260	-.334	.308	-.260	.194
	.8125	.208	-.260	.272	-.256	.224
	.8542	.160	-.202	.220	-.220	.212
	.8958	.112	-.144	.160	-.166	.166
	.9375	.066	-.086	.098	-.100	.102
	.9792	.022	-.028	.034	-.032	.034

Slug Flow

		First Mode	Second Mode	Third Mode
λ^2		11.54	60.8	148.6
C		1.595	-1.076	.876
A		.990	.990	.990
R at r/a =	.0208	1.000	.994	.984
	.0625	.994	.960	.902
	.1042	.982	.908	.780
	.1458	.968	.832	.614
	.1875	.946	.736	.420
	.229	.922	.624	.218
	.271	.896	.500	.024
	.3125	.862	.370	-.148
	.354	.824	.240	-.276
	.396	.782	.110	-.360
	.4375	.740	-.008	-.390
	.479	.692	-.120	-.370
	.521	.642	-.214	-.310
	.5625	.590	-.290	-.212
	.604	.536	-.348	-.098
	.646	.480	-.382	.024
	.6875	.420	-.396	.130
	.729	.364	-.390	.218
	.771	.306	-.362	.272
	.8125	.248	-.318	.290
	.8542	.190	-.260	.270
	.8958	.134	-.192	.216
	.9375	.080	-.116	.140
	.9792	.026	-.040	.048

TABLE IX (Continued)

Reynolds' Number: 8000 Prandtl Number: 0

		First Mode	Second Mode	Third Mode
λ^2		9.84	53.8	134
C		1.570	-.982	.777
A		.910	.800	.744
R at r/a =	.0208	1.000	.996	.984
	.0625	.994	.958	.894
	.1042	.982	.898	.754
	.1458	.966	.812	.572
	.1875	.946	.708	.360
	.229	.918	.586	.142
	.271	.888	.454	-.050
	.3125	.854	.316	-.214
	.354	.814	.180	-.324
	.396	.770	.048	-.380
	.4375	.724	-.072	-.382
	.479	.676	-.178	-.334
	.521	.626	-.264	-.244
	.5625	.570	-.334	-.130
	.604	.516	-.378	-.010
	.646	.460	-.400	.104
	.6875	.404	-.402	.200
	.729	.346	-.388	.266
	.771	.290	-.350	.298
	.8125	.236	-.302	.296
	.8542	.180	-.244	.260
	.8958	.126	-.176	.200
	.9375	.076	-.106	.124
	.9792	.024	-.036	.040

Reynolds' Number: 24,000 Prandtl Number: 0

		First Mode	Second Mode	Third Mode
λ^2		8.96	54.4	134.4
C		1.564	-1.000	.797
A		.915	.835	.790
R at r/a =	.0208	1.000	.992	.982
	.0625	.990	.954	.888
	.1042	.980	.892	.750
	.1458	.962	.810	.570
	.1875	.940	.704	.358
	.229	.914	.584	.140
	.271	.886	.454	-.050
	.3125	.848	.318	-.210
	.354	.810	.180	-.322
	.396	.768	.050	-.380
	.4375	.722	-.070	-.386
	.479	.672	-.174	-.338
	.521	.622	-.260	-.250
	.5625	.568	-.330	-.138
	.604	.514	-.376	-.018
	.646	.458	-.400	.098
	.6875	.400	-.404	.190
	.729	.344	-.390	.260
	.771	.288	-.352	.290
	.8125	.232	-.306	.290
	.8542	.178	-.246	.258
	.8958	.122	-.180	.200
	.9375	.072	-.108	.122
	.9792	.022	-.038	.040

TABLE IX (Continued)

Reynolds' Number: 80,300 Prandtl Number: 0

		First Mode	Second Mode	Third Mode
λ^2		10.10	55.2	136.0
C		1.570	-1.015	.811
A		.919	.860	.820
R at r/a =	.0208	1.000	.992	.986
	.0625	.990	.954	.894
	.1042	.980	.894	.750
	.1458	.962	.810	.574
	.1875	.942	.706	.368
	.229	.916	.586	.160
	.271	.886	.456	-.038
	.3125	.852	.320	-.200
	.354	.812	.182	-.314
	.396	.770	.056	-.374
	.4375	.724	-.064	-.388
	.479	.678	-.170	-.344
	.521	.626	-.258	-.260
	.5625	.572	-.326	-.154
	.604	.518	-.372	-.036
	.646	.462	-.398	.080
	.6875	.404	-.400	.180
	.729	.350	-.388	.250
	.771	.292	-.354	.288
	.8125	.238	-.306	.292
	.8542	.180	-.246	.260
	.8958	.128	-.178	.202
	.9375	.074	-.108	.128
	.9792	.024	-.034	.044

Reynolds' Number: 500,000 Prandtl Number: 0

		First Mode	Second Mode	Third Mode
λ^2		10.22	55.6	137.0
C		1.560	-1.020	.814
A		.922	.874	.839
R at r/a =	.0208	1.000	.996	.986
	.0625	.992	.960	.898
	.1042	.982	.900	.760
	.1458	.968	.820	.580
	.1875	.944	.716	.372
	.229	.918	.594	.160
	.271	.888	.462	-.040
	.3125	.852	.326	-.202
	.354	.812	.194	-.318
	.396	.772	.062	-.380
	.4375	.728	-.060	-.390
	.479	.680	-.164	-.348
	.521	.628	-.254	-.264
	.5625	.574	-.322	-.154
	.604	.520	-.372	-.034
	.646	.466	-.398	.082
	.6875	.408	-.402	.180
	.729	.350	-.390	.252
	.771	.294	-.358	.290
	.8125	.238	-.308	.294
	.8542	.182	-.250	.262
	.8958	.128	-.182	.206
	.9375	.066	-.110	.130
	.9792	.024	-.038	.042

TABLE IX (Continued)

Reynolds' Number: 8000 Prandtl Number: .01

		First Mode	Second Mode	Third Mode
λ^2		10.12	55.6	139.0
C		1.550	-.973	.750
A		.925	.815	.735
R at r/a =	.0208	1.000	.994	.982
	.0625	.994	.954	.888
	.1042	.980	.894	.746
	.1458	.966	.810	.562
	.1875	.944	.706	.352
	.229	.918	.586	.136
	.271	.888	.454	-.080
	.3125	.874	.316	-.218
	.354	.814	.182	-.326
	.396	.772	.052	-.380
	.4375	.726	-.068	-.382
	.479	.680	-.172	-.334
	.521	.628	-.260	-.244
	.5625	.574	-.330	-.134
	.604	.520	-.376	-.010
	.646	.466	-.400	.104
	.6875	.410	-.402	.200
	.729	.352	-.388	.264
	.771	.298	-.354	.296
	.8125	.240	-.306	.294
	.8542	.186	-.246	.260
	.8958	.130	-.180	.200
	.9375	.076	-.108	.124
	.9792	.026	-.038	.042

Reynolds' Number: 14,500 Prandtl Number: .01

		First Mode	Second Mode	Third Mode
λ^2		10.60	57.8	145.2
C		1.560	-.985	.765
A		.980	.866	.797
R at r/a =	.0208	1.000	.994	.984
	.0625	.994	.956	.890
	.1042	.980	.898	.754
	.1458	.966	.816	.576
	.1875	.944	.712	.370
	.229	.920	.594	.158
	.271	.890	.462	-.040
	.3125	.856	.326	-.200
	.354	.818	.192	-.318
	.396	.776	.060	-.380
	.4375	.730	-.060	-.384
	.479	.686	-.166	-.340
	.521	.634	-.254	-.258
	.5625	.582	-.324	-.146
	.604	.528	-.372	-.026
	.646	.474	-.400	.090
	.6875	.420	-.402	.188
	.729	.362	-.392	.256
	.771	.306	-.360	.294
	.8125	.250	-.312	.298
	.8542	.194	-.252	.266
	.8958	.136	-.184	.206
	.9375	.080	-.112	.130
	.9792	.026	-.038	.044

TABLE IX (Continued)

Reynolds' Number: 24,000 Prandtl Number: .01

		First Mode	Second Mode	Third Mode
λ^2		11.00	60.4	150.4
C		1.552	-.967	.768
A		1.020	.895	.840
R at r/a =	.0208	1.000	.996	.980
	.0625	.994	.958	.890
	.1042	.984	.900	.750
	.1458	.966	.818	.568
	.1875	.946	.714	.360
	.229	.920	.596	.148
	.271	.890	.462	-.048
	.3125	.856	.326	-.208
	.354	.820	.194	-.320
	.396	.778	.062	-.382
	.4375	.732	-.056	-.390
	.479	.686	-.160	-.345
	.521	.638	-.250	-.260
	.5625	.586	-.322	-.150
	.604	.532	-.372	-.030
	.646	.478	-.400	.088
	.6875	.420	-.404	.186
	.729	.364	-.394	.258
	.771	.310	-.364	.296
	.8125	.252	-.316	.300
	.8542	.196	-.258	.270
	.8958	.140	-.190	.210
	.9375	.080	-.114	.132
	.9792	.026	-.038	.044

Reynolds' Number: 38,500 Prandtl Number: .01

		First Mode	Second Mode	Third Mode
λ^2		11.30	62.6	156.4
C		1.560	-.982	.770
A		1.055	.937	.859
R at r/a =	.0208	1.000	.992	.984
	.0625	.996	.952	.892
	.1042	.982	.894	.756
	.1458	.968	.814	.580
	.1875	.948	.714	.380
	.229	.922	.598	.166
	.271	.894	.470	-.028
	.3125	.860	.336	-.192
	.354	.822	.200	-.304
	.396	.782	.072	-.370
	.4375	.740	-.046	-.382
	.479	.692	-.152	-.344
	.521	.640	-.240	-.266
	.5625	.590	-.314	-.160
	.604	.536	-.364	-.042
	.646	.482	-.394	.070
	.6875	.426	-.400	.172
	.729	.372	-.392	.248
	.771	.316	-.364	.288
	.8125	.258	-.318	.298
	.8542	.200	-.260	.274
	.8958	.142	-.194	.216
	.9375	.086	-.118	.140
	.9792	.028	-.040	.050

TABLE IX (Continued)

Reynolds' Number: 80,300 Prandtl Number: .01

		First Mode	Second Mode	Third Mode
λ^2		12.48	69.6	176
C		1.545	-.945	.746
A		1.185	.988	.907
R at r/a =	.0208	1.000	.992	.984
	.0625	.992	.954	.894
	.1042	.982	.900	.758
	.1458	.966	.818	.580
	.1875	.946	.720	.382
	.229	.922	.604	.176
	.271	.896	.480	-.020
	.3125	.862	.350	-.180
	.354	.826	.220	-.300
	.396	.788	.090	-.370
	.4375	.744	-.026	-.386
	.479	.700	-.134	-.356
	.521	.654	-.224	-.284
	.5625	.602	-.300	-.184
	.604	.554	-.356	-.068
	.646	.500	-.390	.046
	.6875	.446	-.404	.150
	.729	.394	-.400	.230
	.771	.338	-.376	.280
	.8125	.280	-.336	.296
	.8542	.220	-.280	.278
	.8958	.160	-.206	.224
	.9375	.096	-.128	.144
	.9792	.030	-.040	.046

Reynolds' Number: 150,000 Prandtl Number: .01

		First Mode	Second Mode	Third Mode
λ^2		14.92	83.6	215
C		1.522	-.935	.721
A		1.445	1.135	.997
R at r/a =	.0322	.998	.990	.950
	.0965	.984	.910	.750
	.161	.960	.796	.484
	.225	.926	.638	.186
	.2895	.886	.452	-.092
	.354	.836	.258	-.284
	.418	.780	.068	-.368
	.482	.716	-.100	-.344
	.546	.642	-.238	-.228
	.611	.568	-.334	-.066
	.675	.490	-.384	.096
	.740	.410	-.396	.220
	.804	.322	-.360	.284
	.868	.226	-.280	.266
	.905	.170	-.214	.224
	.915	.154	-.196	.204
	.925	.136	-.176	.188
	.935	.120	-.154	.166
	.945	.100	-.132	.142
	.955	.082	-.110	.120
	.965	.064	-.088	.096
	.975	.044	-.066	.068
	.985	.026	-.040	.040
	.995	.008	-.016	.016

TABLE IX (Continued)

Reynolds' Number: 500,000 Prandtl Number: .01

		First Mode	Second Mode	Third Mode
λ^2		28.5	175.0	454
C		1.462	-.775	.578
A		3.01	1.790	1.418
R at r/a =	.0322	.998	.988	.966
	.0965	.986	.920	.790
	.161	.968	.816	.546
	.225	.942	.676	.260
	.2895	.908	.512	-.010
	.354	.870	.332	-.226
	.418	.822	.154	-.350
	.482	.770	-.018	-.368
	.546	.712	-.160	-.300
	.611	.650	-.274	-.162
	.675	.576	-.350	.000
	.740	.518	-.390	.144
	.804	.440	-.394	.254
	.868	.346	-.350	.300
	.905	.288	-.304	.286
	.915	.268	-.286	.274
	.925	.246	-.264	.260
	.935	.222	-.240	.240
	.945	.194	-.214	.216
	.955	.166	-.184	.188
	.965	.134	-.148	.154
	.975	.100	-.110	.114
	.985	.060	-.068	.070
	.995	.020	-.024	.022

Reynolds' Number: 8000 Prandtl Number: .0240

		First Mode	Second Mode	Third Mode
λ^2		10.62	58.8	147.6
C		1.538	-.948	.740
A		.985	.840	.757
R at r/a =	.0208	1.000	.996	.986
	.0625	.996	.956	.898
	.1042	.982	.898	.758
	.1458	.966	.814	.578
	.1875	.948	.710	.370
	.229	.922	.590	.158
	.271	.894	.460	-.040
	.3125	.858	.324	-.200
	.354	.820	.190	-.336
	.396	.778	.058	-.376
	.4375	.734	-.060	-.384
	.479	.686	-.168	-.340
	.521	.636	-.258	-.258
	.5625	.584	-.326	-.146
	.604	.530	-.374	-.026
	.646	.476	-.400	.090
	.6875	.420	-.404	.186
	.729	.364	-.394	.256
	.771	.306	-.360	.294
	.8125	.252	-.332	.298
	.8542	.194	-.256	.268
	.8958	.140	-.186	.210
	.9375	.082	-.132	.132
	.9792	.026	-.036	.046

TABLE IX (Continued)

Reynolds' Number: 14,500 Prandtl Number: .0240

		First Mode	Second Mode	Third Mode
λ^2		11.44	63.6	159.6
C		1.537	-.944	.742
A		1.072	.906	.835
R at r/a =	.0208	1.000	.996	.982
	.0625	.994	.958	.892
	.1042	.982	.900	.750
	.1458	.968	.820	.574
	.1875	.948	.720	.366
	.229	.922	.600	.160
	.271	.894	.472	-.040
	.3125	.860	.338	-.200
	.354	.824	.202	-.318
	.396	.782	.076	-.380
	.4375	.740	-.048	-.390
	.479	.692	-.152	-.350
	.521	.642	-.242	-.266
	.5625	.592	-.318	-.158
	.604	.540	-.366	-.038
	.646	.488	-.400	.080
	.6875	.434	-.406	.180
	.729	.380	-.400	.252
	.771	.320	-.370	.294
	.8125	.264	-.326	.300
	.8542	.208	-.266	.276
	.8958	.146	-.200	.218
	.9375	.088	-.122	.138
	.9792	.026	-.042	.044

Reynolds' Number: 24,000 Prandtl Number: .0240

		First Mode	Second Mode	Third Mode
λ^2		12.66	70.2	178.8
C		1.530	-.940	.726
A		1.200	.995	.895
R at r/a =	.0208	1.000	.996	.984
	.0625	.994	.958	.898
	.1042	.982	.902	.762
	.1458	.966	.820	.586
	.1875	.950	.722	.390
	.229	.924	.608	.178
	.271	.898	.482	-.018
	.3125	.866	.350	-.182
	.354	.830	.216	-.300
	.396	.790	.086	-.370
	.4375	.748	-.032	-.388
	.479	.702	-.140	-.356
	.521	.674	-.230	-.280
	.5625	.602	-.304	-.180
	.604	.554	-.360	-.062
	.646	.500	-.394	.054
	.6875	.446	-.406	.156
	.729	.394	-.400	.236
	.771	.338	-.376	.286
	.8125	.280	-.334	.300
	.8542	.220	-.278	.280
	.8958	.160	-.208	.228
	.9375	.098	-.130	.150
	.9792	.034	-.044	.054

TABLE IX (Continued)

Reynolds' Number: 38,500 Prandtl Number: .0240

		First Mode	Second Mode	Third Mode
λ^2		14.96	84.4	215
C		1.543	-.933	.710
A		1.465	1.157	1.010
R at r/a =	.0322	1.000	.982	.956
	.0965	.984	.900	.756
	.161	.962	.778	.486
	.225	.932	.612	.182
	.2895	.888	.422	-.090
	.354	.840	.222	-.284
	.418	.780	.040	-.368
	.482	.716	-.130	-.340
	.546	.644	-.260	-.220
	.611	.568	-.348	-.060
	.675	.490	-.392	.110
	.740	.406	-.394	.232
	.804	.320	-.348	.290
	.868	.226	-.262	.266
	.905	.164	-.206	.220
	.915	.148	-.188	.204
	.925	.132	-.170	.184
	.935	.116	-.148	.166
	.945	.100	-.128	.142
	.955	.084	-.106	.120
	.965	.066	-.086	.096
	.975	.048	-.062	.070
	.985	.030	-.038	.042
	.995	.010	-.014	.014

Reynolds' Number: 80,300 Prandtl Number: .0240

		First Mode	Second Mode	Third Mode
λ^2		19.5	117.2	304
C		1.475	-.829	.641
A		1.990	1.335	1.160
R at r/a =	.0322	1.000	.988	.970
	.0965	.986	.914	.794
	.161	.966	.802	.540
	.225	.938	.654	.240
	.2895	.900	.478	-.040
	.354	.856	.286	-.250
	.418	.804	.102	-.360
	.482	.746	-.066	-.364
	.546	.684	-.206	-.272
	.611	.616	-.314	-.120
	.675	.544	-.378	.040
	.740	.472	-.400	.180
	.804	.388	-.380	.274
	.868	.284	-.314	.294
	.905	.220	-.254	.256
	.915	.200	-.234	.242
	.925	.180	-.210	.222
	.935	.160	-.188	.200
	.945	.138	-.162	.178
	.955	.116	-.138	.150
	.965	.090	-.108	.120
	.975	.066	-.080	.088
	.985	.040	-.048	.054
	.995	.014	-.016	.020

TABLE IX (Continued)

Reynolds' Number: 150,000 Prandtl Number: .0240

		First Mode	Second Mode	Third Mode
λ^2		26.1	156.8	410
C		1.460	-.800	.600
A		2.70	1.71	1.388
R at r/a =	.0322	1.000	.990	.956
	.0965	.990	.916	.770
	.161	.970	.806	.520
	.225	.944	.662	.230
	.2895	.910	.496	-.040
	.354	.868	.310	-.242
	.418	.820	.124	-.358
	.482	.764	-.040	-.364
	.546	.702	-.186	-.280
	.611	.640	-.296	-.140
	.675	.570	-.366	.022
	.740	.500	-.400	.164
	.804	.422	-.390	.266
	.868	.326	-.340	.298
	.905	.258	-.284	.276
	.915	.238	-.264	.262
	.925	.218	-.244	.244
	.935	.198	-.220	.224
	.945	.172	-.196	.200
	.955	.144	-.166	.178
	.965	.120	-.138	.142
	.975	.088	-.100	.108
	.985	.056	-.064	.070
	.995	.020	-.024	.024

Reynolds' Number: 500,000 Prandtl Number: .0240

		First Mode	Second Mode	Third Mode
λ^2		62.6	442	1182
C		1.370	-.620	.456
A		6.99	2.99	2.28
R at r/a =	.047	.998	.980	.922
	.141	.978	.858	.600
	.235	.950	.674	.214
	.329	.908	.446	-.124
	.423	.856	.204	-.322
	.517	.794	-.020	-.340
	.610	.722	-.200	-.204
	.705	.646	-.328	.000
	.799	.556	-.386	.194
	.893	.426	-.366	.306
	.9421	.338	-.306	.294
	.9464	.324	-.296	.284
	.9507	.312	-.284	.276
	.9550	.296	-.272	.264
	.9593	.278	-.258	.254
	.9636	.260	-.240	.240
	.9679	.240	-.224	.226
	.9722	.218	-.204	.208
	.9764	.194	-.180	.188
	.9807	.168	-.156	.160
	.9850	.136	-.126	.134
	.9893	.102	-.096	.100
	.99358	.064	-.060	.062
	.99786	.022	-.020	.022

TABLE IX (Continued)

Reynolds' Number: 8000 Prandtl Number: .10

	First Mode	Second Mode	Third Mode
λ^2	17.66	108.8	285
C	1.455	-.763	.546
A	1.807	1.12	.894
R at r/a = .0208	1.000	.994	.986
.0625	.996	.964	.904
.1042	.986	.914	.780
.1458	.974	.844	.616
.1875	.956	.756	.424
.229	.938	.650	.216
.271	.914	.534	.024
.3125	.888	.410	-.144
.354	.878	.284	-.276
.396	.826	.158	-.360
.4375	.790	.038	-.394
.479	.752	-.070	-.380
.521	.712	-.170	-.322
.5625	.677	-.254	-.230
.604	.626	-.320	-.122
.646	.580	-.370	-.008
.6875	.534	-.400	.102
.729	.482	-.412	.200
.771	.428	-.408	.274
.8125	.372	-.384	.316
.8542	.312	-.342	.320
.8958	.240	-.276	.284
.9375	.152	-.180	.196
.9792	.052	-.064	.070

Reynolds' Number: 14,500 Prandtl Number: .10

	First Mode	Second Mode	Third Mode
λ^2	22.6	143.6	380
C	1.430	-.733	.526
A	2.37	1.390	1.138
R at r/a = .0208	1.000	.998	.990
.0625	.996	.968	.914
.1042	.988	.918	.796
.1458	.978	.852	.636
.1875	.962	.764	.450
.229	.944	.664	.250
.271	.922	.554	.054
.3125	.900	.434	-.118
.354	.872	.308	-.252
.396	.842	.186	-.344
.4375	.808	.070	-.390
.479	.776	-.040	-.390
.521	.738	-.140	-.346
.5625	.698	-.228	-.266
.604	.658	-.300	-.166
.646	.616	-.352	-.056
.6875	.572	-.392	.056
.729	.524	-.410	.160
.771	.472	-.416	.250
.8125	.414	-.400	.310
.8542	.354	-.364	.334
.8958	.280	-.304	.312
.9375	.190	-.214	.236
.9792	.074	-.080	.094

TABLE IX (Continued)

Reynolds' Number: 24,000 Prandtl Number: .10

		First Mode	Second Mode	Third Mode
λ^2		30.2	197	520
C		1.420	-.686	.497
A		3.31	1.725	1.423
R at r/a =	.0208	1.000	.996	.986
	.0625	.994	.966	.908
	.1042	.986	.920	.794
	.1458	.978	.856	.640
	.1875	.960	.770	.450
	.229	.944	.672	.254
	.271	.924	.562	.060
	.3125	.902	.448	-.106
	.354	.876	.328	-.242
	.396	.848	.206	-.338
	.4375	.818	.090	-.388
	.479	.784	-.020	-.390
	.521	.748	-.120	-.352
	.5625	.710	-.206	-.278
	.604	.674	-.280	-.180
	.646	.632	-.334	-.074
	.6875	.590	-.376	.040
	.729	.546	-.402	.140
	.771	.500	-.410	.230
	.8125	.444	-.402	.298
	.8542	.386	-.374	.334
	.8958	.314	-.324	.326
	.9375	.222	-.238	.260
	.9792	.084	-.092	.100

Reynolds' Number: 38,500 Prandtl Number: .10

		First Mode	Second Mode	Third Mode
λ^2		36.6	264	712
C		1.400	-.633	.471
A		4.16	1.930	1.730
R at r/a =	.0322	1.000	.990	.968
	.0965	.992	.926	.800
	.161	.976	.828	.566
	.225	.954	.696	.294
	.2895	.926	.536	.020
	.354	.896	.360	-.200
	.418	.856	.184	-.338
	.482	.814	.020	-.378
	.546	.764	-.126	-.326
	.611	.714	-.246	-.204
	.675	.658	-.336	-.050
	.740	.598	-.392	.114
	.804	.524	-.410	.250
	.868	.418	-.380	.342
	.905	.350	-.338	.346
	.915	.328	-.320	.338
	.925	.304	-.300	.324
	.935	.278	-.276	.306
	.945	.248	-.250	.282
	.955	.216	-.220	.252
	.965	.180	-.186	.214
	.975	.136	-.144	.166
	.985	.088	-.092	.106
	.995	.030	-.032	.034

TABLE IX (Continued)

Reynolds' Number: 80,300 Prandtl Number: .10

		First Mode	Second Mode	Third Mode
λ^2		62.6	454	1230
C		1.380	-.568	.436
A		7.23	2.76	2.22
R at r/a =	.05	.998	.974	.924
	.15	.976	.828	.570
	.25	.944	.620	.164
	.35	.900	.374	-.180
	.45	.840	.118	-.342
	.55	.770	-.106	-.304
	.65	.692	-.280	-.120
	.75	.606	-.374	.100
	.85	.494	-.392	.272
	.9033	.420	-.360	.306
	.9100	.408	-.354	.306
	.9167	.394	-.344	.306
	.9233	.380	-.334	.304
	.9300	.364	-.320	.300
	.9367	.348	-.308	.294
	.9433	.330	-.296	.284
	.9500	.310	-.280	.274
	.9567	.290	-.262	.260
	.9633	.264	-.240	.240
	.9700	.234	-.216	.218
	.9767	.200	-.184	.188
	.9833	.158	-.144	.150
	.9900	.100	-.094	.096
	.99667	.034	-.034	.032

Reynolds' Number: 150,000 Prandtl Number: .10

		First Mode	Second Mode	Third Mode
λ^2		93.6	714	1980
C		1.345	-.558	.381
A		10.90	4.01	2.83
R at r/a =	.05	.996	.978	.930
	.15	.980	.840	.586
	.25	.950	.642	.190
	.35	.916	.400	-.160
	.45	.854	.146	-.340
	.55	.794	-.080	-.320
	.65	.724	-.252	-.150
	.75	.644	-.360	.074
	.85	.540	-.400	.266
	.9033	.466	-.380	.316
	.9100	.454	-.374	.318
	.9167	.442	-.366	.320
	.9233	.428	-.358	.320
	.9300	.414	-.350	.320
	.9367	.400	-.340	.316
	.9433	.384	-.326	.310
	.9500	.366	-.314	.302
	.9567	.346	-.298	.290
	.9633	.320	-.280	.276
	.9700	.290	-.254	.254
	.9767	.254	-.222	.226
	.9833	.206	-.180	.186
	.9900	.140	-.124	.130
	.99677	.052	-.046	.050

TABLE IX (Continued)

Reynolds' Number: 500,000 Prandtl Number: .10

		First Mode	Second Mode	Third Mode
λ^2		240	2200	5800
C		1.270	-.428	.298
A		28.8	7.66	5.35
R at r/a =	.0475	1.000	.976	.936
	.1425	.988	.862	.626
	.2375	.970	.696	.260
	.3325	.940	.484	-.080
	.4275	.902	.250	-.300
	.5225	.860	.030	-.354
	.6175	.806	-.158	-.250
	.7125	.752	-.298	-.060
	.8075	.682	-.382	.150
	.9025	.578	-.406	.320
	.9525	.500	-.376	.340
	.9575	.484	-.368	.338
	.9625	.468	-.360	.334
	.9675	.446	-.346	.324
	.9725	.424	-.328	.312
	.9775	.394	-.306	.298
	.9825	.356	-.280	.274
	.9875	.304	-.240	.236
	.99083	.262	-.208	.204
	.99250	.234	-.186	.186
	.99417	.200	-.158	.156
	.99584	.158	-.124	.124
	.99750	.106	-.082	.080
	.99917	.038	-.030	.028

Reynolds' Number: 8000 Prandtl Number: .718

		First Mode	Second Mode	Third Mode
λ^2		59.4	700	1995
C		1.228	-.322	.216
A		7.20	1.48	1.105
R at r/a =	.0322	1.000	.992	.970
	.0965	.998	.938	.814
	.161	.990	.850	.594
	.225	.978	.736	.328
	.2895	.964	.594	.064
	.354	.946	.438	-.160
	.418	.926	.276	-.312
	.482	.902	.116	-.376
	.546	.876	-.032	-.360
	.611	.846	-.160	-.270
	.675	.816	-.266	-.134
	.740	.780	-.352	.026
	.804	.736	-.412	.200
	.868	.674	-.442	.340
	.905	.628	-.440	.386
	.915	.606	-.434	.398
	.925	.580	-.422	.400
	.935	.548	-.404	.400
	.945	.510	-.380	.392
	.955	.460	-.348	.368
	.965	.396	-.302	.326
	.975	.296	-.228	.250
	.985	.180	-.138	.154
	.995	.060	-.046	.054

TABLE IX (Continued)

Reynolds' Number: 14,500 Prandtl Number: .718

		First Mode	Second Mode	Third Mode
λ^2		92.6	110.8	3200
C		1.185	-.321	.203
A		11.25	2.39	1.705
R at r/a =	.0322	1.000	.994	.980
	.0965	.996	.944	.840
	.161	.990	.862	.630
	.225	.980	.748	.378
	.2895	.966	.614	.108
	.354	.948	.460	-.122
	.418	.930	.300	-.292
	.482	.906	.140	-.378
	.546	.882	-.008	-.380
	.611	.856	-.140	-.308
	.675	.826	-.250	-.178
	.740	.792	-.340	-.018
	.804	.744	-.410	.168
	.868	.686	-.450	.336
	.905	.644	-.454	.398
	.915	.630	-.450	.408
	.925	.614	-.444	.418
	.935	.590	-.436	.424
	.945	.562	-.420	.424
	.955	.520	-.398	.414
	.965	.464	-.360	.386
	.975	.380	-.300	.330
	.985	.256	-.204	.226
	.995	.090	-.078	.080

Reynolds' Number: 24,000 Prandtl Number: .718

		First Mode	Second Mode	Third Mode
λ^2		133	1540	4320
C		1.220	-.332	.215
A		16.42	3.30	2.16
R at r/a =	.05	1.000	.974	.920
	.15	.988	.838	.570
	.25	.970	.620	.200
	.35	.946	.440	-.120
	.45	.914	.202	-.304
	.55	.876	-.016	-.318
	.65	.830	-.200	-.186
	.75	.778	-.334	.022
	.85	.704	-.412	.240
	.9033	.654	-.422	.314
	.9100	.644	-.422	.322
	.9167	.634	-.420	.330
	.9233	.622	-.418	.336
	.9300	.610	-.414	.340
	.9367	.600	-.408	.344
	.9433	.586	-.402	.346
	.9500	.570	-.396	.346
	.9567	.550	-.386	.342
	.9633	.524	-.370	.336
	.9700	.488	-.348	.320
	.9767	.436	-.312	.294
	.9833	.362	-.260	.246
	.9900	.246	-.178	.170
	.99667	.088	-.060	.060

TABLE IX (Continued)

Reynolds' Number: 38,500 Prandtl Number: .718

		First Mode	Second Mode	Third Mode
λ^2		193.6	2170	6210
C		1.214	-.334	.217
A		23.8	4.81	3.12
R at r/a =	.047	.998	.982	.944
	.141	.986	.872	.656
	.235	.972	.712	.298
	.329	.950	.504	-.058
	.423	.920	.280	-.288
	.517	.884	.060	-.360
	.610	.844	-.128	-.278
	.705	.800	-.276	-.098
	.799	.742	-.378	-.120
	.893	.654	-.426	.322
	.9421	.598	-.418	.368
	.9464	.590	-.412	.372
	.9507	.580	-.408	.372
	.9550	.574	-.402	.372
	.9593	.560	-.400	.370
	.9636	.548	-.392	.368
	.9679	.534	-.382	.362
	.9722	.516	-.368	.356
	.9764	.488	-.354	.342
	.9807	.454	-.330	.324
	.9850	.404	-.296	.294
	.9893	.332	-.244	.244
	.99358	.220	-.162	.168
	.99786	.076	-.058	.060

Reynolds' Number: 80,300 Prandtl Number: .718

		First Mode	Second Mode	Third Mode
λ^2		339	3820	11,080
C		1.200	-.324	.202
A		41.6	7.94	5.01
R at r/a =	.0404	1.000	.986	.954
	.1212	.992	.902	.724
	.202	.980	.780	.426
	.283	.962	.620	.104
	.364	.940	.432	-.160
	.445	.918	.240	-.326
	.525	.886	.050	-.366
	.606	.854	-.116	-.292
	.686	.816	-.248	-.140
	.768	.776	-.342	.040
	.849	.720	-.404	.222
	.9276	.626	-.420	.364
	.97125	.568	-.394	.380
	.97375	.560	-.388	.376
	.97625	.550	-.382	.372
	.97875	.540	-.376	.366
	.98125	.528	-.368	.362
	.98375	.512	-.358	.354
	.98625	.472	-.342	.340
	.98875	.460	-.322	.322
	.99125	.418	-.294	.294
	.99375	.350	-.246	.246
	.99625	.238	-.170	.170
	.99875	.080	-.064	.060

TABLE IX (Continued)

Reynolds' Number: 150,000 Prandtl Number: .718

		First Mode	Second Mode	Third Mode
λ^2		546	6030	16,860
C		1.210	-.343	.212
A		66.8	14.86	9.20
R at r/a =	.0408	.998	.984	.950
	.1225	.992	.904	.736
	.202	.978	.780	.440
	.286	.960	.620	.124
	.367	.940	.436	-.140
	.449	.912	.238	-.316
	.530	.880	.050	-.368
	.613	.848	-.118	-.312
	.694	.804	-.252	-.162
	.776	.758	-.360	.038
	.858	.690	-.434	.256
	.9392	.582	-.440	.396
	.9808	.520	-.404	.394
	.9825	.514	-.400	.390
	.9842	.504	-.394	.384
	.9858	.494	-.386	.378
	.9875	.480	-.376	.370
	.98916	.466	-.364	.360
	.99084	.448	-.352	.348
	.99250	.424	-.334	.330
	.99416	.388	-.306	.304
	.99584	.330	-.260	.260
	.99750	.236	-.190	.186
	.99917	.084	-.070	.068

Reynolds' Number: 500,000 Prandtl Number: .718

		First Mode	Second Mode	Third Mode
λ^2		1468	17,700	50,800
C		1.185	-.292	.178
A		179	30.5	17.68
R at r/a =	.0485	1.000	.980	.940
	.1455	.990	.868	.646
	.2425	.974	.704	.280
	.3395	.952	.500	-.064
	.436	.922	.270	-.300
	.534	.890	.050	-.366
	.630	.874	-.140	-.272
	.728	.810	-.280	-.084
	.825	.756	-.380	.140
	.9215	.670	-.420	.334
	.9717	.606	-.404	.366
	.9751	.594	-.400	.366
	.9784	.582	-.394	.364
	.9818	.568	-.382	.358
	.9852	.548	-.372	.352
	.98856	.524	-.356	.340
	.99194	.494	-.336	.320
	.99531	.440	-.300	.290
	.99725	.400	-.274	.260
	.99775	.376	-.256	.246
	.99825	.342	-.234	.224
	.99875	.290	-.198	.188
	.99925	.200	-.138	.132
	.99975	.094	-.052	.044

TABLE IX (Continued)

Reynolds' Number: 8000 Prandtl Number: 7.5

		First Mode	Second Mode	Third Mode
λ^2		122	2080	
C		1.060	-.109	
A		14.95	1.03	
R at r/a =	.047	1.000	.978	
	.141	.998	.874	
	.235	.994	.722	
	.329	.984	.526	
	.423	.976	.312	
	.517	.964	.100	
	.610	.952	-.090	
	.705	.936	-.286	
	.799	.916	-.374	
	.893	.878	-.472	
	.9421	.850	-.490	
	.9464	.836	-.490	
	.9507	.820	-.490	
	.9550	.804	-.486	
	.9593	.780	-.480	
	.9636	.752	-.468	
	.9679	.712	-.452	
	.9722	.662	-.426	
	.9764	.598	-.392	
	.9807	.516	-.340	
	.9850	.414	-.280	
	.9893	.300	-.202	
	.99358	.180	-.122	
	.99786	.058	-.042	

Reynolds' Number: 14,500 Prandtl Number: 7.5

		First Mode	Second Mode	Third Mode
λ^2		192	7100	
C		1.060	-.0995	
A		23.8	3.04	
R at r/a =	.045	1.000	.980	
	.135	.998	.880	
	.225	.994	.740	
	.315	.988	.560	
	.405	.978	.360	
	.495	.970	.160	
	.585	.958	-.024	
	.675	.946	-.186	
	.765	.930	-.320	
	.855	.908	-.436	
	.905	.890	-.474	
	.915	.880	-.482	
	.925	.874	-.492	
	.935	.860	-.498	
	.945	.848	-.504	
	.955	.826	-.506	
	.965	.792	-.500	
	.975	.722	-.474	
	.98167	.654	-.436	
	.98500	.580	-.394	
	.98833	.488	-.332	
	.99167	.364	-.248	
	.99500	.220	-.152	
	.99833	.074	-.052	

TABLE IX (Continued)

Reynolds' Number: 38,500 Prandtl Number: 7.5

		First Mode	Second Mode	Third Mode
λ^2		434	15,400	
C		1.060	-.0974	
A		54.3	3.01	
R at r/a =	.0485	1.000	.986	
	.1455	.998	.890	
	.2425	.994	.740	
	.3395	.984	.550	
	.436	.978	.336	
	.534	.964	.120	
	.630	.954	-.054	
	.728	.940	-.234	
	.825	.920	-.362	
	.9215	.880	-.462	
	.9714	.850	-.484	
	.9741	.842	-.482	
	.9769	.834	-.480	
	.9796	.820	-.476	
	.98237	.802	-.468	
	.98512	.778	-.460	
	.98787	.744	-.442	
	.99062	.684	-.412	
	.99267	.620	-.374	
	.99400	.550	-.334	
	.99533	.456	-.276	
	.99667	.338	-.206	
	.99800	.204	-.126	
	.999333	.070	-.042	

Reynolds' Number: 80,300 Prandtl Number: 7.5

		First Mode	Second Mode	Third Mode
λ^2		776	26,600	
C		1.061	-.0965	
A		97.1	5.12	
R at r/a =	.0492	1.000	.978	
	.1478	.998	.874	
	.246	.992	.720	
	.345	.986	.520	
	.443	.976	.300	
	.541	.964	.084	
	.640	.952	-.100	
	.739	.936	-.262	
	.836	.914	-.382	
	.9348	.874	-.474	
	.98475	.840	-.480	
	.98625	.830	-.476	
	.98775	.818	-.470	
	.98925	.802	-.464	
	.99075	.784	-.452	
	.99225	.758	-.440	
	.99375	.718	-.414	
	.99525	.650	-.374	
	.99633	.574	-.336	
	.99700	.502	-.292	
	.99767	.408	-.238	
	.99833	.300	-.172	
	.99900	.182	-.104	
	.999667	.062	-.034	

TABLE IX (Concluded)

Reynolds' Number: 150,000 Prandtl Number: 7.5

		First Mode	Second Mode	Third Mode
λ^2		1260	46,400	
C		1.053	-.0878	
A		158	7.51	
R at r/a =	.0495	1.000	.980	
	.149	.998	.878	
	.248	.994	.722	
	.347	.986	.526	
	.446	.978	.304	
	.545	.966	.086	
	.645	.956	-.102	
	.744	.940	-.256	
	.844	.920	-.374	
	.9425	.880	-.470	
	.992375	.842	-.478	
	.993125	.830	-.468	
	.993875	.814	-.460	
	.994625	.794	-.450	
	.995375	.766	-.436	
	.996125	.730	-.416	
	.996875	.676	-.386	
	.997625	.590	-.336	
	.998165	.504	-.284	
	.998500	.426	-.242	
	.998833	.320	-.192	
	.999165	.246	-.136	
	.999500	.148	-.084	
	.999833	.050	-.032	

Reynolds' Number: 500,000 Prandtl Number: 7.5

		First Mode	Second Mode	Third Mode
λ^2		3250	139,600	
C		1.045	-.0731	
A		408	15.95	
R at r/a =	.0495	1.000	.980	
	.150	.998	.878	
	.250	.994	.722	
	.349	.988	.530	
	.449	.980	.310	
	.549	.972	.100	
	.648	.960	-.094	
	.748	.950	-.248	
	.848	.934	-.376	
	.9475	.896	-.482	
	.99714	.860	-.486	
	.99741	.844	-.478	
	.99769	.826	-.468	
	.99796	.804	-.456	
	.99824	.774	-.438	
	.998513	.736	-.416	
	.998788	.680	-.386	
	.999063	.596	-.340	
	.999267	.514	-.294	
	.999400	.440	-.252	
	.999534	.350	-.202	
	.999667	.254	-.148	
	.999800	.152	-.086	
	.999933	.050	-.030	

APPENDIX D

SAMPLE CALCULATIONS AND DERIVATIONS

In this appendix are calculations referred to earlier in the report.

Nusselt Number for Uniform Wall Temperature

By definition

$$Nu = \frac{hD}{k} = \frac{qD}{k(t_w - t_{mm})} \tag{52}$$

Equation (6) is the expression for q and it now remains to find t_{mm} as follows:

$$t_{mm} = \frac{\int_o^a urtdr}{\int_o^a urdr}$$

$$= \frac{\int_o^1 fr_* tdr_*}{\int_o^1 fr_* dr_*} = 2\int_o^1 fr_* tdr_* \tag{53}$$

Substitution of equation (4) into (53) and carrying out the indicated integration yields

$$t_{mm} = t_w + 2(t_o - t_w) \sum_n C_n e^{-\lambda_n^2 \beta x} \int_o^1 fr_* R_n dr_* \tag{54}$$

Substitution of equations (6) and (54) into (52) yields

$$Nu(x) = \frac{2\sum_n A_n e^{-\lambda_n^2 \beta x}}{\sum_n C_n e^{-\lambda_n^2 \beta x} \int_o^1 fr_* R_n dr_*} \tag{55}$$

One integration of equation (5) shows that

$$C_n \int_o^1 f r_* R_n dr_* = \frac{4A_n}{\lambda_n^2} \tag{56}$$

Substitution of (56) into (55) yields the final result

$$Nu(x) = \frac{\sum_n A_n e^{-\lambda_n^2 \beta x}}{2\sum_n \frac{A_n}{\lambda_n^2} e^{-\lambda_n^2 \beta x}} \tag{36}$$

Temperature Distribution for Linear Wall Temperature

This calculation will illustrate the method of Tribus and Klein (57) for finding fluid-temperature distribution or heat flux for arbitrary wall-temperature distribution. From Tribus and Klein

$$t - t_o = \int_{\xi=o}^{x_*} \left[1 - \theta(x_*-\xi, r_*)\, dt_w(\xi)\right] \tag{57}$$

and if

$$t_w(x_*) - t_o = Bx_* \tag{58}$$

$$\frac{dt_w(x_*)}{dx_*} = B$$

Substituting the expression for θ in (57), one may write

$$t - t_o = \int_o^{x_*} \left[1 - \sum_n C_n R_n e^{-\lambda_n^2 (x_*-\xi)}\right] \frac{dt_w(\xi)}{d\xi}\, d\xi$$

$$= Bx_* - B\sum_n C_n R_n e^{-\lambda_n^2 x_*} \int_o^{x_*} e^{\lambda_n^2 \xi}\, d\xi$$

Carrying out the integration yields the final result

$$t - t_o = Bx_* - B\sum_n \frac{C_n R_n}{\lambda_n^2}\left(1 - e^{-\lambda_n^2 x_*}\right) \qquad (38)$$

The heat flux at the wall and the Nusselt number can be calculated from (38) by the same procedures outlined for the uniform wall-temperature case.

Uniform Heat Flux at the Wall

The equations for this case are derived in Tribus and Klein (57) and Sellars, Tribus, and Klein (51) and are given on page 76. A few remarks about their equations are appropriate, however.

The Nusselt number for uniform heat flux has been shown by the above authors to be

$$Nu = \frac{1}{-\frac{1}{2}\sum_m \frac{1}{\gamma_m^4 H'(-\gamma_m^2)} - \frac{1}{2}\sum_m \frac{e^{-\gamma_m^2 \beta x}}{\gamma_m^4 H'(-\gamma_m^2)}} \qquad (59)$$

From (59) the fully developed Nusselt number is

$$Nu = \frac{1}{-\frac{1}{2}\sum_m \frac{1}{\gamma_m^4 H'(-\gamma_m^2)}} \qquad (60)$$

It has been shown by the above authors and others, however, that after entrance effects have decayed, the wall temperature for the case of uniform heat flux is linear. Therefore, the asymptotic Nusselt number must be the same as that of the linear wall temperature, which is easily shown to be

$$Nu = \frac{1}{16\sum \frac{A_n}{\lambda_n^4}} \tag{61}$$

Hence, the denominators must be equal. The advantage of equation (61) is that it converges much more rapidly than (60).

As an example of the use of (59), the thermal entry length for a fluid of Pr = .024, Re = 120,000 will be found. From Figures 10-18 the following constants are found:

$$\lambda_o^2 = 23.2 \qquad C_o = 1.465 \qquad A_1 = 2.40$$
$$\lambda_1^2 = 140 \qquad C_1 = -.810 \qquad A_2 = 1.58$$
$$\lambda_2^2 = 360 \qquad C_2 = .620 \qquad A_3 = 1.30$$

With these values it is possible to calculate approximately the first two roots of H(s) = 0. Thus from equation (42)

$$H(s) = \frac{(2)(2.40)}{s + 23.2} + \frac{(2)(1.58)}{s + 140} + \frac{2(1.30)}{s + 360}$$

The roots of this equation are

$$\gamma_o^2 = 89.5$$
$$\gamma_1^2 = 292 \tag{62}$$

Also

$$16\sum_n \frac{A_n}{\lambda_n^4} = 16\left[\frac{2.40}{23.2^2} + \frac{1.58}{140^2} + \frac{1.30}{360^2}\right]$$

$$= 0.0725$$

Substituting the above values into (59) gives

$$Nu = \frac{1}{0.0725 - .0232e^{-89.5x_*} - .0075e^{-292x_*}} \tag{63}$$

The value of x/D for which the Nusselt number is 2% greater than Nu_a is easily calculated from (63) and is about 44.

Temperature Distribution of Run 6

The calculation of the temperature distribution within the air stream of Run 6 at 3.06 ft from the thermal entrance proceeds as follows: For a Reynolds number of 38,900 and Prandtl number of 0.718, Figures 10-18 give

$$\lambda_0^2 = 193 \qquad C_0 = 1.218 \qquad A_0 = 23.8$$
$$\lambda_2^2 = 2200 \qquad C_1 = -.350 \qquad A_1 = 4.7$$
$$\lambda_3^2 = 6200 \qquad C_2 = .212 \qquad A_2 = 3.15$$

The wall-temperature distribution is approximated by the straight lines shown in Figure 20, i.e.,

$$\begin{aligned}
t - t_o &= 0 \quad ^\circ F && x < 0 \quad \text{ft} \\
&= 0.75 && 0 < x < 1.217 \\
&= 2.60 && 1.217 < x < 1.734 \\
&= 2.60 + 12.98x && 1.734 < x < 2.55 \\
&= 13.20 + 5.65x && 2.55 < x < 2.835 \\
&= 14.80 && x < 2.835
\end{aligned}$$

This representation of wall temperature is substituted into the equation of Tribus and Klein

$$t - t_o = \int_{\xi=o}^{x} \left[1 - \sum_n C_n R_n e^{-\lambda_n^2 \beta x} \right] \frac{dt_w(\xi)}{d\xi} \, d\xi$$

The result is

$$t(r_*,x=3.06) = 0.75\left[1 - \sum_n C_n R_n e^{-\lambda_n^2\beta(3.06)}\right]$$

$$+ 1.85\left[1 - \sum_n C_n R_n e^{-\lambda_n^2\beta(1.838)}\right]$$

$$+ 12.98\int_{1.734}^{3.06}\left[1 - \sum_n C_n R_n e^{-\lambda_n^2\beta(3.06-\xi)}\right]d\xi$$

$$- 12.98\int_{2.55}^{3.06}\left[1 - \sum_n C_n R_n e^{-\lambda_n^2\beta(3.06-\xi)}\right]d\xi$$

$$+ 5.65\int_{2.55}^{3.06}\left[1 - \sum_n C_n R_n e^{-\lambda_n^2\beta(3.06-\xi)}\right]d\xi$$

$$- 5.65\int_{2.83}^{3.05}\left[1 - \sum_n C_n R_n e^{-\lambda_n^2(3.05-\xi)}\right]d\xi$$

Note that the above equation satisfies the wall-temperature boundary condition. When the constants are put into the above equation and the integrations carried out, the result is

$$t(r_*,x=3.06) = 14.80 - 15.84R_0 + 1.578\,R_1 - 0.288R_2 \qquad (64)$$

The values of R_0, R_1, and R_2 are read from Table IX, and the result of their substitution into (64) has been shown in Figure 21.

The Nusselt number can be calculated in a manner analogous to the the above. The result is 101.5, and the experimental value is 101 $\pm$ 2%.

APPENDIX F

NOMENCLATURE

a	pipe radius, ft
A_n	constant, $-C_n R_n'(1)/2$
B	a constant, axial temperature gradient, °F/unit dimensionless length
C_p	specific heat at constant pressure, Btu/lb °F
C_n	constant defined by equation (4) or (7)
D	pipe diameter, ft
f	$f(r_*)$, dimensionless velocity, u/u_{max}; also friction factor
g	dimensionless total thermal diffusivity, $1 + Pr\epsilon_c/\nu$
g_c	conversion factor, 32.2 lb-mass ft/lb-force sec^2
h	heat-transfer coefficient, $qD/k(t_w-t_{mm})$, Btu/hr ft^2 °F
H	function defined by equation (42)
J	778 ft-lb/Btu
k	thermal conductivity, Btu/hr ft °F
K	constant in velocity distribution equations, usually 0.4
L	length, ft
Nu	local Nusselt number, hD/k
Nu_a	asymptotic or fully developed Nusselt number
Pe	Peclet number, $RePr$
Pr	Prandtl number, $C_p\mu/k$
q	heat flux, Btu/hr ft^2
r	radial distance, ft
r_*	r/a
R_a-R_d	electrical resistances, ohms, in analog circuit
Re	Reynolds number, $Du\rho/\mu$

R_n eigenfunction defined by equation (5)

s variable in equation (42)

t total temperature, °F

t_g static temperature of a moving gas stream, °F

t_{mm} mixed-mean temperature, °F

t_o inlet temperature, °F

t_w wall temperature, °F (sometimes wire temp)

u mean velocity at a point, ft/sec

u^+ dimensionless velocity, u/U_τ

u' root mean square of instantaneous velocity fluctuations in x direction

u_x instantaneous velocity fluctuation in x direction

u_{av} average velocity in pipe

u_{max} maximum velocity in pipe

U_τ friction velocity, $\sqrt{\tau_w/\rho}$

x axial distance, ft

x_* dimensionless axial length, βx

y a-r

y_* (a-r)/a

y^+ dimensionless distance from wall, $U_\tau y/\nu$

α ϵ_c/ϵ_ν, ratio of eddy diffusivities

β 2/RePrD

$-\gamma^2$ the zeros of equation (42); γ is also recovery factor on page 97

ϵ_c eddy conductivity, ft^2/sec

ϵ_ν eddy viscosity, ft^2/sec

θ dimensionless temperature, $(t-t_w)/(t_o-t_w)$, solution of equation (3)

λ_n eigenvalue in equation (5)

μ viscosity, lb-force sec/ft^2

ν kinematic viscosity, ft^2/sec

ξ dummy variable

ρ density, $lb\ sec^2/ft^4$

σ specific weight, lb/ft^3

τ shear stress, $lb\text{-}force/ft^2$

τ_w shear stress at the wall

ψ functional relationship defined on page 96

APPENDIX E

LITERATURE CITATIONS

1. Aladyev, I. T., "Experimental Determination of Local and Mean Coefficients of Heat Transfer for Turbulent Flow in Pipes," NACA TM 1356 (1954). Original is a 1951 Russian report.

2. Bakhmeteff, B. A., "The Mechanics of Turbulent Flow," Princeton University Press (1936).

3. Berry, V. J., "Non-Uniform Heat Transfer to Fluids Flowing in Conduits, Appl. Sci. Res., Sec. A, Vol. 4, 61-75 (1953).

4. Boelter, L. K. M., Young, D., and Iversen, H. W., "An Investigation of Aircraft Heaters - XXVII. Distribution of Heat Transfer Rate in the Entrance Section of a Circular Tube," NACA TN 1451 (1948).

5. Carslaw, H. S. and Jaeger, J. C., "Heat Conduction in Solids," p. 175, Oxford University Press (1947).

6. Churchill, R. V., "Modern Operational Mathematics in Engineering," 242-266, McGraw-Hill Book Co., Inc. (1944).

7. Corcoran, W. H., Page, F., Jr., Schlinger, W. G., and Sage, B. H., "Temperature Gradients in Turbulent Gas Streams," Ind. Eng. Chem., 44, 410-430 (1952).

8. Deissler, R. G., "Analytical and Experimental Investigation of Adiabatic Turbulent Flow in Smooth Tubes," NACN TN 2138 (1950).

9. Deissler, R. G., "Analysis of Turbulent Heat Transfer, Mass Transfer, and Friction in Smooth Tubes at High Prandtl and Schmidt Numbers," NACA TN 3145 (1954).

10. Deissler, R. G., "Turbulent Heat Transfer and Friction in the Entrance Regions of Smooth Passages," A.S.M.E. Paper No. 54-A-154 (1955). Also "Analysis of Turbulent Heat Transfer in the Entrance Regions of Smooth Passages," NACA TN 3016 (1953).

11. Eucken, A., "Allgemeine Gesetzmässigkeiten für das Wärmeleitvermögen verschiedener Stoffanten und Aggregatzustände," Forsch. a.d. Geb. d. Ing., 11, No. 1, 6-20 (1940).

12. Gilliland, E. R., Musser, R. J., and Page, W. R., "Heat Transfer to Mercury," General Discussion on Heat Transfer, 402-404, Institution of Mechanical Engineers, London (1951).

13. Hagelbarger, D. W., Howe, C. E., and Howe, R. M., "Investigation of the Utility of an Electronic Analog Computer in Engineering Problems," UMM-28, Engineering Research Institute, Univ. of Mich., Ann Arbor (1949).

14. Hartnett, J. P., "Experimental Determination of the Thermal Entrance Length for the Flow of Water and of Oil in Circular Pipes," A.S.M.E. Preprint of Paper No. 54-A-184 (1954).

15. Hoffman, H. W., "Turbulent Forced Convection Heat Transfer in Circular Tubes Containing Molten Sodium Hydroxide," 1953 Heat Transfer and Fluid Mechanics Institute, Preprints of Papers, p. 83, Stanford University Press, Stanford, California (1952).

16. Hottel, H. C. and Kalitinsky, A., J. Appl. Mech., 12, A25-32 (1945).

17. Isakoff, S. E. and Drew, T. B., "Heat and Momentum Transfer in Turbulent Flow of Mercury," General Discussion on Heat Transfer, 405-409, Institution of Mechanical Engineers, London (1951). Also Ph.D. Thesis of Isakoff, University Microfilms, Ann Arbor, Michigan, Microfilm No. 4200.

18. Jakob, M., "Heat Transfer," Vol. I, 451-464, John Wiley and Sons, Inc., New York (1949).

19. Jenkins, R., "Variation of Eddy Conductivity with Prandtl Modulus and Its Use in Prediction of Turbulent Heat Transfer Coefficients," Heat Transfer and Fluid Mechanics Institute Preprints, 147-158, Stanford University Press, Stanford, California (1951).

20. Johnson, H. A., Hartnett, J. P., and Clabaugh, W. J., "Heat Transfer to Molten Lead-Bismuth Eutectic in Turbulent Pipe Flow," 1952 Heat Transfer and Fluid Mechanics Institute, Preprints of Papers, p. 5, Stanford University Press, Stanford, California (1952).

21. Keys, F. G. and Sandell, D. J., "New Measurements of the Heat Conductivity of Steam and Nitrogen," Trans. A.S.M.E., 72, 767 (1950).

22. Knudsen, J. G., "Heat Transfer, Friction, and Velocity Gradients in Annuli Containing Plain and Fin Tubes," Ph.D. Thesis, Univ. of Mich., Ann Arbor (1949).

23. Kovásznay, L. S. G., "Development of Turbulence-Measuring Equipment," NACA TN 2839 (1953).

24. Latzko, H., "Heat Transfer in a Turbulent Liquid or Gas Stream," NACA TM 1068 (1944); original in Zeitschrift für angewandte Mathematik und Mechanik, 1, No. 4 (1921).

25. Laufer, J., "Some Recent Measurements in a Two-Dimensional Turbulent Channel," J. Aero. Sci., 17, 277-287 (1950).

26. Laufer, J., "The Structure of Turbulence in Fully Developed Pipe Flow," NACA TN 2954 (1953).

27. Levy, S., "Heat Conduction Methods in Forced Convection Flow," A.S.M.E. Preprint of Paper No. 54-A-142 (1955).

28. Lipkis, R., Comments on A.S.M.E. Paper by Sellars, Tribus, and Klein; A.S.M.E. Preprint No. 55-SA-66.

29. Lubarsky, B., "Experimental Investigation of Forced-Convection Heat-Transfer Characteristics of Lead-Bismuth Eutectic," NACA-RME 51G02 (1951).

30. Lyon, R. N., "Heat Transfer at High Fluxes in Confined Spaces," Ph.D. Thesis in Chemical Engineering, Univ. of Mich., Ann Arbor (1949).

31. Lyon, R. N., "Liquid Metal Heat-Transfer Coefficients," Chem. Eng. Progress, 47, No. 2, 75-79 (1951).

32. Lyon, R. N., "Liquid-Metals Handbook," 2nd ed. revised, 184-194, U.S. Government Printing Office, Washington (1954).

33. Martinelli, R. C., "Heat Transfer to Molten Metals," Trans. A.S.M.E., 69, 947-959 (1947).

34. McAdams, W. H., "Heat Transmission," 3rd ed., 202-251, New York, McGraw-Hill Book Co., Inc. (1954).

35. Ibid., p. 259.

36. Micromatic Hone Co., Detroit, Mich., Personal Communication.

37. Nikuradse, J., "Gestzmässigkeiten der turbulenten Strömung in glatten Röhren," V.D.I. Forschungsheft, 356 (1932).

38. Poppendiek, H. F., "Forced Convection Heat Transfer in Thermal Entrance Regions - Part I," Oak Ridge National Laboratory, Tennessee, ORNL 913 Series A Physics (March, 1951).

39. Poppendiek, H. F. and Palmer, L. D., "Forced Convection Heat Transfer in Thermal Entrance Regions - Part II," Oak Ridge National Laboratory, Tennessee, ORNL 914 Metallurgy and Ceramics (March, 1951).

40. Poppendiek, H. F. and Harrison, W. B.,"Remarks on Thermal Entrance-Region Heat Transfer in Liquid-Metal Systems," Paper Presented at Heat Transfer Symposium in St. Louis, Missouri, December 13-16, 1953; A.I.Ch.E. Preprint No. 7.

41. Prandtl, L., "Über die ausgebildete Turbulenz," Proceedings of the Second International Congress for Applied Mechanics, 62-74, Zurich, Switzerland (1926).

42. Reichardt, H., "Heat Transfer Through Turbulent Friction Layers," NACN TM 1047 (1943).

43. Reynolds, O., "On the Extent and Action of the Heating Surface for Steam Boilers," Proceedings of the Manchester Literary and Philosophical Society, 14, 7 (1874).

44. Ross, D., "Turbulent Flow in Smooth Pipes, A Reanalysis of Nikuradse's Experiments," Ordnance Research Laboratory, Pennsylvania State College, State College, Pennsylvania (September 1952).

45. Rothman, A. J., "Thermal Conductivity of Gases at High Temperature," U.S. Atomic Energy Commission UCRL 2339 (1953).

46. Schenk, J., A Letter to the Editor, Appl. Sci. Res., A4, 222 (1954).

47. Schlinger, W. G., Berry, V. J., Mason, J. L., and Sage, B. H., "Temperature Gradients in Turbulent Gas Streams," Ind. Eng. Chem., 45, No. 3, 662-666 (1953).

48. Schlinger, W. G., Hsu, N. T., Cavers, S. D., and Sage, B. H., "Temperature Gradients in Turbulent Gas Streams," Ind. Eng. Chem., 45, 864-870 (1953).

49. Seban, R. A. and Shimazaki, T. T., "Calculations Relative to the Thermal Entry Length for Fluids of Low Prandtl Number," Univ. of Calif., Division of Engineering Research Report, Series No. 16, Issue No. 4, Berkeley, California (1950).

50. Seban, R. A. and Shimazaki, T. T., "Heat Transfer to a Fluid Flowing Turbulently in a Smooth Pipe with Walls at Constant Temperature," Trans. A.S.M.E., 73, 803-808 (1951).

51. Sellars, J., Tribus, M., and Klein, J., "Heat Transfer to Laminar Flow in a Round Tube or Flat Conduit, The Graetz Problem Extended," WADC Technical Report 54-255, Engineering Research Institute, Univ. of Mich., Ann Arbor (April, 1954). Also A.S.M.E. Preprint No. 55-SA-66.

52. Sherwood, T. T. and Reed, C. E., "Applied Mathematics in Chemical Engineering," p. 287, Mc Graw-Hill Book Co., Inc., New York (1939).

53. Stops, D. W., "Effect of Temperature on the Thermal Conductivity of Gases," Nature, 164, 966 (1949).

54. Taylor, W. J. and Johnson, H. L., "An Improved Hot Wire Cell for Accurate Measurements of Gases over a Wide Temperature Range," J. Chem. Phys., 14, 219 (1946).

55. Trefethen, L. M., "Heat Transfer Properties of Liquid Metals," Cambridge University in Collaboration with Atomic Energy Research Extablishment, Harwell, Berks. (1950). Published by Atomic Energy Commission, Technical Information Service, as "NP-1788" (1951).

56. Tribus, M. and Boelter, L. K. M., "An Investigation of Aircraft Heaters, II - Properties of Gases," NACA Wartime Report W-9 (October, 1942).

57. Tribus, M. and Klein, J., "Forced Convection from Nonisothermal Surfaces," in "Heat Transfer, a Symposium held at the University of Michigan during the summer of 1952," 211-235, Engineering Research Institute, Univ. of Mich., Ann Arbor (1953).

58. Van Driest, E. R., "On Turbulent Flow Near a Wall," 1955 Heat Transfer and Fluid Mechanics Institute, Preprints of Papers, Paper XII, Univ. of Calif., Los Angeles (1955).

59. von Kármán, Th., "The Analogy Between Fluid Friction and Heat Transfer," Trans. A.S.M.E., 61, 705-710 (1939).

60. Werner, R. C., King, E. C., and Tidball, R. A., "Forced Convection Heat Transfer with Liquid Metals," Presented at the Annual Meeting of A.I.Ch.E., December, 1949. Also, "Final Report, Research with Sodium and Sodium Potassium Alloys from July, 1948 to May 31, 1949," Mine Safety Appliances Co., p. 17-24.

61. Willis, J. B., Australian Council Aeronautical Report ACA-19 (1945).

62. Moody, L. F., "Friction Factors for Pipe Flow," Trans. A.S.M.E., 66, 671 (1944).